An investigation of novel coatings for the protection of organic coated iron based substrates and the industrialisation of dye-sensitised solar cell technology.

Reynolds, Gavin James

Swansea University
Prifysgol Abertawe

An Investigation of Novel Coatings for the Protection of Organic Coated Iron Based Substrates and the Industrialisation of Dye-sensitised Solar Cell Technology

Gavin James Reynolds

Eng.D.

Materials Research Centre
College of Engineering
Swansea University

2013

DECLARATION

Declaration: This work has not previously been accepted in substance for any degree and is not being concurrently submitted in candidature for any degree.

Signed: Date: 4/11/13

Statement: This thesis is the result of my own investigations, except where otherwise stated. Other sources are acknowledged by footnotes giving explicit references.

Signed: Date: 4/11/13

Statement: I hereby give consent for my thesis, if accepted, to be available for photocopying and interlibrary loan and for the title and summary to be made available to outside organisations.

Signed: Date: 4/11/13

Thesis Summary

A high-throughput method of investigating organic coating delamination from iron substrates incorporating interfacial thin metallic films of varying thickness is presented. Physical vapour deposited aluminium is demonstrated as a means of limiting underfilm oxygen reduction and slowing rates of corrosion-driven cathodic disbondment. A wedge of graded thickness is deposited on an iron surface and over-coated with a model organic layer. After initiating corrosion by applying corrosive electrolyte to a penetrative defect, rates of corrosion-driven delamination are determined by in-situ scanning Kelvin probe measurements, enabling the influence of a range of Al thicknesses to be studied on a single sample.

A novel method of monitoring corrosion activity when an iodide/ triiodide dye-sensitized solar cell redox electrolyte is placed in contact with a range of metallic substrates is also described. Corrosion of the metallic substrate results from anodic dissolution of the metallic surface coupled with cathodic reduction of triiodide (I_3^-) to colorless iodide ions in solution. In the work described here, UV/Vis spectrophotometry in reflectance mode is used in conjunction with encapsulation cells that incorporate a 25 μm thick electrolyte layer, prepared using a range of polished metallic substrates. The corrosion rate is quantified by monitoring changes in the absorption spectra with respect to time. Of the metals evaluated, only titanium was wholly resistant to corrosion and did not show evidence of reaction with the electrolyte for periods of up to 3 months. Other metals such as zinc reacted within seconds and complete and irreversible loss of I_3^- was observed after only a few minutes.

Dye sensitized solar cells (DSCs) have been assembled directly onto a pre-painted construction steel substrate. This has been achieved by chemically isolating the underlying substrate through the application of a high temperature resistant organic polymer rendered conducting by applying a 1.2 μm collection electrode of magnetron sputtered titanium. The resultant DSC achieved 2.9 % energy conversion efficiency under one sun illumination compared to 3.2 % for identical cells

manufactured on 1mm thick Ti coupons. The slight reduction in efficiency reflects the increasing resistance of the substrate 1.2 □m Ti layer that results from micro-cracking during the titania sintering step.

Dye sensitized solar cells (DSCs) have also been assembled directly onto an electro-chromium coated steel substrate that has been both chemically and electrically isolated through the application of a high temperature resistant organic polymer (polyimide) coating. The surface of the coated product has been rendered conducting through the application of 0.5μm aluminium and titanium films deposited directly by DC magnetron sputtering. The resultant DSCs achieved very poor energy conversion efficiencies under one sun illumination as did cells produced on bulk Al substrates. Cells manufactured on 1mm thick Ti coupons gave efficiencies of around 3.2%. The poor efficiencies for the sputtered Ti and Al films can be related to the increasing resistance of the Ti film due to the formation of micro cracking during the titania sintering step, and the inadequate corrosion performance of Al when in contact with an iodine triiodide redox electrolyte. An Al-Ti bilayer has been proposed where the Ti film has been used as a barrier layer to corrosion, cells fabricated on this substrate have showed much promise, and efficiencies of 2.2 % have been achieved.

Acknowledgements

I would like to take this opportunity to gratefully acknowledge the Engineering and Physical Sciences Research Council and Tata Steel for their continued funding throughout the course of this project. In particular I would like to thank my academic supervisor Dr. Geraint Williams. Dr. Geraint Williams' constant input of energy, suggestions and ideas helped keep the project fun and relevant. Without his vote of confidence, this work would not have been possible. Also from the university side I owe a huge debt of gratitude to those who showed me patience in mentoring me through the intricacies of experimental science.

Another guiding hand came in the form of Dr. Trystan Watson who gave so generously his time and energy to help me along the way, and also became a friend and role model during my study. I would also like to thank Prof. Dave Worsley for his patience and support, and also Prof. Neil McMurray for lending me his superior knowledge whenever I needed it. Help from Tata Steel came in the form of Debbie Hammond, Tim English and those involved in the PV team, who all offered their experience at one stage or another during the project. I'd also like to thank all the members of the Eng.D. for their friendship and support over the 4 years and wish them all the best in the future.

Finally I would like to dedicate this thesis to my parents for their unrelenting support, advice and patience over the last 5 years and who have, and continue to, support me in every aspect of my life. I would also like to dedicate it to my Grampa Jim who sadly passed away during third year. He was always interested in what I was doing and gave me lots of support and encouragement.

Gavin James Reynolds

Table of Contents

Chapter 2: Experimental Procedures

Chapter 1

Introduction

1.1 Area of Study

There is currently significant interest towards using so-called "clean" coating technologies to replace traditional methods of depositing sacrificial, wear resistant or decorative metallic coatings on to industrial steel panels. The word "clean" can be used to describe products, processes or services that reduce waste and require as few non-renewable resources as possible. Environmental considerations are largely responsible for recent developments in this area, since conventional metal finishing technologies such as hot-dip galvanising or electroplating consume substantial quantities of energy and generate waste, incurring considerable disposal costs. With fossil fuels slowly nearing depletion [1], along with the threat of global warming, research, development and implementation of renewable energy is one of the most crucial challenges of today's mankind [1, 64]. Some may argue that nuclear power is the answer to all our problems. However despite the tight safety regulations and procedures in modern nuclear power plants, nuclear energy still raises much opposition amongst consumers through a concern in the nature of the waste produced by nuclear processes.

Of the various technologies available, physical vapour deposition (PVD) is considered to be the most promising and economically viable methods of depositing thinner coatings on to steel products on an industrial scale through a cleaner process [64, 75]. Apart from protecting steel, it would also be ideal if a coating could be applied to roofing and cladding material that has the ability to harness 'free' energy from the sun.

Technologies that can harness the energy that is emitted by the sun, know as photovoltaic devices, have existed for many years. The term "photovoltaic" refers to the utilisation of a generated voltage when radiant energy falls on the boundary between dissimilar substances such as semiconductors [1]. The main drawbacks of this technology to date are high production costs and being suitable for a limited variety of applications only, which in turn has hindered the development of such technology on a large scale [93]. This is why development of new, more advanced, cheaper and efficient solar energy technologies is called for to bring this form of renewable energy available to even larger number of customers. This project seeks to investigate a solution to both of these scenarios.

1.2 Objectives of the Study

The focus of work in chapter 3 intends to investigate a PVD layer over-coated with an organic-based protective layer as detailed in Figure 1.1, to replicate the action of a paint film in providing corrosion protection to a metal substrate. The inclusion of the PVD layer upon an iron substrate is explored as a method of preventing underfilm corrosion processes. Aluminium has been selected as the PVD layer.

Chapter 4 explores the large-scale development and fabrication of photovoltaic technology on to strip metal products. A developing member of the family of photovoltaic devices, known as dye-sensitised solar cells (DSCs) [2,93], has shown huge potential regarding suitability toward up scaling [4]. DSC technology uses materials that are relatively low cost when compared to more traditional silicon based photovoltaics [2], and the materials required are readily available in large quantities [3,5]. Production costs are also low, as no specialised environments are needed. However, one of the main drawbacks of incorporating DSC technology on to a metallic substrate is the aggressive nature of a redox-mediating electrolyte that is an essential part of the operation of the technology. The most commonly used DSC electrolyte to date consists of an iodide/triiodide (I^-/I_3^-) redox mediator in aqueous solution [76,93]. During the interaction between triiodide within the DSC electrolyte

and a metallic surface, corrosion of the metallic substrate occurs [76]. Initially the electrolyte has a characteristic dark brown colour due to the presence of triiodide.

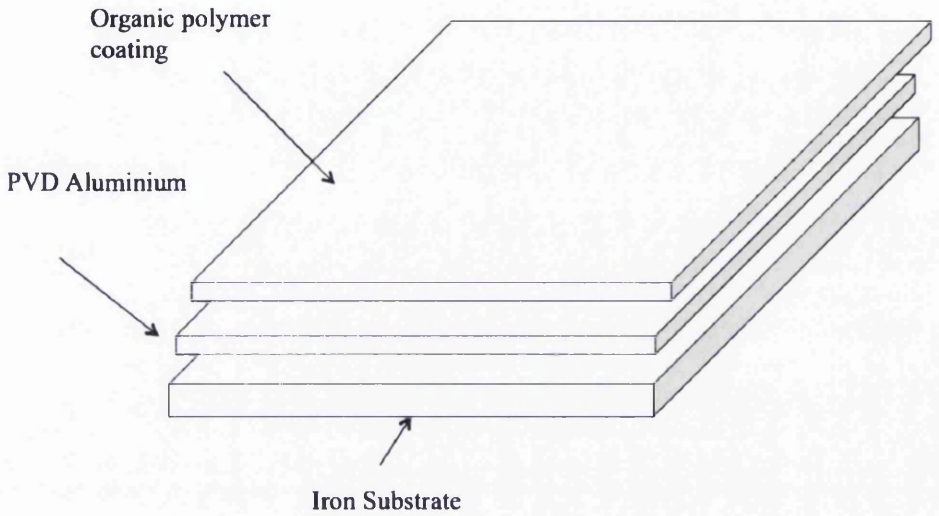

Figure 1.1: *A schematic of an iron substrate coated with a PVD Al layer, which has been over coated with a polymer organic paint layer, in order to improve underfilm organic coating delamination.*

The corrosion is a consequence of anodic dissolution of the metallic surface coupled with cathodic reduction of triiodide ions (I_3^-) to colorless iodide ions (I^-) in solution. This means that any triiodide in contact with a metal surface will be totally depleted from the electrolyte over a period of time as a result of the corrosion reaction and there will be a colour transformation from dark brown to colourless. This effect will eventually terminate the operation of a DSC as the important redox couple (I^-/I_3^-) has been destroyed. This work set out to explore the interaction between a range of different metallic substrates and the DSC electrolyte to scope out metals that may have a potential to remain inert in the presence of the triiodide-containing electrolyte. The development of a novel method of monitoring the corrosion activity has also been investigated. In the work described, it was the intention to develop a technique using UV/Vis spectrophotometry in reflectance mode and used in conjunction with electrolyte encapsulation cells, to provide a more quantitative method of testing

substrate compatibility. The corrosion rate is quantified by monitoring changes in electrolyte colour through accurate measurement of the absorption spectra for various different metal samples with respect to time.

In chapter 5, dye sensitized solar cells DSCs have been assembled directly onto a pre-painted construction steel substrate. It is the intention here to explore the potential of sputtering titanium onto pre-existing roofing or cladding products as a substrate for the industrialisation of DSC technology.

Finally, chapter 6 sets out to study the assembly of DSCs directly onto an electro-chromium coated steel substrate, that has been both chemically and electrically isolated through the application of a high temperature resistant organic polymer (polyimide) coating. The surface of the organic coated product has been rendered conducting through the application of 0.5μm Aluminium and Titanium films deposited directly by DC magnetron sputtering. The resultant DSCs achieved very poor energy conversion efficiencies under one sun illumination as did cells produced on bulk Al substrates. Cells manufactured on 1mm thick Ti coupons however gave efficiencies of around 3.2%. This section explores the reason for the poor performance for the cells fabricated on thin metallic films and as a solution an Al-Ti bilayer has been proposed. It is the intention of this work to unveil the successes of such a bilayer configuration on the operation of DSCs built on thin metallic films.

1.3 Literature Review

1.3.1 Novel PVD Protective Coatings for Iron Based Substrates

The first section of work reported in Chapter 3 focuses on the development of physical vapour deposited (PVD) aluminium thin films as corrosion protection coatings on iron substrates, with the intention of halting the cathodic disbondment process of organic polymer coatings, which have been exposed to atmospheric conditions. It is therefore necessary to review work that has been reported on coating

technologies that have been used for the purpose of corrosion protection, and in particular as methods of preventing underfilm organic coating delamination. However, to make sense of the work being investigated in Chapter 3, we shall first concentrate on work that has been carried out regarding cathodic disbondment mechanisms and the techniques developed to monitor its effects. The PVD process will be detailed in section 1.3.2.

1.3.1.1 Cathodic Disbondment of Polymer Coatings on Iron Based Substrates

One of the main modes of failure regarding the separation of an organic polymer coating from iron based substrates is corrosion-driven cathodic coating disbondment, which has previously been reviewed [6-12]. This process can occur wherever the metallic substrate becomes exposed to the environment *via* scratches or cut edges during manufacturing or through in-service damage. A review by McMurray and Williams suggests that numerous studies have indicated that when iron or zinc substrates are exposed to aqueous electrolyte through penetrative defects in an organic coating, a cathodic delamination cell may become established [6].

Figure 1.2 shows a schematic of a cathodic delamination cell for a defective organic polymer coating on an iron substrate. Within this cell, a thin layer of electrolyte ingresses through a defect in the coating and means that an anodic reaction, and consequently anodic dissolution of the metal, signified by reaction (2) in the diagram is allowed to occur. This reaction is coupled to cathodic oxygen reduction at the area of organic coating disbondment, where oxygen penetration through the coating is greatest. This cathodic oxygen reduction process is signified by reaction (1). Due to the nature of the electrolyte, an alkaline environment forms at the cathode due to the migration of alkali metal cations from the defect and through the delamination zone. Within the delamination zone, a breakdown of the polymer-metal bond is witnessed.

There have been various mechanisms suggested as why the bond between the substrate and the polymer coating breaks down and are detailed by McMurray and Williams [1,6,13,14,15,16,17,18,19]. It has been suggested that there are many mechanisms, such as the increase in alkalinity and the consequence of the cathodic

reaction, that aid the process of organic coating disbondment that may work alone or in combination with one another. A more in-depth explanation of this process is detailed in Chapter 3 of this thesis.

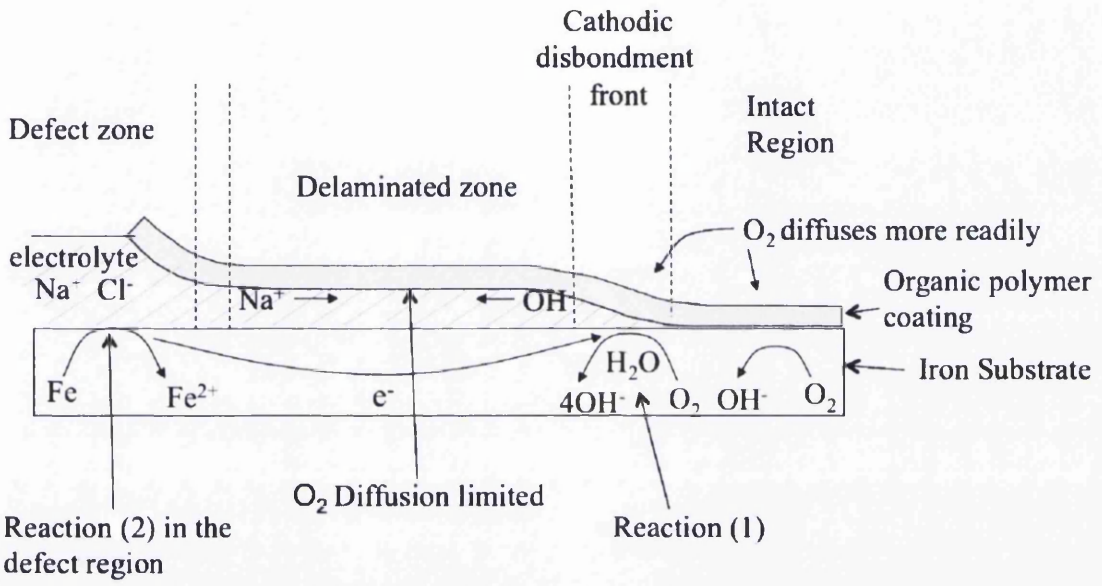

Figure 1.2 *A schematic showing a cathodic delamination cell for a defective organic polymer coating on an iron substrate.*

The idea behind the work reported in Chapter 3 is to apply thin physical vapour deposited metallic film on to the surface of the iron substrate prior to the application of an organic polymer coating. The metallic film however, must be known to exhibit characteristics of a poor cathode, which means that the ability for the oxygen reaction (2) to occur is strictly prevented at the surface of the metallic film. As aluminium is known to be a poor cathode it has been chosen for use in the work reported.

1.3.1.2 The Scanning Kelvin Probe Technique (SKPT)

A technique for investigating the mechanisms of cathodic coating disbondment has been detailed in the literature [48-63]. With strong relevance to Chapter 3 of this thesis, pioneering investigations on organic coating delamination from iron substrates in atmospheric environments [20-22] with the use of a Scanning Kelvin Probe Technique (SKPT) have been carried out by Stratmann *et al.,* and provide a reproducible method of studying the kinetics of underfilm delamination when thin layers of electrolyte ingress beneath organic polymer coatings on metallic substrates [6, 26, 27]. The Scanning Kelvin Probe Technique was an advancement of an earlier method used, the Kelvin Probe Technique, and details of the advancement can be found in work by McMurray and Worsley [23]. The SKPT has its benefits in that it allows the electrochemical mapping of localised corrosion phenomena occurring beneath thin electrolyte films on un-coated metals and beneath intact polymer coatings on metal substrates [23, 24, 25]. Through the use of electrochemical maps produced by the technique it is possible to build knowledge of the corrosion mechanisms occurring beneath a polymer coated metal substrate. McMurray and Worsley have fully detailed the operating principles behind the Scanning Kelvin Probe Technique [23]. The technique is one of the most sensitive measuring procedures in surface physics and is a well established means of determining metallic work functions [47].

1.3.1.2.1 Theory of the Kelvin Probe

Figure 1.3 shows a schematic of the Kelvin Probe Technique apparatus. The surface of the metal sample under investigation and the tip the vibrating probe electrode represents a parallel plate capacitor. The capacitor dielectric is the presence of a non-conducting medium (typically air gap or a mixture of air gap and insulating polymer) in the space between the plates. The capacitance, C, is therefore given by,

$$C = \frac{\varepsilon \varepsilon_0 A}{d} \qquad (1.1)[23]$$

d is the distance between the plates, A the plate area, ε_0 the permittivity of vacuum, and ε the dielectric constant of the capacitor dielectric.

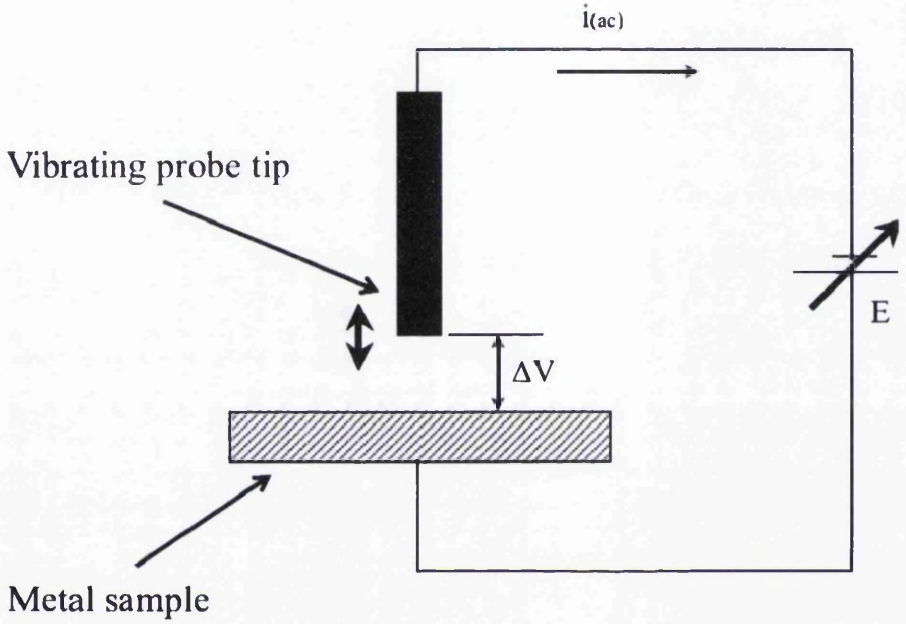

Figure 1.3: *A schematic diagram illustrating the Kelvin probe (vibrating capacitor method) for measuring surface (Volta) potential* [23].

The probe electrode is vibrated sinusoidally, relative to the surface of the metal sample, at a frequency of ω so that the plate separation distance, d, varies with in time, t, according to;

$$d = d_0 + d_1 \sin(\omega t) \qquad (1.2)[23]$$

d_0 is the mean plate separation distance, and d_1 is the amplitude of vibration. Due to the change in separation distance, d, there exists and variation in the capacitance, C.

If any external potential difference (ΔV) is established between the metal sample surface and the vibrating probe tip, an alternating current will flow through the circuit. The Kelvin probe signal current is not used directly to infer the open circuit value of ΔV. Instead ΔV is obtained indirectly by adjusting the voltage value of the externally applied DC bias voltage, E, so that the signal current becomes zero *i.e.* the null current condition. By doing so,

$$E = E_{i=0} = -\Delta V \qquad (1.3)[23]$$

The value of ΔV can be obtained by introducing a parameter E_{kp}, Kelvin probe potential, which is equal to $-E_{i=0}$. The quantity of E_{kp} will be directly equivalent to the measured value of ΔV. The meaning of E_{KP} depends on the conditions under which the measurement is performed. When pristine metal surfaces are measured in a vacuum, E_{KP} will be equivalent to the difference in the work functions of the metals composing the probe and the sample. When the measurements are performed in air the presence of surface oxide films may cause E_{KP} to deviate values expected purely of the basis of metallic work functions [50]. Further changes in E_{KP} are likely when humidity is present in the experimental atmosphere as a consequence of water adsorption and the hydration of any surface oxide layer [50].

For the purposes of using this technique to investigate corrosion occurring on a metal surface due to the presence of a thin electrolyte layer, measurements of E_{KP} are more complex. In this situation volta potential differences, ΔV, will not be measured between the vibrating tip electrode and the metal sample electrode, but between the vibrating tip electrode and outer surface of the electrolyte film [23]. It has been reported that the value of E_{KP} for this system can be related directly to the corrosion potential plus a constant {23].

$$E_{kp} = E_{corr} + constant \qquad 1.4[23]$$

E_{corr} is the free corrosion potential of the metal surface relative to a real or hypothetical reference electrode immersed in the electrolyte film immediately over the point of measurement. One significant advantage of the Kevin probe technique is that the measurement is indifferent to the nature of the dielectric overlaying the metal or the electrolyte surface. Thus E_{KP} measurements may be carried out with samples over coated with, for example, an insulating polymer film. The value of the constant can be determined *via* calibration techniques as discussed in Chapter 2.

1.3.1.2.2 Scanning Kelvin Probe Apparatus

The advancement of this technique, as mentioned earlier, allows the measurement of free corrosion potentials to be made, within a given atmospheric environment, over a larger sample surface area. The apparatus used is shown in Figure 1.4. The apparatus allows a spatially resolved surface map of free corrosion potential to be generated. The apparatus can be set up to repeat measurements in a time-lapse fashion over desired lengths of time. Studying the change in the detail of the surface maps over time, gives a view of the corrosion mechanisms occurring on metal surfaces with or without the addition of an organic polymer coating. From the information generated corrosion it is possible to produce corrosion rates. This has been explained extensively in Chapter 3, and examples of corrosion maps and kinetics plots can be found there.

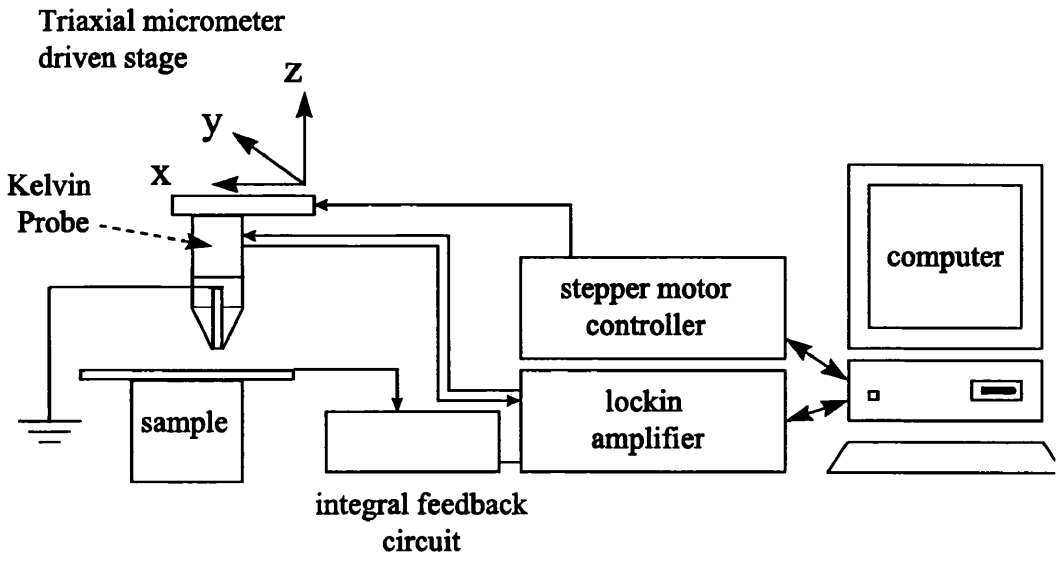

Figure 1.4: *Schematic illustration of a Scanning Kelvin Probe Apparatus for monitoring atmospheric and underfilm corrosion phenomena. A stepper motor provides the x, y, z, movement of the tip electrode. The vibrator drive is obtained by amplifying the local oscillator output of a lock-in amplifier that also detects the a.c. Kelvin probe signal current (i). However, an additional feedback circuit is required to control the d.c. bias voltage (E) and maintain a null current condition* ($E_{i=0}$) [23].

1.3.1.3 Preventing Cathodic Coating Delamination

Where a coating has become detached from the surface of a metal through physical means it might reasonably be assumed that disbondment could be discouraged by promoting coating adhesion. Funke has described adhesion as the most important and decisive property of a coating [28-30].

1.3.1.3.1 Silane Treatment

Improvements in adhesion of organic coatings on steel have been witnessed through the use of silanes. There is evidence of various different types of silanes that are used for different purposes as reported here [31,32]. Silanisation has also been found to

improve wet and dry adhesion by Marsh *et al.* through threating steel substrates prior to applying the organic coating [33]. However, no relationship between adhesion and coating delamination was reported in this work. Leidheiser did find that treating an iron surface with silane prior to coating with polybutadiene resulted in significantly reduced rates of cathodic delamination [5]. Overall, it would seem that improving coating adhesion alone might not improve resistance to cathodic delamination if an alternative disbondment mechanism, such as hydrolysis of the coating polymer, is available [34].

1.3.1.3.2 Inorganic Pretreatments

Other forms of pretreatments are available as in-organic phosphate or chromium based treatments that react with the substrate in order to replace the air formed oxides on the surface with oxide of phosphate or chromium [35]. SKP Studies have shown that inorganic pretreatments or conversion coatings, such as thin phosphate based conversion coatings, that are applied to metal substrates prior to coating with paint or lacquer, inhibit the ability for cathodic oxygen reduction to take place [36]. Hence, as a consequence they are seen to reduce the effects of cathodic coating delamination of polymer coatings on metal substrates.

1.3.1.3.3 Smart Release Pigments

Corrosion inhibitor pigments have been reported in retarding the corrosion driven coating delamination through the use of an SKP in conjunction with strontium chromate based inhibiton pigments in polyvinylbutyral applied to galvanised steel [37]. Novel Zn^{2+} and Ca^{2+} -exchanged cross-linked sulphonated polystyrene (CSP) pigments have been used in model polymer coatings to inhibit corrosion-driven cathodic delamination on galvanised steel surfaces [37].

1.3.1.3.4 Conducting Polymers (ICPs)

There has been interest in the use of conducting polymers (ICPs) for corrosion control and also reviewed [38,39]. Many studies have focused on polyaniline ES (PAni ES) [38-40]. PAni ES may be applied to metal surfaces directly by electrodeposition [41,42]. PAni ES particles may also be dispersed in a conventional polymer binder [43,44]. The protection of carbon steel by PAni ES has been ascribed to the formation of a passive oxide film and anodic inhibition through precipitation of an insoluble metal salt of the dopant anion [45,46].

1.3.1.3.5 Thin Metallic Films

The possibility of inhibiting corrosion driven cathodic coating delamination on iron based substrates has recently gained positive interest. The subject of PVD based coatings as direct replacements for traditional galvanic (zinc or cadmium) or barrier-type nickel corrosion resistant metallic layers has been reviewed [64]. Only recent developments since the 1999 publication date of this review will be discussed here. In the intervening period, and as a substitute for coatings mentioned above, there has been a number of reports investigating PVD coatings for improving corrosion resistance of iron based substrates. One report by Lauwerens *et al.* has detailed that mixed coatings of multilayer Al/Ti coatings, of 3-4 μm thickness, deposited on steel substrates *via* magnetron sputtering, provide corrosion resistance that is comparable or even better than a 20-μm thick Al-Si hot-dip coating [65]. However in this report coatings have undergone corrosion tests before and after a heat treatment step, where a thick protective oxide film was allowed to grow. However, good corrosion resistance has been reported. Work by Charrier *et al.* on Ti/Al multilayers, deposited on steel via PVD, showed, through corrosion tests using 5% salt spray and electrochemical characterisation *via* voltamperometric, that corrosion resistance was superior to that witnessed from monolayer coatings [73]. This confirms the findings of Lauwerens *et al.* mentioned above.

In this intervening period, there has also been a change in focus from single or multiple metal thin films to alloy systems [66, 67], or single metals which can subsequently be thermally interdiffused with the substrate to form an alloyed surface layer, such as magnesium on zinc-coated (galvanised) steel [68, 69]. The corrosion resistance of such systems has been said to strongly depend on the magnesium content within the coating [69]. In addition, highly efficient, corrosion-resistant thin coatings based on metals such as titanium [70] and tantalum [71], which develop highly protective passive films, have also been demonstrated on surfaces such as stainless and carbon steels respectively. Another report regarding stainless steel has been detailed in the literature, where PVD coatings of TiCN, CrN and DLC (diamond like carbon), have been applied to stainless steel substrates and subjected to NaCl, HCl and H_2SO_4 aqueous solutions. Corrosion studies were performed via polarisation curve testing and immersion testing [72]. Results revealed that DLC films performed better in chloride containing environments such as NaCl and HCL, TiCN and CrN films proved not to be as protective. In H_2SO_4 the DLC film produced better corrosion resistance and was matched by CrN. However, after a period of 100 hours, the corrosion resistance of CrN and TiCN began to diminish.

Despite the evidence collected for the use of PVD metallic films as sacrificial corrosion protection for iron based substrates, very little attention has been paid to the corrosion studies of PVD metallic films on iron substrates coated with organic polymer coatings. There is also little evidence of the SKPT being used to investigate corrosion mechanisms occurring beneath organic polymer coatings on PVD coated iron substrates. To our knowledge work described in Chapter 3 of this thesis is the only investigation of it's kind so far.

1.3.2 Thin Film coating Technologies

1.3.2.1 Vapour Coating Processes

Atomistic deposition processes such as physical vapour deposition (PVD) and chemical vapour deposition (CVD), are the two main methods of providing hard, fracture resistant film coatings to a given substrate [74]. CVD and PVD processes have been around for many years with regards to small scale coating requirements e.g. for depositing materials onto semiconductor wafers due to the ability to create very thin layers of a given material, such as silicon. Essentially both methods allow an atom-by-atom transfer of a given material from a target source on to the substrate under vacuum conditions. However, CVD and PVD differ by the way in which this process is carried out.

1.3.2.2 PVD

Interest from Tata Steel is currently being paid towards the use of physical vapour deposition process for the fabrication of dye-sensitised solar cells (DSCs). The main drive behind the development of this process is due to its economical advantages over the current methods used [80,82]. A low cost coating on flexible metallic or plastic sheet and strip can be achieved by this process and substantial PVD coating deposition rates can be achieved [75]. The process is very versatile allowing the deposition of many elements and alloys of elements to be achieved. PVD produces a quality coating and is environmentally friendly. There are a range of PVD techniques available for coating metal strip; vapourisation by resistive or inductive heating, Electron Beam Evaporation (EB), Jet Vapour Deposition (JVD) and Electro-Magnetic Levitation (EML-PVD). There is a level of efficiency associated with each method and this is crucial during the decision making process regarding the technique to incorporate into the business.

The method in which a target material is vapourised distinguishes a PVD process from that of a CVD process. In a PVD process the atoms within in a solid target material become physically separated from the target producing a vapour phase. There are many methods by which a target material can be vapourised and these are detailed in Figure 1.6 and are summarised in the preceding sections. The particular example in Figure 1.5 is that of a magnetron sputtering process, which is performed in a stainless steel chamber under vacuum conditions. Argon gas is introduced to the chamber and ionised through the application of a D.C. source, and hence an Ar plasma is created in the vicinity of the target material. With the use of a magnetron, the Ar plasma is attracted towards the surface of the target material. The plasma ions bombard the surface causing atoms of the target material to dislodge. The dislodged atoms then move away from the source producing the vapour phase. The atoms are then transported in a straight line to the substrate, where they condense on the surface, building up a layer of material on the substrate.

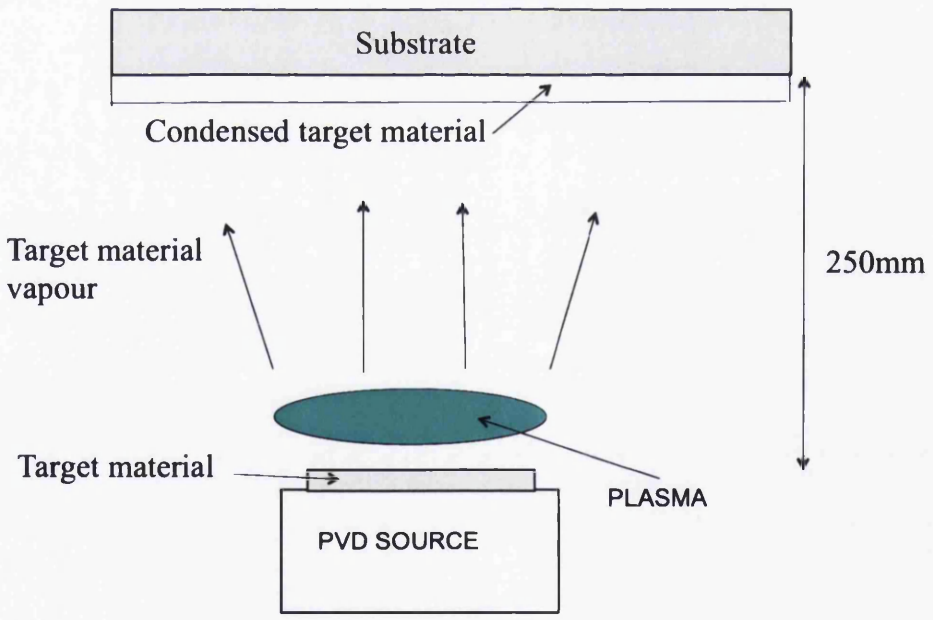

Figure 1.5: *A schematic to show material build up from target to substrate for a PVD process.*

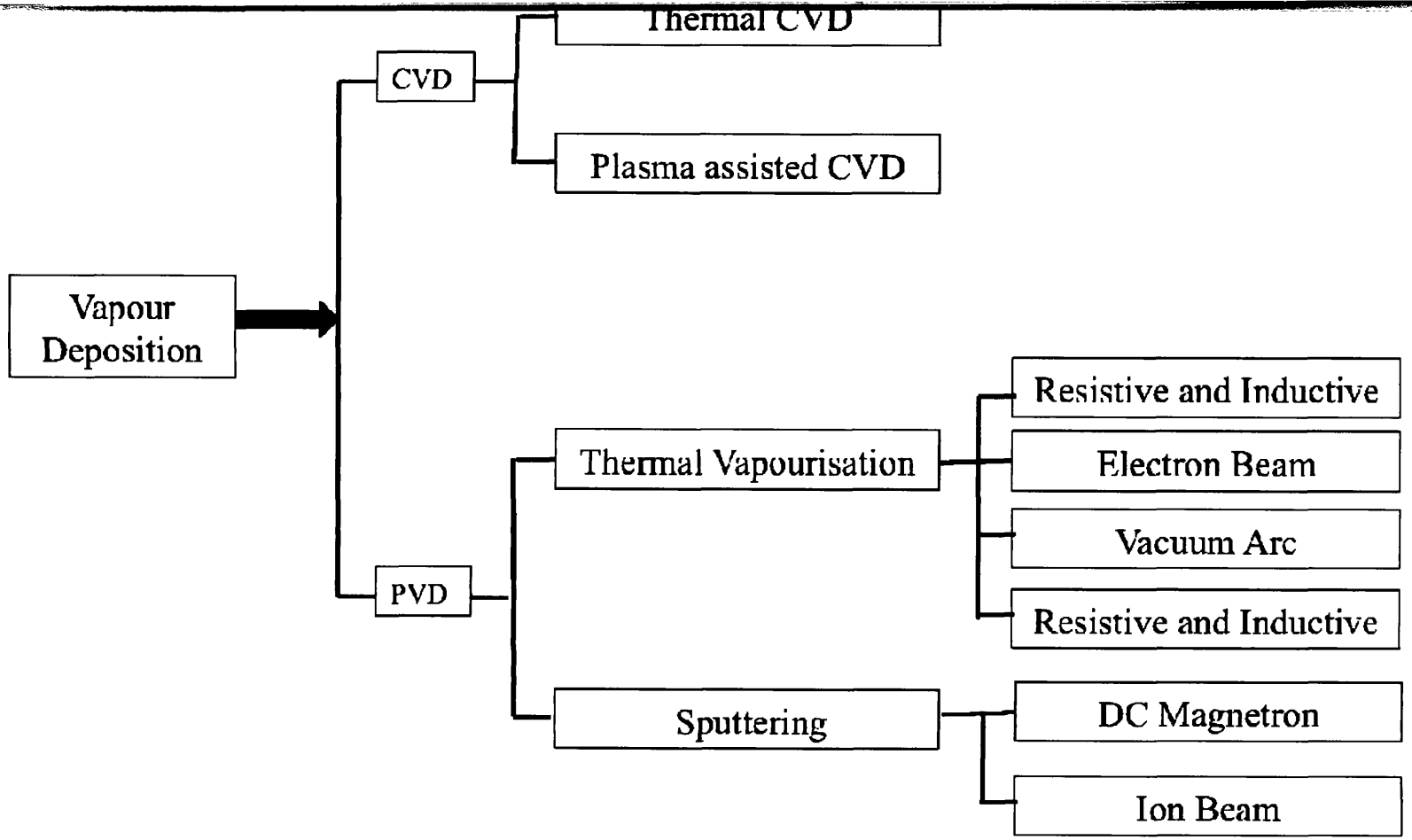

Fig 1.6: *A diagram of CVD and PVD processes and different types of thin film deposition of each [74].*

1.3.2.2.1 PVD Vapourisation Methods

One method of vapourising a target material is through the use of a thermal evaporation process. The process comprises of vaporising the target material in a vacuum within a pressure range of 10^{-5} and 10^{-9} Torr, through one of several types of thermal vapourisation techniques shown below:

- Resistive or inductive heating.
- Electron Beam heating.
- Vacuum arc vapourisation.
- Laser vapourisation.

Each method provides heat to a given target material and it is this that that excites the atoms within the material to become detached and enter in to the vapour phase.

1.3.2.2.1.1 Laser Vapourisation

Laser vapouration is mainly connected with small-scale depositions and the heat generated through focussing the laser beam on the surface of the target material allows atoms of the material to be vapourised. It has been reported that laser method is a good method of producing vapours of compound materials [126].

1.3.2.2.1.2 Vacuum Arc Vapourisation

Vacuum arc deposition utilises an anode and cathode that are arranged so that when a discharge is triggered between them, an arc is emitted, creating local melts in the surface of the target material and a vapour phase is created.

1.3.2.2.1.3 Electron Beam Vapourisation

The electron beam heating method of vapourisation consists of an energetic electron beam directed towards the surface of the target material. The beam of electrons is accelerated through electric fields typically in the range of 5 to 10kV. The target material is held in a crucible that is usually water-cooled. Temperatures exceeding 3000k may be achieved. Due to high energy bombardment the material heats up, melts and vapourises. The electron beam is usually produced through thermo-ionic emission of a tungsten filament. Reactions between the target material and the crucible lining are normally minimised as the beams are focused on the surface and the melt is local. Deposition rates of 60m/min can be achieved by electron beam processes on strip metal sheets of 300mm in width [75].

1.3.2.2.1.4 Resistive and Inductive Heating

Resistive heating vapourisation of target materials witnesses crucibles of the target material that are usually heated by radiation from metal filaments. However, radiation shields must be used to maximise efficiency as a small percentage of the emitted light is actually in the direction of the source. Inductive heating or radio frequency induction heating has some advantages over resistive heating. Part of the energy is coupled directly into the target metal, it is not necessary to produce temperatures higher than the vaporisation temperature for maintaining heat flow. Interactions between the target material and container walls are minimised. Energy efficiency is also better as radiation and conduction heat losses are lower. Disadvantages are that RF induction heating has greater costs and space requirements of the power supply.

1.3.2.2.1.5 Structure of Films Produced by Heating Vapourisation Techniques

The coating processes carried out by thermal vapourisation are said to produce a very porous film upon the substrate due to the fact that the thermally produced

particles have low energies in comparison with other vapourisation methods such as sputtering. Thermal vapouration processes are generally assisted by a plasma generated between substrates and source material. Substrate ions are accelerated towards the growing film surface and the impact creates a denser film deposition (ion plating). Ion beams can also be used instead of using plasma.

1.3.2.2.2 Sputtering Processes

The type of vaporisation method used utilised in this thesis was that of a sputtering process. Sputtering processes are achieved when the target material to be vaporized is bombarded with ions from a plasma as mentioned in section 1.3.2.2. The most common method used in technological and industrial applications is magnetron sputtering, realised through the generation of an Ar^+ plasma created under vacuum conditions.

1.3.2.2.2.1 Magnetron Sputtering

Magnetron sputtering is a state of the art technology for large area coating in both semi-continuous and continuous modes. Generally the process is used for coating glass with anti-reflection coatings, low emission coatings to prevent heat loss, for photovoltaic applications and for solar control coatings to prevent heating by solar radiation. Most of these applications require the use of oxide coatings with well-controlled thickness distribution.

However developments are under way and large area magnetron sputtering is a well-established deposition technique for industrial applications. Effort is being made to improve deposition rates through improved design of magnetic fields and cathode channels. Deposition rates as high as 20μm/min [64] have been reported, depending on the material being deposited.

1.3.2.2.2 Ion Beam and Ion Assisted Sputtering

Instead of producing a plasma in the vicinity of a target material, an ion beam can be used to carry out the same function by bombarding the surface and dislodging atoms to produce a vapour phase. This method of sputtering is called ion beam or ion-assisted sputtering deposition. Ions of gases such as Ar are formed can accelerated towards the surface of the target material. This method has found use for many different purposes, mainly for production of various environmentally stable dielectric multilayer products in instrument optics and ophthalmics [108]. It has however found applications in solar cells, electro-optical devices and flat panel displays [109]. Work reported also shows that ion beam sputtering can be used in conjunction with a target material that consists of 2 different materials. By focussing the ion beam on the interface between both materials, combinatorial deposition of the both materials can be achieved in order to produce a desired coating.

Ion-assisted processes may also be incorporated in the thermal vapourisation techniques explained earlier, in order to modify coating properties, and can be used as an alternative process to plasma assisted processes which are explained in section 1.3.2.2.3. Much evidence of the use of this technique can be found in the literature and example of which is detailed [108,110,111].

1.3.2.2.3 Plasma Assisted Processes

Plasma assisted PVD processes have been reported to produce hard coatings [107]. At high deposition rates like we see with EB evaporation, the condensation rate is also high, and as the energy of the impacting particles is relatively low the coating forms a porous columnar microstructure. To form a denser and harder structure the particles need more time and energy. The energy can be increased in two ways, by increasing the substrate temperature or by plasma activation. Changing the temperature of the substrate can be difficult as it may alter the properties of the substrate product. So plasma assisted Electron Beam was developed.

1.3.2.2.4 PVD Coating Process at Swansea University

Swansea University has recently installed and commissioned a PVD coating system called the Kurt J. Lesker PVD 75. The company has been manufacturing thin-film deposition systems for over 20 years, and is based in Pittsburg in the U.S. The unit is configured to suit a large range of deposition for small scale batch production. The system will be extremely useful for this project and will help build an understanding of the underfilm corrosion properties of thin metallic films, such as Al, deposited on iron. The process will also be suited to investigate the affects of thin metallic films incorporated into the manufacturing of laboratory sized DSCs with functionalised PVD layers as discussed in the proceeding sections. A whole range of experiments can be carried out on samples of many different types of depositions to gain an understanding of how the properties of the film relate to the efficiency of a typical cell.

The facility utilises magnetron sputtering techniques in order to deposit material. It also has the ability to clean the substrate before deposition through an ion source, the ability to produce a variable thickness of film across the substrate through the use of a sliding shutter and can also heat or cool the substrate. Figure 1.7 shows a picture of the inside of the deposition chamber.

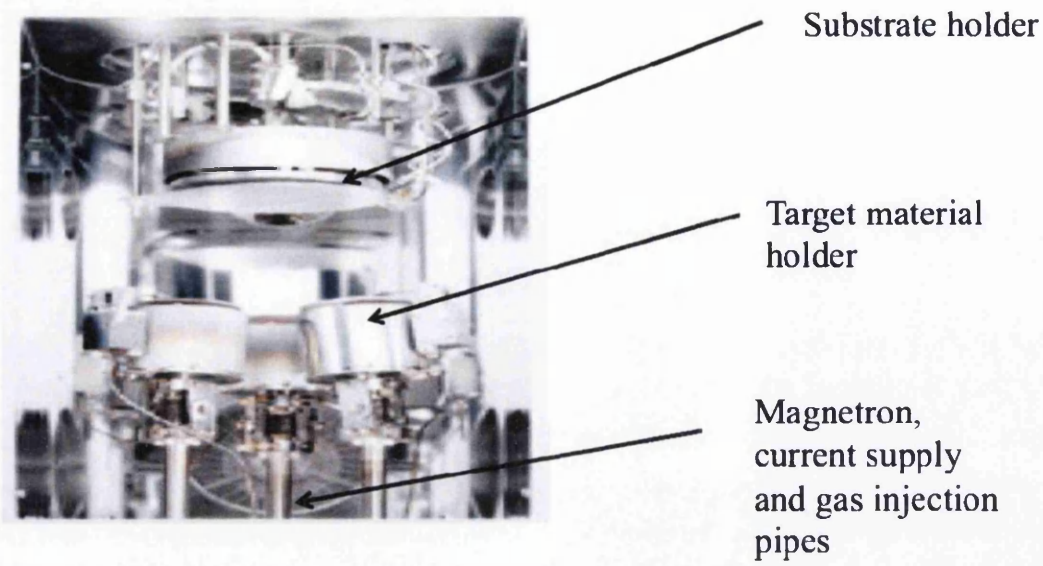

Figure 1.7: *A picture showing the inside of the deposition chamber, within the PVD unit, at Swansea University.*

1.3.2.2.5. Thin Film Growth of PVD Thin Films

Any thin film deposition method such as PVD processes allows the build up material on to a given substrate through the adhesion of vapourised target material atoms to the substrate surface, in order to produce a solid film [88].

Formation of the thin film takes place *via* nucleation and growth processes [88]. On impacting the substrate, an atom of target material will lose its velocity component normal to the surface and will become physically absorbed onto the substrate surface. This creates single atoms on the substrate (number density nl (t)) on a substrate with N_o sites per unit area, so that the single-atom concentration is (nl/N_o). These single atoms may then diffuse over the surface until they are entered into one of several processes.

These processes include re-vaporisation, nucleation of 2D or 3D clusters, capture by existing clusters, possibly diffusion into the substrate and capture at special (defect)

sites such as steps. On an ideally flat, 'inert' substrate, these last two processes would be excluded, though they may often be present in practice. The target material atoms are not in thermal equilibrium with the substrate initially and upon movement over the substrate surface, interaction causes them to form bigger clusters or nuclei. The nuclei are thermodynamically unstable and may tend to desorb in time depending on the deposition parameters such as substrate heating, deposition rate or vacuum pressure. If the deposition parameters are such that a cluster collides with other absorbed species before it desorbs, it will start to grow in size. After reaching a certain critical size the cluster will then become thermodynamically stable and the nucleation barrier will have been overcome. This stage is called nucleation.

The critical nuclei grow in number as well as in size until a saturation nucleation density is reached. The density and size depend on a number of parameters: energy of the impacting species, the rate of impingement, the activation energies of absorption, desorption, thermal diffusion, the temperature, the substrate surface topography, and the chemical nature of the substrate. Nuclei can grow parallel to the substrate as well as perpendicular to it by direct impingement of the incident species. At this stage in the process the grown nuclei are called islands.

The next stage in the process is called the coalescence stage. Small islands start coalescing with each other to try and reduce the surface area. Agglomeration is taking place, where bigger islands are being formed. This is enhanced by increasing the surface mobility of the absorbed species, i.e. by increasing the surface temperature of the substrate. Larger islands grow together leaving holes or channels of exposed substrate. The structure is sometimes seen as a porous network, and a completely continuous network is achieved by filling up the holes and channels.

1.3.2.2.5.1 Film microstructure

As discussed previously, it is known that the main influences on microstructure of vapour deposited films are the substrate temperature, the deposition rate and the energy of the impinging particles [88]. However the substrate temperature is limited by the maximum thermal load of the substrate material. Microstructures of magnetron sputtered zinc coatings have been described by Shedden *et al.* [86]. Economical issues often demand a very high deposition rate, especially in the strip coating industry. There are only a few PVD technologies that can reach a desired deposition rate of more than 20μm/min. The highest deposition rate is achieved by ion plating and sputtering process which produce deposition rates of between 0.02-20μm/min [64]. The only down side is that a high deposition rate has its disadvantages; a deposition rate greater than 1μm/s generally results in a columnar microstructure and a high porosity of the deposited film [85, 86]. Due to the fact that the energy of the vaporised particles is low, by use of plasma is the only way we can improve the microstructure of deposited film. A layer structure can be changed decisively by altering the substrate temperature or by action of plasmas during condensation [16]. From the work on magnetron sputtering by Shedden *et al.*, it may be possible to change the microstructure of the zinc film by altering various process parameters. The appearance is affected by the microstructure and it was found that a matte appearance could be achieved by decreasing the substrate bias voltage or a mirror like appearance could be achieved by increasing the bias. The matte finish was due to the presence of randomly oriented rough grains protruding from the densely packed columnar grains [15]. An example of this structure is shown in Figure 1.8. At higher bias's these protruding grains were attacked by ion bombardment and only a columnar grain persisted.

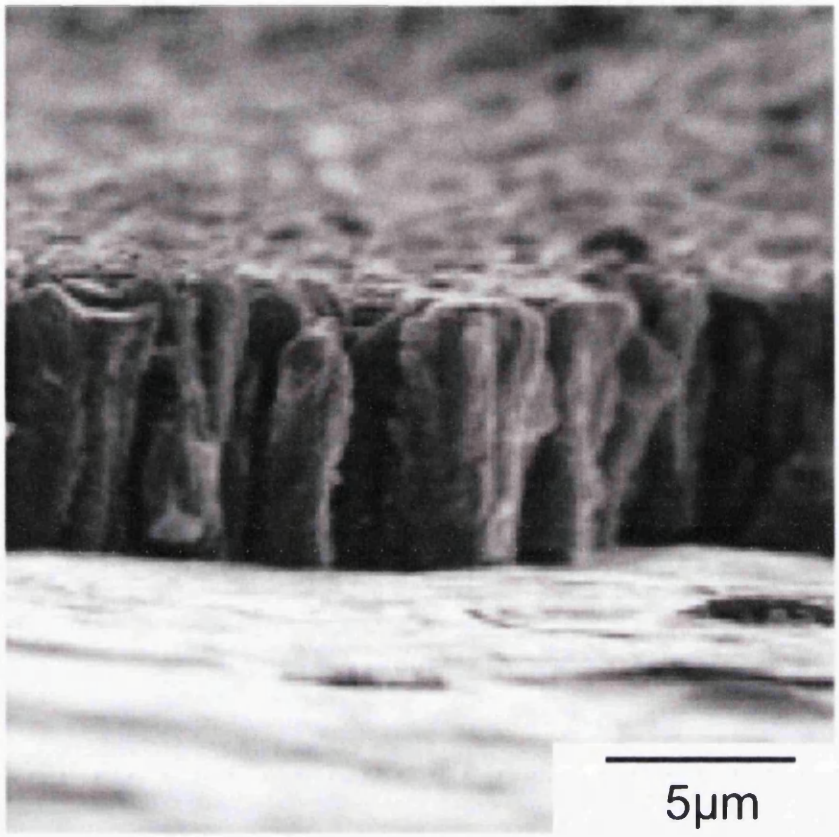

Figure 1.8: *An SEM image to show an example of a columnar coating structure of a material deposited by PVD [16].*

1.3.2.2.5.2 Plasma Activation

As mentioned in section 1.3.3.3.7, it is possible through the use of plasma-assisted or plasma activation processes, in order to produce harder and more dense film microstructure. At high deposition rates, the only way to produce a dense deposit of coating upon a substrate is by the use of plasma activation since substrate temperatures achievable otherwise are limited to 400 - 800ºC. In the 1970's CVD processes seemed to lead the way in being prime facilities for producing hard, dense and relatively thick coatings. However, since the 1980's plasma-assisted PVD techniques have become investigated more and more in the literature [112]. Reports here suggest that it is possible to create a microstructure that is comparable to CVD

through plasma assisted PVD techniques. Figure 1.9 shows a SEM image of a dense film microstructure achievable through plasma activation.

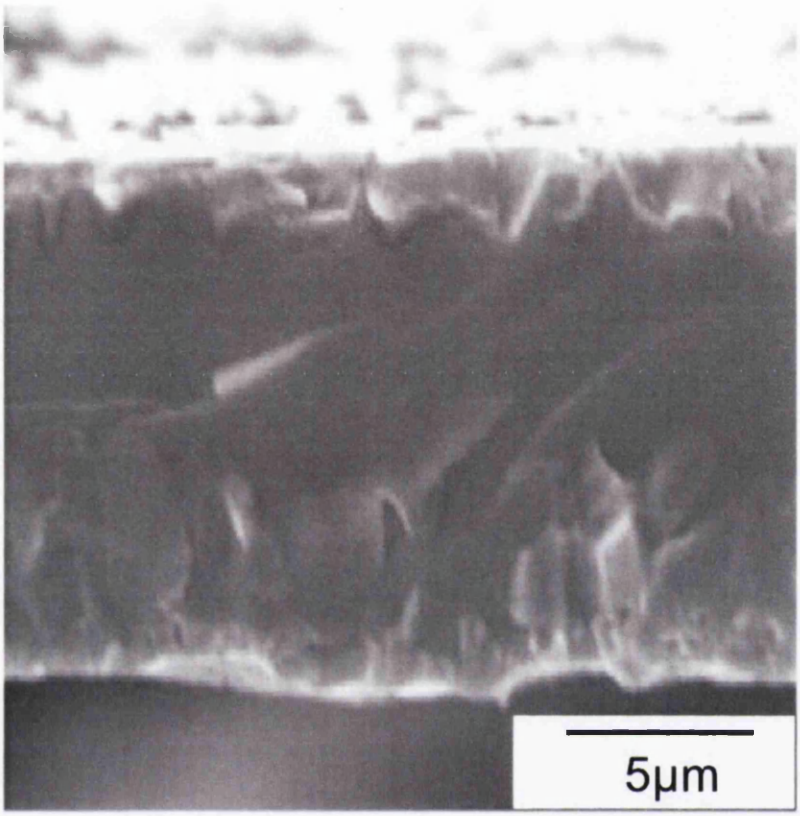

***Figure 1.9**: Dense coating structure [112]*

1.3.2.2.5.3 Surface Effects

The morphology of a deposited thin film can be affected by what are called shadowing effects. Figure 1.10 shows the effects of the surface roughness upon the distribution of the deposited film material and the film morphology. The direction in which the vapour is attacking the surface is a concern when looking at surface affects on thin films. A film builds up in a line of sight manner as mentioned earlier. At a defect in the surface, such as a surface bump, as witnessed on a rougher surface, the film will start building up on it's top side, leaving it's bottom side exposed (assuming that the vapour is entering at an angle normal to the surface). These

shadowing effects are greatly affected by larger sized defects or bumps on the surface. To put this into context when depositing thin films via PVD on to substrates for investigation during the work carried out in the thesis, it will be essential to take into account any defects or debris laying on the surface of the samples used, so cleaning procedures and polishing techniques shall be adopted.

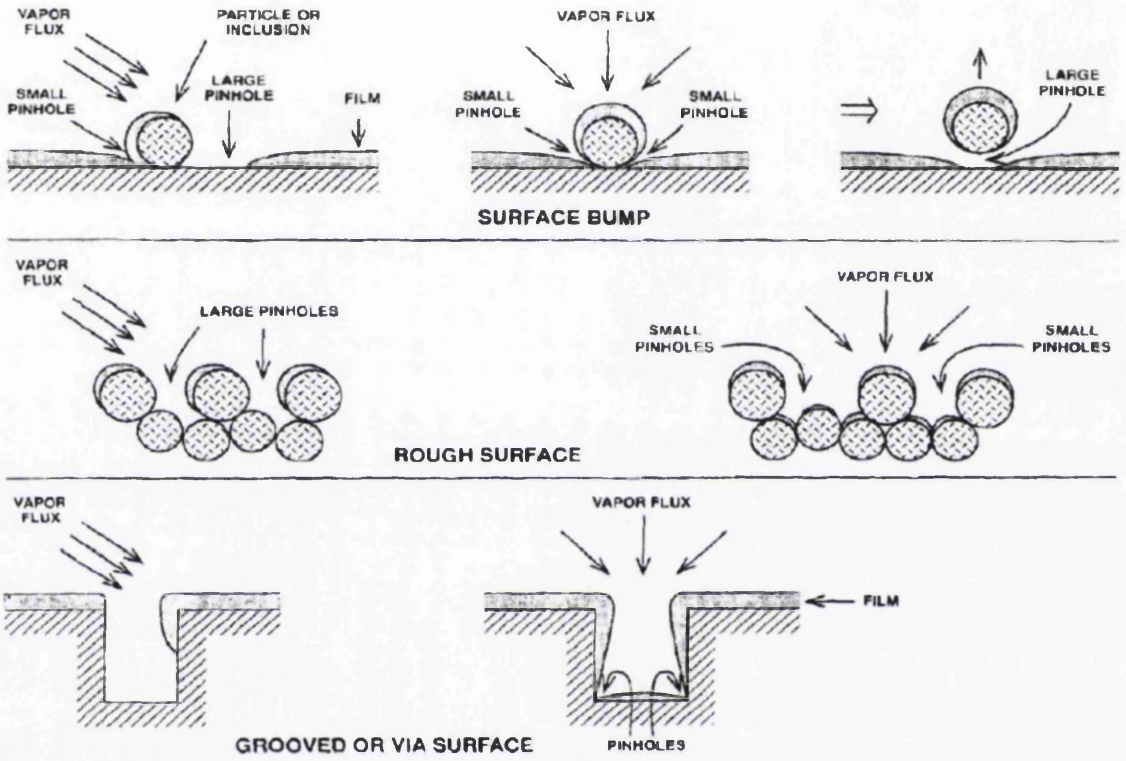

Figure 1.10. *A diagram to show how the type of surface affects the morphology of thin films deposited via vapour deposition processes.*

1.3.2.2.5.4 Adhesion of Thin Films

There are many properties related to both the substrate and the film that govern the adhesive nature of the two. These include stresses in the film, contamination, chemical nature between the film and the substrate and the microscopic topography

of the substrate. No intermetallic layers are formed between the substrate and the coating in the PVD process, the adhesion of the deposited species relies ultimately upon a mechanical bond with the substrate. Adhesion is usually better when the kinetic energy of the incident species is higher, when the absorption energy of the deposit is higher and when the initial nucleation density is also higher. Contaminants may cause the absorption energy to increase or decrease, and in turn may affect the adhesion. Milde *et al.* have alluded that well-adhering coatings on plastic films require a pre-treatment. Pre-treatments such as plasma etching and ion beam bombardment provide a purposeful method of removing contaminants or defects off the surface of the substrate prior to the application of the thin film [113].

1.3.2.3 CVD

Chemical vapour deposition is a process that has been in existence from the early part of the last century and is termed a mature technology [114]. A CVD coating differs from a PVD coating in that there are four stages carried out during deposition of material on to a substrate: formulation of the reactant vapour, transport of this vapour, chemical reaction between the vapour and the heated substrate and finally removal of by-products. These must be carried out in a contained vessel or reactor due to the volatile nature of the chemicals involved. The pressure within the vessel is either at or below atmospheric. The temperatures within the reactor can reach up to 1500°C depending on the specific process underway [82,115]. A general schematic of the CVD process is shown in Figure 1.11.

The early CVD processes had advantages over electroplating coating methods of the time in that the coverage for complex geometries or sharp edges was better. However its high level of toxic products was problematic, and is one of the main drawbacks of using this process on a large industrial scale.

Coating properties produced by CVD are dependent on the materials used, the deposition temperature, the pressure within the vessel, the type and flow rate of the

carrier gas. A very wide range of materials can be deposited using this technique ranging from nickel and chrome to the refractory type metals. The latter are used extensively with this process to improve the mechanical, thermodynamic or electrical properties of a substrate. TiN and TiC have been used extensively in the manufacture of cutting tools and can increase wear resistance of a D3 tool steel by up to 24% [116,117]. In the case of TiN CVD coatings the hardness is affected by the deposition temperature, to a large degree, with hardness increasing with higher temperatures [118].

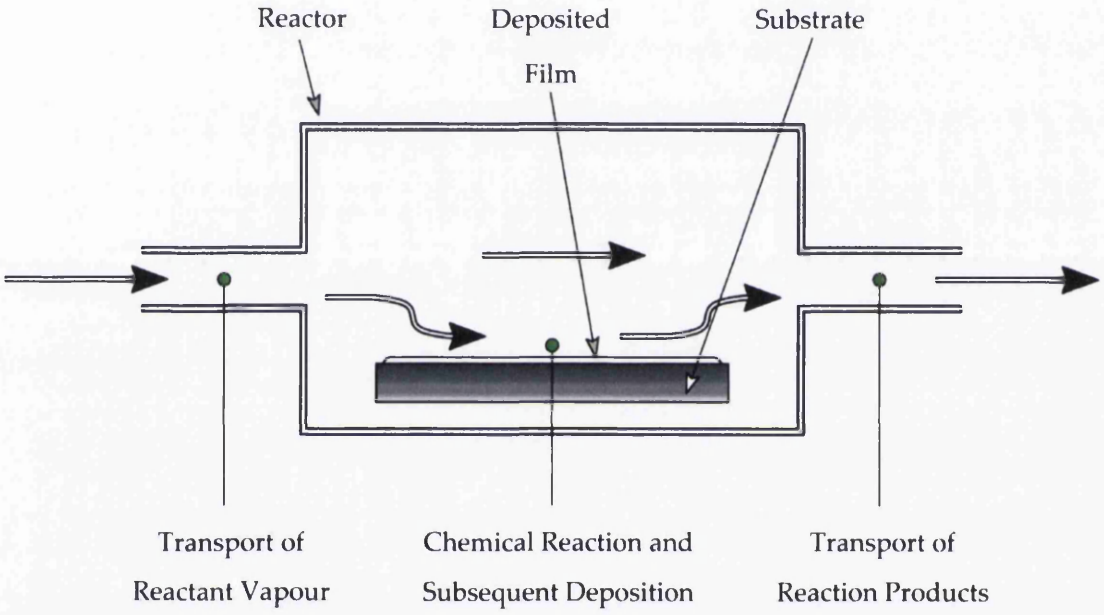

Figure 1.11: *A schematic of a CVD Process*

1.3.2.3.1 CVD Applications

CVD has applications across a wide range of industries such as. Coatings for a variety of applications such as wear resistance, corrosion resistance, high temperature protection, erosion protection and combinations thereof (small scale). It has also found use in the production of semiconductors and related devices, as well as integrated circuits, sensors and optoelectronic devices. The process is less

economical than PVD due to the high temperatures used during the process. This is one reason why CVD technology would not be suitable for large area coating in a continuous industrialised process. There has been no literature found where this process has been used for coating strip products. The chemicals used in the process are also extremely hazardous, and in large quantities within a coating plant will not be accepted by health and safety regulations.

1.3.2.4. PVD Scale Up Potential and Dynamic Deposition Rates

Any PVD coating facility for strip product must allow a coating width of up to 2m. In order for the process to be profitable the velocity at which the strip is moving during the coating procedure is also of high importance. Essentially time is money and the more throughput that can be achieved in a set interval of time means increased profit. So, in turn this impinges on the rate of deposition that is achieved by the evaporation method that has been chosen to produce the vapour.

It is obvious, that when the speed of strip is higher then the thickness of the coating is going to be less. This means that the coating thickness is inversely proportional to the strip speed:

$$T = R_{dyn}/V \qquad (1.5)$$

Where T is the thickness of the deposited layer, V is the speed and R_{dyn} is the dynamic deposition rate. This means that if a 2μm layer of zinc is required upon a strip substrate at a speed of 400m/min, then the rate of deposition will need to be around 800μm/m or 13.3μm/sec. The assumption is that the deposition along the length of the strip is homogeneous. Currently as reported in the preceding sections, on a laboratory scale deposition rates of this kind are impossible. For these deposition rates to be realised on a large-scale process, much consideration should be made towards the feasibility of such a process.

1.3.3 Solar Cell Technology

1.3.3.1 Introduction

This section of the introduction to this thesis focuses on dye-sensitised solar cell technology and reviews developments that have been made regarding industrialisation and commercialisation. It is therefore essential at this point to discuss the production and operation of such technology. This section also explains the scale up potential of incorporating thin film technology into the industrialisation of dye-sensitised solar cells. There is also a synopsis of any drawbacks that may arise as a consequence of the industrialisation process.

1.3.3.2 Organic Photovoltaics – Dye Sensitized Solar Cells (DSC)

The DSC differs from other types of solar cells by its basic construction and operation. A typical DSC configuration incorporates a number of different mediums in harmony. Excited electrons are produced within a nanoporous TiO_2 film which has been sensitised with a layer of visible light absorbing dye and penetrated with a redox electrolyte [93]. The TiO_2-electrolyte network is sandwiched between two conductive substrates that also work as current collectors. The opposite substrate to the TiO_2 layer, the counter electrode, is coated with a material capable of catalysing the redox reaction in the electrolyte, such as Pt or C. A diagram showing the operation of a DSC is shown in Figure 1.12.

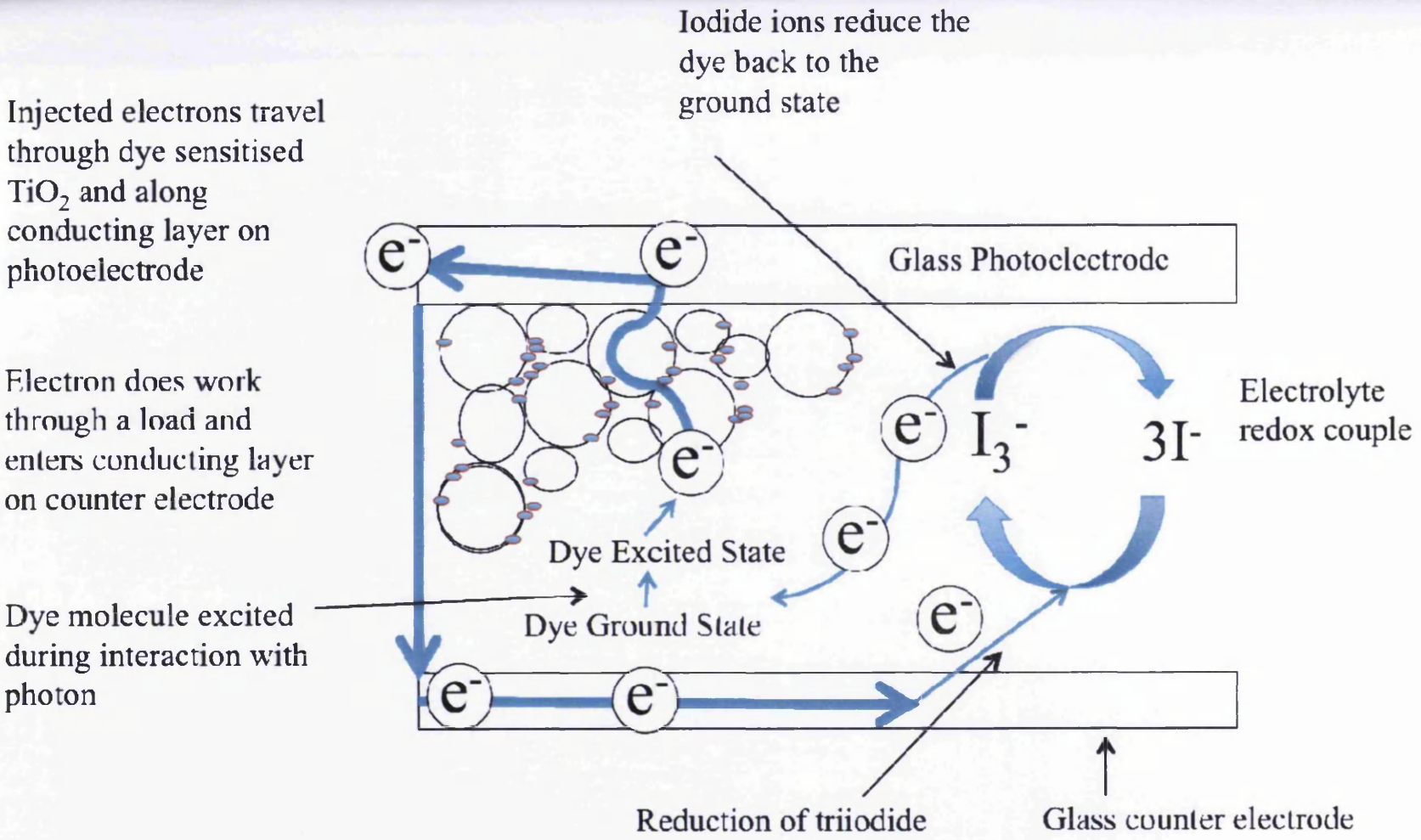

Figure 1.12: *The operation of a DSC*

Photon absorption induces an electron injection to the TiO_2. After injection, electrons diffuse in the nanocrystalline TiO_2 network to the conductive coating of the photoelectrode substrate, which is attached to the TiO_2 network, from which they can be transferred to an external circuit. There exist various models for the electron diffusion in the TiO_2 film but thermally activated trapping/detrapping mechanism along localised energy levels below the TiO_2 conduction band edge seems the most realistic one, in the light of experimental evidence [89-92]. The electron injection to the TiO_2 leaves the dye molecule in an oxidised state. In order for current generation to continue, the dye must be reduced back to its ground state. The redox couple in the electrolyte is responsible for reducing the dye molecules back to the ground state. The most commonly used redox couple, and the one that gives the best cell efficiencies when combined with TiO_2, is iodide/triiodide [119]. An oxidized dye molecule receives an electron from the iodide ions present, which, in turn, become oxidised, to triiodide in the process. The triiodide ions then diffuse to the counter electrode, where they become reduced back to iodide by the electrons returning from the external load. Thus, the cell operation is based on consecutive reduction/oxidation cycles. The most often used counter electrode catalyst for the triiodide/iodide reduction reaction is platinum.

Of all the sequences involved in creating a successful DSC, this thesis concentrates on the photoelectrode system. This work concentrates on investigating materials in which DSC technology can be fabricated. The materials, preferentially of a metallic species, will act as a substrate for the electrode contacts of a DSC. The materials must show to be compatible with the various stages of production and operation of DSC technology that will be discussed throughout the thesis. The next section looks at materials used in DSC technology.

1.3.3.3 DSC basic materials

1.3.3.3.1 Metallic Substrates

For efficient transfer of the electrical energy produced from light incident upon a dye-sensitised solar cell, it is necessary that the titanium dioxide semiconductor material is in contact with a conducting layer at the photoeelectrode (figure 1.13). Work within this thesis investigates the possibility of vacuum metallising metallic and organic coated steel substrates, to act as electrical conducting layers for electron transport; with a range of metallic elements which will not only transport electrons but also withstand the aggression of the redox electrolyte should they come in contact with one another by permeation through the porous titania layer.

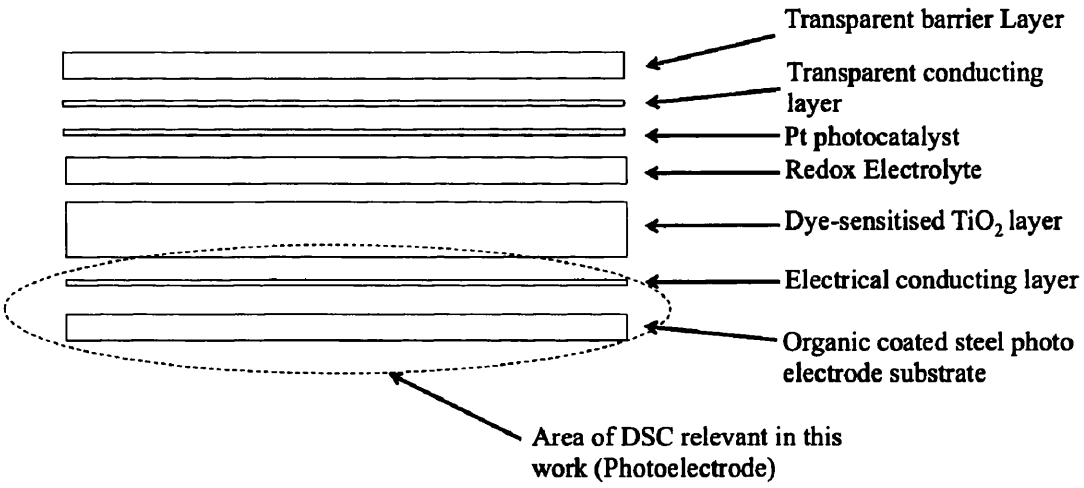

Figure 1.13: *A schematic showing the various layers of a DSC, in reverse illumination, fabricated on an organic coated steel product. The photoelectrode has been circled to emphasis the area of investigation. The diagram is not to scale.*

In this setup, when DSC technology is fabricated on metallic substrates, light has to travel through more layers, as opposed to when the TiO_2 network is deposited onto a glass electrode cell as shown in Figure 1.12.

There are a number of requirements that a DSC photoelectrode substrate, shown within the dashed line in Figure 1.13, must possess. Firstly, electrical conductivity must be good in order to ensure electrical losses are minimum in order to achieve maximum output from a cell. Due to the high processing temperatures experienced during the production of DSCs, namely the titania treatment step, the substrate material must have the ability to withstand high temperatures of up to 500°C. Another important feature is the ability to prevent impurities such as water and oxygen from entering into the cell. The traditional approach is to build the DSC on transparent conducting oxide (TCO) coated glass sheets. The most often used TCOs are fluorine- and indium-doped tin oxides, whose sheet resistances are around 10 Ω/□ [119,120]. Whilst glass is obviously an effective barrier towards water and oxygen penetration into the cell, its disadvantages are fragility, rigidity, heavy weight and high price [121].

Alternative substrate materials such as plastic foils and metal sheets overcome most of the glass' problems. Conductive plastics, like ITO-PET and ITO-PEN (indium-doped tin oxide coated polyethylenenaphtalate), used for counter electrodes, are light weight and flexible, whereas metals are also mechanically robust, cheap, and their electrical conductivity is superior compared to most other substrate materials [121]. The last factor plays a crucial role in cell size up-scaling, since the main part of the total ohmic losses in the cell are due to lateral resistance of the substrate surface. It has also been noticed that substrate-mediated electron recombination, is lower from stainless steel than from glass [89]. Disadvantages of plastics include low temperature tolerance, max. 150 – 160°C, for ITO-PET higher sheet resistance, around 60 Ω/□, and uncertainties considering the oxygen and water penetration.

For metals, the main problem is the traditionally used, iodine-containing electrolyte. Triiodide ions are corrosive, and thus far only stainless steel and titanium have shown enough chemical stability in the iodine electrolyte to be successfully employed as DSC substrates [93-101]. Long-term stability of metal-based cells is still unknown and requires further studies before this DSC type can be transferred to large scale manufacturing hence the reason for carrying out the work detailed in this

thesis. However, the main push behind the alternative substrate research is the flexibility of both the plastic and metal substrates that may enable continuous roll-to-roll type manufacturing of the DSC, potentially leading to high volume production of low cost solar cells with wide variety of applications.

The vast majority of research thus far has concentrated on DSCs constructed using indium or fluorine doped tin oxide as a conducting layer coated on a glass substrate. As far as metal based cells are concerned, a patent application was made for the use of zinc and titanium foils to fill the dual role of supporting and conducting substrates for ZnO and TiO_2 photoelectrodes respectively [102]. Two papers have been written, one reporting on the use of a TiO_2 coated titanium sheet [103] and the other reporting a 4.2% efficient (100 $mWcm^{-2}$) flexible dye-sensitised solar cell using a stainless steel substrate [104].

1.3.3.3.2 Novel Thin films for Dye -Sensitized Solar Cells

Due to a major interest in the fabrication of dye-sensitised solar cells on to metallic strip substrates, as detailed in Chapter 2, investigations are being made into the feasibility of incorporating thin film technology into the manufacturing process. Using thin metallic films as opposed to bulk metallic substrates as cell collector electrodes, may offer substantial reduction in material costs. These films may be vapour deposited onto less expensive flexible substrates at thicknesses ranging from nanometers to microns. There are a number constraints issued upon the metallic film-substrate system; it must have the ability to conduct electrons through the cell circuitry, it must chemically withstand the aggression of the DSC electrolyte and any oxide formed must be compatible with that of the TiO_2 semiconductor for efficient charge transfer at the semiconductor-metallic film interface.

There is no evidence in the literature to suggest that metallic vapour deposition of cell photo electrodes has been used in manufacturing of DSC products, and part of

the investigation work in this thesis is aimed at gaining a better understanding of this process.

Vapour deposition techniques can also be used in generating the porous nanocrystalline TiO_2 semiconductor layer. It has been shown that magnetron sputtering techniques have found application within the DSC field, in a series of papers by Gomez *et al.* [77-81], and it can be seen that titania layers can be deposited on to photoelectrode substrates by reactive sputtering of titanium with oxygen, as opposed to titania paste deposition via various printing methods. It has been reported that cells with efficiencies as high as 7% have been produced using titania layers applied through sputtering. Apart from this, to the best of my knowledge, there is no other evidence of thin metallic film technology being used as electrodes for DSCs.

1.3.3.4 DSC Scale-up Potential

Many institutes and companies have developed commercialisation research on the up-scaling of DSC technology. Toin University of Yokohama, Japan, have fabricated full-plastic DSC modules based on low-temperature coating techniques of TiO_2 photoelectrodes [122]. Peccell Technologies, Japan, and Konarka US, have practiced the utility and commercialisation of a study on flexible DSC modules on polymer substrates [123,124]. There are reports that a company called STI completed the first pilot-plant production of DSCs. They produced a DSC roof of $200m^2$ in Newcastle that showed the potential of DSC commercialisation [125].

The possibility of industrialising DSC technology on a large area scale has also been reviewed extensively [105]. G. Hashmi *et al.* have reported that to reduce costs of producing DSCs in a continuous roll-to-roll process, the use of flexible metal and plastic sheets must be adopted. They suggest that Al sheet may be used as substrates and alternative conducting layers for plastics are needed. Work in Chapter 3 of this thesis concentrates on this very idea. It has also been reported that lower processing

temperatures must be realised in order to reduce large-scale industrialisation costs. Work in this review alludes to the fact that low temperature processes and materials have been developed and have produced highly efficient cells [106]. They propose concern regarding the nature of the redox electrolyte used in DSCs. With the corrosive nature of the electrolyte commonly employed in this technology, alternative electrolyte systems may be needed and optimised. Cell longevity and stability is also critical for large-scale industrialisation and needs to be a main focus incorporated into studies carried out.

As far as industrialisation of DSC technology with an incorporated PVD process, for depositing thin metallic films as electronic conducting layers, there is no evidence of research in the literature of work in this area. Work in Chapters 5 and 6 of this thesis lead on from corrosion investigations relating to suitable metals for use as DSC substrates, and sets out to investigate the possibility of producing DSCs on such thin film metallic layers.

1.3.3.3 DSC Electrolyte and Corrosion mechanisms

The electrolyte used in the production of DSCs can vary significantly in its makeup related to inclusion of additives. The most basic redox couple consists of only lithium iodide and iodine dissolved in 3-methoxypropionitrile or acetonitrile. 4-tert-butylpyridine (TBP) or N-methylbenzimidazole are also widely added to the electrolyte and said to significantly improve open circuit voltage (Voc) and cell efficiency due to their ability in reducing back reaction effects by blocking the triiodide molecule from interacting with the titania surface [136]. Additions of guanidinium thiocyanate are used to enhance ion transport efficiency [137], and iodine-based ionic liquids such as 1- propyl-3-methylimidazolium iodide (PMII) are added to reduce viscosity and in turn enhance ion mobility within the electrolyte.

Various species of metal substrate materials when in contact with the non aqueous I_3^- /I^- based DSC electrolyte explained in Chapter 1 and 2, were investigated. However,

with production and material costs a major issue, the choice of substrate has to be economically viable in order to make the final product feasible for large-scale commercialisation [127]. Unfortunately, DSC electrolyte is an aggressive iodide-containing medium, and is capable of depassivating an oxide covered metal surface (in an analogous manner to chloride ions) and the reduction of triiodide providing a facile cathodic reaction to couple with anodic metal dissolution. When the reduction of the triiodide into iodide ions occurs, the result is a loss of the brown colouration of the solution due to the generation of colourless I^- ions according to the following reaction.

$$I_3^- + 2e^- \rightarrow 3I^- \qquad (1.6)$$

To date relatively little research has been carried out into the corrosion mechanisms of metal substrates in contact with the constituents of DSC electrolyte. Toivola *et al.* have investigated DSCs fabricated on metal substrates as photoelectrodes, studying the outcome when DSC electrolyte is placed contact with zinc coated steel products, stainless steel and mild steel, through both immersion and encapsulation tests, using both visual examination and atomic absorption spectroscopic analysis [74,128,129]. It was reported that zinc reacted quickly, while stainless steel, and perhaps more controversially, mild steel remained inert for many months in the presence of the electrolyte. Work by Miettunen has shown that titanium, stainless steel and Inconel (Ni-Cr) alloys do not seen to corrode in the presence of the redox electrolyte used as photoelectrodes within a cell set up [130–132]. Fang *et al.* have also studied the possibility of using stainless steel, nickel, aluminium, copper, of various purities, as well as various conducting polymers for use as counter electrodes. They found that aluminium and copper became degraded whereas stainless steel and nickel remained stable [133, 134]. These findings were supported by tests consisting of visual inspection and elemental analysis of the electrolyte. Apart from the inherent degradation of both metal substrate and DSC electrolyte by corrosion, metal ion contamination may also cause surface contamination of the TiO_2 layer, to the detriment of DSC performance. Iron oxide mixed in the porous TiO_2 layer has been shown to significantly decrease the photocurrent 132, 135], therefore raising issues about the compatibility of ferrous-based electrode substrates with the TiO_2, especially if some corrosion takes place.

However, despite the reported work described above, after a long search of the available literature, no convenient quantitative method of studying the time dependent interaction of metallic substrates with DSC electrolyte currently exists.

1.4 Summary

From conducting a literature review it is evident that technology has been development for preventing underfilm corrosion of organic coated metallic substrates. What is not known is the potential of PVD thin films to act as direct replacements for these technologies. It is clear that current technologies have drawbacks associated with them such as negative impacts on the environment. Hence, the work explained in Chapter 3, studies the possibility of using PVD films of Al to halt the process of corrosion-driven organic polymer coatings on iron.

With regards to dye-sensitised solar cells, limited quantitative assessment of the corrosion mechanisms involved, during industrialisation and commercialisation of the technology on to strip metal products, has been found. It is not exactly known what metals are suitable to act as photoelectrode substrates for DSC technology up-scaling, nor is there a great deal of evidence relating to the use of PVD thin film layers, to act as corrosion resistant and conducting layers within the fabrication of industrialised DSC technology. Chapter 4, 5 and 6 study these unknown quantities in order to investigate the possibilities of producing DSC technology fabricated on metallic based substrates.

1.5 References

1. B. Parida, S. Iniyan, R. Goic, "A review of photovoltaic technologies", *Renewable and Sustainable Energy Reviews*, 2011, 15, p. 1625-1636.
2. M. Gratzel, "Dye-sensitized solar cells", *Journal of Photochemistry and Photobiology C: Photochemistry Reviews*", 2003, 4, p. 145-153.
3. Md. K. Nazeeruddin, E. Baranoff, M. Gratzel, "Dye-sensitized solar cells: A brief overview", *Solar Energy*, 2011, 85, p. 1172-1178.
4. P. Sommeling, M. de Wild-Scholten, T. Veltkamp, J. Krohn, "Life cycle assessment and testing of dye solar cells, 2nd Dye Solar Cell Industrialisation Conference, St. Gallen, Switzerland, 11-13 September, 2007.
5. H. Desilvestro, M. Bertoz, Sylvia Tulloch and G. Tulloch, "Packaging, scale-up and commercialization of dye solar cells", in Dye-sensitized solar cells, K. Kalyanasundaram, Editor, p. 209, CRC Press-Taylor & Francis Group, Boca Raton (2010).
6. H.N. McMurray and G. Williams, "2.14 Under Film/Coating Corrosion" in Corrosion in liquids – Vol 2: Types of Corrosion in Liquids, Shreir's Corrosion, 4th Edition, T.A.J. Richardson (Ed.), Elsevier Ltd, (2009), p. 988-1004.
7. H. J. Leidheiser, "Cathodic delamination of polybutadiene from steel - A review", *Adhesion Science and Technology*, 1987, 1, p. 79-98.
8. D. Greenfield, D. J. Scantlebury, "The Protective Action of Organic Coatings on Steel: A Review", *Journal of Corrosion Science Engineering*, 2000, 2.
9. G. Grundmeyer, A. Simeos, in Encyclopaedia of Electrochemistry, A. J. Bard, M. Stratmann, J. Frankel, Eds, Wiley-VCH, New York, 2003, Vol.5, p. 500-566.
10. K. Ogle, A. Simeos, in Encyclopaedia of Electrochemistry, A. J. Bard, M. Stratmann, J. Frankel, Eds, Wiley-VCH, New York, 2003, Vol.4, p. 460-499.
11. T. Skoulikidis, A. Ragoussis, "Diffusion of iron ions through protective coatings on steel", *Corrosion*, 1992, 48, p. 666-670.

12. W. Furbeth, M. Stratmann, "Scanning Kelvinprobe investigations on the delamination of polymeric coatings from metallic surfaces", *Progress in Organic Coatings*, 2000, 39, p. 23-29.

13. E. L. Koehler, "Technical Note: The mechanism of cathodic disbondment of protective organic coatings: aqueous displacement at elevated pH", *Corrosion*, 1984, 40, p. 5-8.

14. J. D. B Sharman, J. M. Sykes, T. Handyside, "Cathodic disbonding of chlorinated rubber coatings from steel", *Corrosion Science*, 1993, 35, 1375-1383.

15. J. W. Lorimer, Ed, Solubility Data Series, Alkaline Earth Hydroxides in Water and Aqueous Solutions, IUPAC, Pergammon Press, Oxford, 1992, Vol. 52.

16. J. J. Ritter, J. Kruger, in Corrosion Control by Organic Coatings, H. Leidheiser, Ed, NACE, Houston, 1981, p. 28.

17. H. Leidheiser, L. Igetoft, W. Wang, "The mechanism for the cathodic delamination of organic coatings from a metal surface", *Progress in Organic Coatings*, 1983, 11, p. 19-40.

18. H. Leidheiser, W. Wang, "Some substrate and environmental influences on the cathodic delamination of organic coatings", *Journal of Coating Technology*, 1981, 53, p. 77-84.

19. J. F. Watts, J. E. Castle, "The application of x-ray photoelectron spectroscopy to the study of polymer-to-metal adhesion", *Journal of Material Science*, 1984, 19, p. 2259-2272.

20. A. Leng, H. Streckel, M. Stratmann, "The delamination of polymeric coatings from steel. Part 1: Calibration of the Kelvinprobe and basic delamination mechanism", *Corrosion Science*, 1999, 41, p. 547-578.

21. A. Leng, H. Streckel, M. Stratmann, "The delamination of polymeric coatings from steel. Part 2: First stage of delamination, effect of type and concentration of cations on delamination, chemical analysis of the interface", *Corrosion Science*, 1999, 41, p. 579-597.

22. A. Leng, H. Streckel, K. Hoffmann, M. Stratmann, "The delamination of polymeric coatings from steel Part 3: Effect of the oxygen partial pressure on the delamination reaction and current distribution at the metal/polymer interface", *Corrosion Science*, 1999, 41, p. 599-620.

23. H. N. McMurray, D. A. Worsley, "Scanning electrochemical techniques for the study of localised metallic corrosion", *Research in Chemical Kinetics*, 1997, 4, p. 149.

24. M. Stratmann, "The investigation of the corrosion properties of metals, covered with adsorbed electrolyte layers—A new experimental technique", *Corrosion Science*, 1987, 27, p. 869-872.

25. A. Leng, M. Stratmann, "The inhibition of the atmospheric corrosion of iron by vapour-phase-inhibitors", *Corrosion Science*, 1993, 34, p. 1657-1683.

26. M. Stratmann, H. Streckel and R. Feser, "A new technique able to measure directly the delamination of organic polymer films", *Corrosion Science*, 1991,32, p. 467-470.

27. M. Stratmann, R. Feser and A. Leng "Corrosion protection by organic films". *Electrochimica Acta*, 1994, 39, p. 1207-1214.

28. W. Funke, *Journal of the Oil and Colour Chemists' Association*, 1979, 62, p. 63.

29. W. Funke, "The role of adhesion in corrosion protection by organic coatings", *Journal of Oil and Colour Chemists Association*, 1985, 68, p. 229-232.

30. W. Funke, H. Leidheiser, *Journal of the Oil and Colour Chemists' Association*, 1987, 70, p. 121.

31. J. Marsh, Scantlebury, S. B. Lyon, in Surfaced Engineering: Fundamentals of Coatings, P. K. Datta, J. S. Gray, Eds, Royal Society of Chemistry, Cambridge, 1993, Vol.1, p. 568.

32. A. Sabata, W. J. Van Ooij, R. J. Koch, "The interphase in painted metals pretreated by functional silanes" *Journal of Adhesion Science Technology*, 1993, 7, p. 1153-1170.

33. J. Marsh, Scantlebury, S. B. Lyon, "The effect of surface/primer treatments on the performance of alkyd coated steel", *Corrosion Science*, 2001,43, p. 829-852.

34. M. K. Harun, J. Marsh, S. B. Lyon, "The effect of surface modification on the cathodic disbondment rate of epoxy and alkyd coatings", *Progress in Organic Coatings*, 2005, 54, p. 317-321.

35. I. Suzuki, Corrosion Resistant Coating Technology, Marcel Dekker, New York, 1989, p. 167-205.

36. G. Klimow, N. Fink, G. Grundmeier, "Electrochemical studies of the inhibition of the cathodic delamination of organically coated galvanised steel by thin conversion films", *Electrochemica Acta*, 2007, 53, p. 1290-1299.

37. G. Williams, H. N. McMurray, "Chromate inhibition of corrosion driven organic coating delamination studied using a scanning kelvin probe technique", *Journal of the Electrochemistry Society*, 2001, 148, p. B377-B385.

38. B. Wessling, "Passivation of metals by coating with polyaniline – corrosion potential shift and morphological changes", *Advanced Materials*, 1994, 6, p. 226-228.

39. B. Wessling, "Scientific and commercial breakthrough for organic metals" *Synthetic Materials*, 1997, 85, p. 1313-1318.

40. P. J. Kinlen, Y. Ding, D. C. Silverman, ""Corrosion Protection Using Polyaniline Coating Formulations", *Synthetic Materials*, 1997, 85, p. 1327.

41. M. C. Bernard, A. Hugot-Le Goff, S. Joiret, N. N. Ginh, N. N. Toan, "Polyanaline layer for iron protection in sulphate medium", *Journal of the Electrochemical Society*, 1999, 146, 995-998.

42. M. Galkowski, M. A. Malik, P. J. Kulesza, H. Bala, K. Miecznikowsk, R. Wlodarczyk, L. Adamczyk, M. Chojak, "Protection of steel against corrosion in aggressive medium by surface modification with multilayer polyaniline – based composite film", *Journal of the Electrochemical Society*, 2003, 150, p. B249-B253.

43. A. Talo, O. Forsen, S. Ylasaari, "Corrosion protective polyaniline epoxy blend coatings on mild steel", *Synthetic Materials*, 1999, 102, p. 1394-1395.

44. A. B. Kaiser, C. J. Liu, P. W. Gilberd, B. Chapman, N. T. Kemp, B. Wessling, A. C. Partidge, W. T. Smith, J. S. Shapiro, "Comparison of electronic transport in polyaniline and polypyrrole", *Synthetic Meterials*, 1997, 84, p. 699-702.

45. D. E. Tallman, G. M. Spinks, A. J. Dominis, G. G. Wallace, ""Electroactive Conducting Polymers for Corrosion Control. Part 1. General Introduction and a Review of Non-Ferrous Metals," *Journal of Solid State Electrochemistry*, 2002, 6, p. 73-84.

46. G. M. Spinks, A. J. Dominis, G. G. Wallace, D. E. Tallman, "Electroactive Conducting Polymers for Corrosion Control. Part 2. Ferrous Metals," *Journal of Solid State Electrochemistry*, 2002, 6, p. 85-100.

47. F. Kohlrausch, Practische Physik, 2 (1968) 320.

48. M. Stratmann, "The investigation of the corrosion properties of metals, covered with adsorbed electrolyte layers—A new experimental technique", *Corrosion Science*, 1987, 27, p. 869-872.

49. K. Doblhofer, M. Cappadonia, "Calibration of the kelvin vibrator for measurements of electronic work functions in a humid atmosphere", *Journal of Electroanalytical Chemistry*, 1989, 243, p. 337-342.

50. S. Yee, R.A. Oriani, M. Stratmann, "Application of a Kelvin Microprobe to the Corrosion of Metals in Humid Atmospheres", *Journal of the Electrochemical Society*, 1991, 128, p. 55-61.

51. M. Stratmann, H. Streckel, "On the atmospheric corrosion of metals which are covered with thin electrolyte layers—I. Verification of the experimental technique", *Corrosion Science*, 1990, 30, p. 681-696.

52. M. Stratmann, H. Streckel, "On the atmospheric corrosion of metals which are covered with thin electrolyte layers—II. Experimental results",*Corrosion Science*, 1990, 30, p. 697-714.

53. M. Stratmann, H. Streckel, K.T. Kim, S. Crockett, "On the atmospheric corrosion of metals which are covered with thin electrolyte layers-iii. the measurement of polarisation curves on metal surfaces which are covered by thin electrolyte layers", *Corrosion Science*, 1990, 30, p. 715-734.

54. A. Leng, M. Stratmann, "The inhibition of the atmospheric corrosion of iron by vapour-phase-inhibitors", *Corrosion Science*, 1993, 34, p. 1657

55. M. Stratmann, H. Streckel, R. Feser, "A new technique able to measure directly the delamination of organic polymer films", *Corrosion Science*, 1991, 32, p. 467-470.

56. M. Stratmann, H. Streckel, *Werkstoffe und Korrosion*, 1992, 43, p. 316.

57. M. Stratmann, M. Wolpers, H. Streckel, R. Feser, "Use of a Scanning□Kelvinprobe in the Investigation of Electrochemical Reactions at the Metal/Polymer Interface", *Berichte der Bunsengesellschaft für physikalische Chemie,* 2010, 95, p. 1365-1375.

58. M. Stratmann, R. Feser and A. Leng, *Electrochimica Acta*, 1994, 39, p. 1207.

59. W. Furbeth and M. Stratmann, *Fresenius Journal of Analytical Chemistry*, 1995, 353, p. 337.

60. A. J. Bard, M. V. Mirkin, P. R. Unwin, D. O. Wipf, "Scanning Electrochemical Microscopy 12. Theory and Experiment of the Feedback Mode with Finite Heterogeneous Electron-Transfer Kinetics and Arbitrary Substrate Size", *Journal of Physical Chemistry*, 96 (1992) p. 1861-1868.

61. A. J. Bard and Fu-Ren Fan, "Introductory lecture. Studies of the liquid/solid interface by scanning tunnelling microscopy and scanning electrochemical microscopy", *Faraday Discuss*, 1992, 94, p. 1-22.

62. A. J. Bard, F. Fan, J. Kwak, O. Lev, *Journal of Analytical Chemistry*, 1989, 61, p. 132.

63. M. V. Mirkin, "Recent Advances in Scanning Electrochemical Microscopy (SECM)", Journal of Analytical Chemistry, 1996, 68, p. 117A.

64. B. Navinsek, M. Panjan, I. Milosev, "PVD coatings as an environmentally clean alternative to electroplating and electroless processes", *Surface Coatings Technology*, 1999, 116–119, p. 476–487.

65. W. Lauwerens, A. De Boeck, M. Thijs, S. Claaessens, M. Van Stappen, P. Steenackers, "PVD Al-Ti and Al-Mn coatings for high temperature corrosion protection of sheet steel", *Surface and Coatings Technology*, 2001, 146 – 147, p. 27-32.

66. C. Metzner, B. Scheffel, "Special aspects concerning the electron beam deposition of multicomponent alloys", *Surface Coatings Technology*, 2001, 146 –147, p. 491-497.

67. B Scheffel, C Metzner, O Zywitzki, J Faber, "High-rate physical vapour deposition in combination with plasma processes for metal strip coating", *Galvatech 2001: 5th International Conference on Zinc and Zinc Alloy Coated Steel Sheet*; Brussels; Belgium; June 2001, p. 35-41.

68. N. C. Hosking, M.A. Strom, P.H. Shipway, C.D. Rudd, "Corrosion resistance of zinc-magnesium coated steel", *Corrosion Science*, 2007, 49, p. 3669–3695.

69. Myeong-Hoon, K. Yeon-Won, L. Kyung-Min, L. Seung-Hyo, M. Kyung-Man, "Electrochemical evaluation of zinc and magnesium alloy coatings deposited on electrogalvanized steel by PVD", *Transactions of Nonferrous Metals Society of China*, 2013, 23, p. 876-880.

70. M. H. Fathi, M. Salehi, A. Saatchi, V. Mortazavi, S. B. Moosavi, "In vitro corrosion behaviour of bioceramic, metallic and bioceramic metallic coated stainless steel implants", *Dental Materials*, 2003, 19, p. 188-198.

71. S. Maeng. T. A. Axe, L. Tyson, M. Gladczuk, M. Sosnowski, "Corrosion behaviour of magnetron sputtered α- and β-Ta coatings on AISI 4340 steel as a function of coating thickness", *Corrosion Science*, 2006, 48, p. 2154-2171.

72. F. Hui-Ping, H. Cheng-Hsun, L. Jung-Kai, S. Yih-Hsun, "Effects of PVD sputtered coatings on the corrosion resistance of AISI 304 stainless steel", *Material Science and Engineering A*", 2003, 347, p. 123-129.

73. C. Charrier, P. Jacquot, E. Denisse, J. P. Millet, H. Mazille, "Aluminium and Ti/Al multilayer PVD coatings for enhanced corrosion resistance", *Surface and Coatings Technology*, 1997, 90, p. 29-34.

74. D. M. Mattox, "Surface effects on the growth, adhesion and properties of reactively deposited hard coatings", *Surface and Coatings Technology,* 1996, 81, p. 8-16.

75. B. Schuhmacher, C. Schwerdt, U. Seyfert, O. Zimmer, "Innovative steel strip coatings by means of PVD in a continuous pilot line: process technology and coating development", Surface and Coatings Technology, 2003, 163-164, p. 703-709.

76. M. Toivola, F. Ahlskog, P. Lund, "Industrial sheet metals for nanocrystalline dye-sensitized solar cell structures", 2006, 90, p. 2881-2893.

77. M. M. Gómez, J. Rodríguez, S. -E. Lindquist and C. G. Granqvist, "Photoelectrochemical studies of dye-sensitized polycrystalline titanium oxide thin films prepared by sputtering", *Thin Solid Films,* 1999, 342, p. 148-152.

78. M. M. Gómez, J. Rodríguez, S. Tingry, A. Hagfeldt, S.-E. Lindquist, C.G. Granqvist "Photoelectrochemical effect in dye sensitized, sputter deposited Ti oxide films: The role of thickness-dependent roughness and porosity", *Solar Energy Materials and Solar Cells*, 1999, 59, p. 277-287.

79. M. M. Gómez, N. Beermann, J. Lu, E. Olsson, A. Hagfeldt, G.A. Niklasson, C.G. Granqvist', "Dye-sensitized sputtered titanium oxide films for photovoltaic applications: influence of the O-2/Ar gas flow ratio during the deposition", *Solar Energy Materials and Solar Cells*, 2003, 76, p. 37-56.

80. M. M. Gómez, J. Lu, E. Olsson, A. Hagfeldt, C. G. Granqvist "*High efficiency dye-sensitized nanocrystalline solar cells based on sputter deposited Ti oxide films", Solar Energy Materials and Solar Cells*, 2000, 64, p. 385-392.

81. M. Gómez, J. Lu, J. L. Solis, E. Olsson, A. Hagfeldt, C. G. Granqvist, "Dye-sensitized nanocrystalline titanium-oxide-based solar cells prepared by sputtering: Influence of the substrate temperature during deposition", *Journal of Physical Chemistry B*, 2000, 104, p. 8712-8718.

82. C. Metzner, B. Scheffel, "Special aspects concerning the electron beam deposition of multicomponent alloys", *Surface Coatings Technology*, 2001, 146–147, p. 491-497.

83. D.M. Mattox, "Surface effects on the growth, adhesion and properties of reactively deposited hard coatings", *Surface and Coatings Technology,* 1996, 81, p. 8-16.

84. D. M. Mattox, *Physical Vapour Deposition Processes*, Society of Vacuum Coaters, Albuquerque, N.M.

85. B. Scheffel, C. Metzner, O. Zywitzki, J. Faber, "High-rate physical vapour deposition in combination with plasma processes for metal strip coating", *5th International Conference on Zinc and Zinc Alloy Coated Steel Sheet, GALVATECH 2001: June 26-28, 2001, Brussels, Belgium*

86. B. A. Shedden, I. V. Katardjiev, S. Berg, M. Samandi, B. Window, "Ion assisted deposition of Zn-Mg coatings by unbalanced magnetron sputtering", *Surface and Coatings Technology,* 1999, 116-119, p. 751-754.

87. K. Wasa, S. Hayakawa, in *Handbook of Sputter Deposition Technologies*, 1992, p. 1-27.

88. J.A. Venables, G.D.T. Spiller, M. Hanbucken, *"Nucleation and Growth of Thin Films"*, School of Mathematical and Physical Sciences, University of Sussex, Brighton BNl 9QH, UK, 1983, p 403.

89. B, O'Regan, J. R. Durrant, "Calculation of activation energies for transport and recombination in mesoporous TiO2/dye/electrolyte films - Taking into account surface charge shifts with temperature", *Journal of Physical Chemistry B*, 2006, 110, p. 8544-8547.

90. J. Bisquert, "Chemical Diffusion Coefficient of Electrons in Nanostructured Semiconductor Electrodes and Dye-Sensitized Solar Cells", *Journal of Physical Chemistry B*, 2004, 108, p. 2323-2332.

91. R. Kern, R. Sastrawan, J. Ferber, R. Stangl, J. Luther, "Modeling and interpretation of electrical impedance spectra of dye solar cells operated under open-circuit conditions", *Electrochimica Acta*, 2002, 47, p. 4213-4225.

92. L. Peter, N. Duffy, R. Wang, K. Wijayantha, "Transport and interfacial transfer of electrons in dye-sensitized nanocrystalline solar cells", *Journal of Electroanalytical Chemistry*, 2002, 524, p. 127-136.

93. M. Grätzel, "Conversion of sunlight to electric power by nanocrystalline dye-sensitized solar cells", *Journal of Photochemistry. and Photobiology. A: Chemistry,* 2004, 164, p. 3-14

94. S. D. Burnside, V. Shklover, Barbé Ch, P. Comte, F. Arendse, K. Brooks, M. Grätzel, Self-organisation of TiO_2 nanoparticles in thin-films", *Chemical Materials,* 1998, 10, p. 2419-2425.

95. U. Bach, Y. Tachibana, J. E. Moser, S. A. Haque, D. R. Klug, M. Grätzel, J. R. Durrant, "Charge separation in solid-state dye-sensitized heterojunction solar cells" *Journal of the American Chemical So*ciety, 1999, 121, p. 7445-7446.

96. K. Kalyanasundaram, M. Grätzel, "Applications of functionalized transition metal complexes in photonic and optoelectronic devices", *Coordination Chemistry Review,* 1998, 177, p. 347-414.

97. J. Ferber, J. Luther, "Computer simulations of light scattering and absorption in dye-sensitized solar cells", *Solar Energy Material and Solar Cells,* 1998, 54, p. 265-275.

98. M. K. Nazeeruddin, A. Kay, I. Rodicio, R. Humphry-Baker, E. Müller, P. Liska, N. Vlachopoulos, M. Gratzel, "Conversion of light to electricity by cis-X2 (dcbpy)2Ru(II) CT sensitizers on nanocrystalline TiO2 electrodes", *Journal of the American Chemical Society,* 1993, 115, p. 6382-6390.

99. K. Tennakone, G. Kumara, I. Kottegoda, V. Perera, "An efficient dye-sensitized photoelectrochemical solar cell made from oxides of tin and zinc", *Chemical Communications,* 1999, 1, p. 15-16.

100. K. Tennakone, G. K. R. Senadeera, V. P. S. Perera, I. R. M. Kottegoda, L. A. A. De Silva, "Dye-sensitized photoelectrochemical cells based on porous SnO2/ZnO composite and TiO2 films with a polymer electrolyte", *Chemical Materials*, 11, 1999, p. 2474-2477.

101. A. Zaban, S. Chen, B. Gregg, "Bilayer nanoporous electrodes for dye sensitized solar cells", *Chemical Communications,* 2000, 22, p. 2231-2232.

102. J. Van Roosmalen, E. Rijnberg, P. M. Sommeling, EP 1095387B1 (2004).

103. N. Vlachopoulos, P. Liska, J. Augustynski, M. Grätzel, "Very efficient visible light energy harvesting and conversion by spectral sensitization of high surface area polycrystalline titanium dioxide films", *Journal of the American Chemical Society*, 1988, 110, p. 1216-1220.

104. M. G. Kang, N-G. Park, K. S. Ryu, S. H. Chang, K-J. Kim, "A 4.2% efficient flexible dye-sensitized TiO_2 solar cells using stainless steel substrate", *Solar Energy Materials for Solar cells,* 2006, 90, p. 574-581.

105. G. Hashmi, K. Miettunen, T. Peltola, H. Halme, I. Asghar, K. Aitola, M. Toivola, P. Lund, "Review of materials and manufacturing options for large area flexible dye solar cells", Renewable and Sustainable Energy Review, 2001, 15, p. 3717-3732.

106. T. Yamaguchi, N. Tobe, D. Matsumoto, T. Nagai, H. Arakawa, "Highly efficient plastic-substrate dye-sensitized solar cells with validated conversion efficiency of 7.6%", *Solar Energy Material and Solar Cells*, 2010, 94, p. 812-816.

107. E. Moll, E. Bergmann, "Hard coatings by plasma assisted PVD technologies: Industrial practice", *Surface and Coatings Technology*, 1989, 37, p. 483-509.

108. H. K. Pulker, "Optical coatings deposited by ion and plasma PVD processes", *Surface and Coatings Technology*, 1999, 112, p. 250-256.

109. Yu-Yun Chen, Jin-Cherng Hsu, P. W. Wang, Yao-Wei Pai, Chih-Yuan Wu, Yung-Hsin Lin, "Dependence of resistivity on structure and composition of AZO films produced by ion beam co-sputtering deposition.

110. E. Roos, K. Maile, A. Lytovich, A. Gusko, A. Udoh, "(Cr-Al) bi-layer coatings obtained by ion beam assisted EB PVD on C/C-SiC composites and Ni-based alloys", *Surface and Coatings Technology*, 2002, 151-152, p. 429-433.

111. D. E. Wolfe, J. Singh, "Titanium carbide coatings deposited by reactive ion beam-assisted, electron beam-physical vapour deposition", *Surface and Coatings Technology*, 2000, 124, p. 142-153.

112. A. Schutze, D. T. Quinto, "Pulsed plasma-assisted PVD sputter-deposited alumina thin films", *Surface and Coatings Technology*, 2003, 162, p. 174-182.

113. F. Milde, K. Goedicke, M. Fahland, "Adhesion behaviour of PVD coatings on ECR plasma and ion beam treated polymer films", Thin Solid Films, 1996, 279, p. 169-173.

114. L. F. Pochet, P. Howard, S. Safaie, "CVD coatings: from cutting tools to aerospace applications and its future potential", *Surface and Coatings Technology*, 1997, 94-95, p. 70-75.

115. S. Grainger, "Engineering coatings: design and application", 1989, [S.l.]: Industrial Press, Inc.

116. A. E. Zeghni, and M. S. J. Hashmi, "Comparative wear characteristics of tin and tic coated and uncoated tool steel", *Journal of Materials Processing Technology*, 2004, 155-156, p. 1923-1926.

117. ASM Handbook. Vol. 18. 1992.

118. J. Wagner, et al., "The effect of deposition temperature on microstructure and properties of thermal CVD TiN coatings", *International Journal of Refractory Metals and Hard Materials*, 2008. 26, p. 120-126.

119. J. Gong, J. Liang, K. Sumathy, "Review on dye-sensitized solar cells (DSSCs): Fundamental concepts and novel materials", *Renewable and Sustainable Energy Reviews*, 2012, 16, p. 5848-5860.

120. L. Wang, X. Fang, Z. Zhang, "Design methods for large scale dye-sensitized solar modules and the progress of stability research", *Renewable and Sustainable Energy*, 2010, 14, p. 3178-3184.

121. Dong-Joo Kwak. Ji-Hoon Kim, Byung-Wook Park, Youl-Moon Sung, Min-Woo Park, Young-Bae Choo, "Growth of ZnO:Al transparent conducting layer on polymer substrate for flexible film types dye-sensitized solar cell", *Current Applied Physics*, 2010, 10, p. S282-S285.

122. T. Miyasaka, Y. Kijitori, M. Ikegami, "Fabrication of full plastic dye-sensitized solar cell modules based on low-temperature coating techniques", *The 16th international conference of photochemical conversion and solar storage (2006).*

123. K. J. Wang, S. Y. Dai, "The research progess in dye-sensitized nano-film solar cells", *Proceedings of the 8th China photovoltaic conference*, 2004, p. 57-62.

124. H. M. Tian, B. Liu, T. Yu, Z. G. Zou, "Analysis of dye-sensitized solar cells industrialization progress", *World Science and Technology Research and Development*, 2008, 30, p. 49-55.

125. F. Robert, "Tricks for beating the heat help panels see the light", *Science*, 2003, 300, p. 1219-1223.

126. V. G. Babaev, M. B. Guseva, A. Yu. Bregadze, V. K. Khvostov, A. N. Obraztsov, M. A. Timofeyev, "Diamond film formation by laser evaporation of highly dispersive diamond in a hydrogen plasma environment", *Diamond and Related Materials*, 1995, 4, p. 1200 – 1204.

127. M. Toivola, F. Ahlskog, and P. Lund, "Industrial sheet metals for nanocrystalline dye-sensitized solar cell structures", *Solar Energy Materials and Solar Cells*, 2006, 90, p. 2881-2893

128. M. Toivola, K. Miettunen, J. Halme, and P. Lund, "Thin nanostructured solar cells on metal sheets", in *Clean Technology 2008: Bio Energy, Renewables, Green Building, Smart Grid, Storage, and Water*, M. Laudon, B. Romanowicz, and D.L. Laird, Editors, p. 96-99, CRC Press-Taylor & Francis Group, Boca Raton (2008).

129. M. Toivola, T. Peltola, K. Miettunen, J. Halme, and P. Lund, "Thin film nano solar cells - from device optimization to upscaling", *Journal of Nanoscience and Nanotechnology*, 2010, 10, p.1078-1084

130. K. Miettunen, X. L. Ruan, T. Saukkonen, J. Halme, M. Toivola, G. S. Huang, and P. Lund, "Stability of Dye Solar Cells with Photoelectrode on Metal Substrates", *Journal of the Electrochemical Society*, 2010, 157, B814-B819..

131. K. Miettunen, J. Halme, and P. Lund, "Segmented Cell Design for Improved Factoring of Aging Effects in Dye Solar Cells", *Journal of Physical Chemistry C*, 2009, 113, p. 10297-10302

132. K. Miettunen, J. Halme, M. Toivola, and P. Lund, "Initial performance of dye solar cells on stainless steel substrates", *Journal of Physical Chemistry C*, 2008, 112, p. 4011-4017.

133. X. M. Fang, T. L. Ma, M. Akiyama, G. Q. Guan, S. Tsunematsu, and E. Abe, "Flexible counter electrodes based on metal sheet and polymer film for dye-sensitized solarcells", *Thin Solid Films*, 2005, 472, p. 242-245.

134. T. L. Ma, X. M. Fang, M. Akiyama, K. Inoue, H. Noma, and E. Abe, "Properties of several types of novel counter electrodes for dye-sensitized solar cells", *Journal of Electroanalytical Chemistry*, 2004, 574 , p. 77-83.

135. A. Kay, "Solar cells based on dye-sensitized nanocrystalline TiO_2 electrodes, PhD thesis", Ecole Polytechnique Federale de Lausanne, Switzerland, (1994).

136. H. Kusama, H. Arakawa, 'Influence of benzimidazole additives electrolytic solution on dye-sensitized solar cell performance", *Journal of Photochemistry and Photobiology A: Chemistry*, 2004, 162, p. 441-448.

137. Z. Yu, M. Gorlov, G. Boschloo, K. Kloo, "Synergistic effect of N-methylbenzimidazole and guanidinium thiocyanate on the performance of dye-sensitised solar cells based on ionic liquid electrolytes", *Journal of Physical Chemistry C*, 2010, 114, p. 22330-22337.

Chapter 2

Experimental Procedures

2.1 Substrates Investigated

The metal substrates tested during the course of these investigations cover a broad cross section from common roofing materials such as aluminium to more exotic metals such as titanium, packaging steels, e.g. coatings developed specifically for the DSC photovoltaic project such as the polyimide coatings. To provide a detailed description of the diverse production methods and physical attributes of the numerous different substrates that were tested would be impractical, therefore a brief overview of each will be given.

The substrates fall into three broad categories; bulk metals, thin metallic coatings and non-metallic coatings, as shown in Table 1.1. Bulk metal substrates and metallic coatings have been employed in order to explore, firstly, corrosion underneath organic paint systems and then as potential substrates for the fabrication of DSC technology. Non-metallic organic coatings have been employed to act primarily as protective barrier layers. All bulk metallic substrates, with the exception of 'black plate', were sourced from Goodfellow. The PVD titanium and aluminium coated layers were applied on polyimide coated ECCS and supplied by Tata Steel but coated in house by Plasma Vapour Deposition. Tata Steel also provided the black plate substrates.

Table 2.1. *Categories of metal substrates tested. Coatings were deposited on cold rolled steel unless otherwise stated.*

BULK METALS	METALLIC COATINGS
Aluminium (99.0%)	PVD Aluminium coated Iron
Aluminium (99.999%)	PVD Titanium (99.995%) coated Polyimide
Titanium (99.6%)	PVD Aluminium coated Polyimide
Molybdenum (99.9%)	PVD Aluminium-Titanium bilayer coated polyimide
Stainless Steel 304	PVD Titanium coated bakeware
Stainless Steel 316	Polyimide coated Electro-chromium coated steel
Electro-chromium Coated Steel (ECCS)	
Iron Foil (99.5%)	
Zinc (99.999%)	
Black Plate	

2.1.1 Aluminium

Aluminium is a silvery white reactive metal that is covered, in ambient conditions, by a dense oxide coating that provides good corrosion resistance [52]. The metal has good thermal properties and is malleable and ductile. Aluminium and its alloys are widely used for various engineering applications including engine parts and building materials. Extracting aluminium from its ore is particularly expensive due to the electricity intensive extraction method of electrolysis. Aluminium of higher purity is also substantially more expensive than lesser pure examples. The presence of

impurities and alloying elements (for example copper) can lead to pitting corrosion, especially in the presence of electrolytes containing dissolved salts. The purity of the aluminium used in this work was 99% and 99.9%.

2.1.2 Titanium

Titanium is a hard, lustrous, silvery metal that forms a protective oxide coating and, hence, resists corrosion. It tends to be inert at low temperatures but will combine with a variety of reagents at elevated temperatures. Titanium is characteristically light, strong and corrosion resistant; as such they are used widely in aerospace and medical applications. The titanium used in this work had purity of 99.6%.

2.1.3 Molybdenum

Molybdenum is a lustrous, silvery metal that has a melting point of 2,623°C; a property that is exploited in applications such as resistance heating elements in furnaces, manufacturing of armour and aircraft parts, industrial motors, filaments and electrical contacts. The purity of the molybdenum used in this work was 99.9%.

2.1.4 Stainless steel

Stainless steels are iron based alloys containing at least 10.5% Chromium. Their stainless characteristics are developed through the formation of an invisible and adherent Chromium rich oxide film. Both 304 and 316 grades are general-purpose austenitic stainless steel with a face centred cubic structure. They are non-magnetic in the annealed condition and can only be hardened by cold working. The lower Carbon content compared to other stainless grades gives better corrosion resistance in welded structures. Both grades contain iron plus 18% Chromium and 10% Nickel. The 316 grade also contains 3% Molybdenum to increase corrosion resistance particularly in chloride containing environments.

2.1.5 Black plate

Black plate is a name within the strip steel industry given to cold reduced mild steel that contains 0.12% carbon and 0.6% manganese additions to iron. Cold reduced steel is made from de-scaled hot rolled coils by cold rolling to the desired thickness. Further processing such as annealing and temper rolling may be used to impart the desired formability, surface texture, and flatness properties. Black plate is used in a variety of applications from automobile panels and door braces, to deep drawn items such as oil filters, or post painted and formed into roofing panels. Black plate corrodes readily in ambient conditions if it is not given some form of corrosion protection, e.g. a protective organic based paint layer or sacrificial galvanic coating such as Zinc.

2.1.6 PVD Titanium and Aluminium on Polyimide (PI) coated ECCS

Polyimide coated electro-chromium coated steel (ECCS) used in this work was sourced by Tata Steel. Polyimides are the most important group of high temperature resistant plastics, and are prime candidates for use as a corrosion barrier upon a steel substrate for large-scale dye-sensitised solar cell applications. It has excellent chemical resistance and has no known solvents. Polyimide films are produced by the polymerisation of an aromatic dianhydride with an aromatic diamine. There are many companies that produce polyimide films one being DuPont, whose brand of polyimide film has the name KAPON®. The film has no melting point and does not burn [53]. The chemical structure of PI can be seen in Figure 2.1.

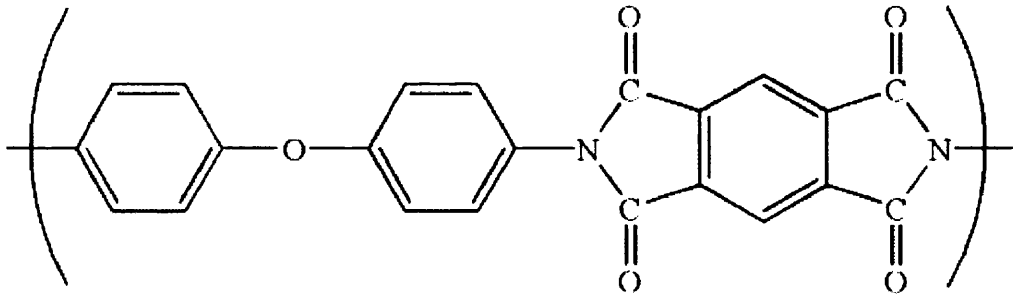

Figure 2.1: Chemical structure of polyimide

The polyimide coated ECCS was coated with a various thicknesses of titanium and aluminium using a Kurt J Lesker PVD 75. Due to the high cost of titanium sheet it would not be viable to produce a building integrated DSC photovoltaic system on this substrate at present. However as demonstrated throughout this work, titanium is ideally suited to the purpose. The reason for producing the PVD coated substrate was to investigate whether deposition of a thin layer of titanium could provide the same properties as those demonstrated by the bulk material.

2.1.7 Tata Research, Development and Technology coatings

Tata R,D and T coatings were supplied in order to study the two main criteria required of a successful DSC substrate, i.e. the coating should provide corrosion protection to the underlying metal and be capable of withstanding the high sintering temperature, the temperature treatment which is applied to the titania layer in order to achieve a mesoporous structure as explained in section 1.3.1.4. A Tata Steel customer who produces vitreous enamelled steel for oven and bake ware applications sourced the enamelled steel. Enamelled steel is essentially a glass layer that has been applied to a steel substrate. This system may celebrate a whole host of advantages properties such as providing barrier protection to the underlying steel, providing resistance to high temperature environments and high durability. The coatings provided by the costumer were very thick (~500μm) and proved to be extremely brittle

2.2 Surface investigation using the Scanning Electron Microscope (SEM)

Samples of the PVD films exposed to high temperatures during the DSC calcining process were examined using a *Philips XL30 CP* Scanning Electron Microscope (SEM). Both 'secondary electron' and 'back scattered electron' detection techniques were used to try to establish whether the surface chemistries of the PVD titanium and aluminium bilayer coatings altered when a variety of different thicknesses of PVD titanium were deposited on to a constant thickness of PVD aluminium. The technique was also used to reveal any areas of the bilayer coating that had features such as tears or cracking that could potentially expose Al at the surface. This would be unfavourable for use in DSC fabrication due to the findings in chapter 3.

2.3 Surface investigation using Energy Dispersive X-ray analysis (EDX)

Further analysis of the elemental composition of areas of specific interest on the surfaces of the selected samples were further examined using Energy Dispersive X-ray analysis with the aid of a *JEOL JSM-35C SEM.* A cobalt standard was used to calibrate the machine prior to measurements made on each sample.

2.4 DSC Cell building technique

This section describes the various steps involved in the construction of a DSC consisting of a metal based working electrode and a glass counter electrode. Though the ultimate aim of this project is to produce a flexible solar cell, a direct comparison of substrate performance is more easily assessed if the counter (non-metal) electrode was rigid. For a DSC to operate at least one of the electrodes is required to be transparent in order to allow light to enter the cell. Fluorine doped Tin Oxide (FTO) coated glass is typically used for this purpose. These glass electrodes are rated according to the sheet resistance of the FTO layer; TEC 8 having a sheet resistance of 8 Ohms/square and TEC 15 with 15 Ohms/square are most commonly quoted in

the literature. In this work TEC 15 was used. A schematic representation of a DSC is shown in figure 2.2.

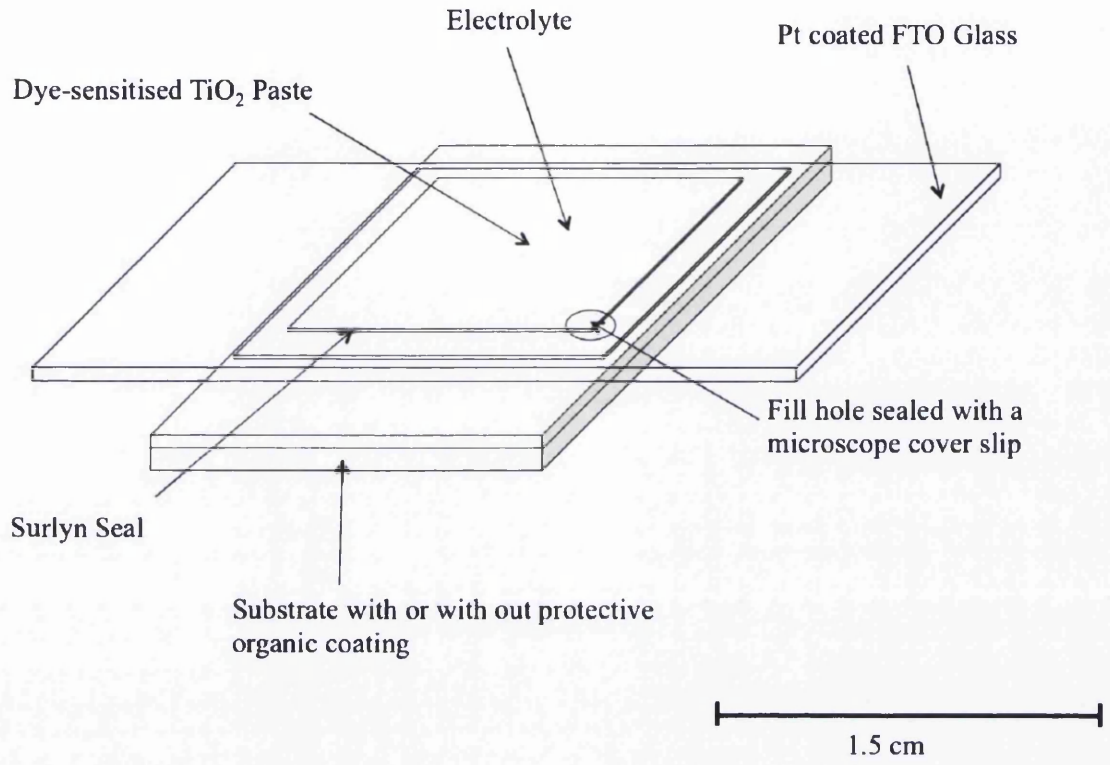

Figure 2.2: *A schematic representation of the constituent parts of a dye-sensitised solar test cell.*

The active area of test cells can vary considerably depending on where they were made. Generally, very small area cells produce the highest reported DSC efficiencies. Small area cells meaning that the active area of the cell that is responsible for generating electrical current is small, typically less than a square centimetre. The reason for this is to minimise the losses associated with sheet resistance of the Transparent Conducting Oxide (TCO) layer on the glass electrodes. Cell areas of one square centimetre (1cm x 1cm) were chosen for all efficiency test cell measurements. Unless otherwise stated all procedures were conducted at room temperature.

2.4.1 Preparation of dye solution

1. 50ml of acetonitrile was measured into a 120ml graduated bottle
2. The volume was made up to 100ml with tert-butanol crystals
3. Tert-butanol crystals were allowed time to dissolve
4. 119mg of N719 ruthenium dye crystals were weighed out (Dyesol B2(N719))
5. Dye crystals were added to tert-butanol/acetonitrile to create 0.25mM solution.
6. The mixture was sonicated for one hour and then stored in the dark until needed.

2.4.2 Preparation of the DSC Photoelectrode

1. Cutting metal substrates – A guillotine was used to cut the samples into strips 15mm wide by 25mm long (if the substrate material was not delivered pre-cut).
2. Cleaning – The cleaning technique varied depending on the substrate composition. Pure metals such as titanium and aluminium were given a light polish with an alumina paste prior to washing with soapy water, rinsing with deionised water and finally with acetone. Coated substrates (e.g. Physical Vapour Deposited (PVD) titanium and aluminium on organic polymer coatings) were not subjected to the polishing step.
3. Applying TiO_2 – A 1cm x 1cm square was removed from two layers of Scotch Magic tape, in order to provide a template for the deposition of the TiO_2 layer. The template was applied to the substrate coupon leaving the 1cm x 1cm square of exposed substrate in the centre of the coupon. Having stirred the TiO_2 paste (DSL 18NRT), supplied by Dyesol, for at least thirty minutes to ensure homogeneity, 200-300µl was applied to the edge of the removed square and a glass bar was then used to draw the paste across the exposed metal as shown in Figure 2.3. The paste was air dried for 30 minutes and then sintered for a further 30mins at 450°C to remove a terpineol solvent, and finally left to cool to room temperature in a covered Petri dish. The titania paste used in this process is a variation of available titania pastes which is capable of much higher sintering

temperatures in order to create a desired mesoporous structure through enhanced solvent and ethyl cellulose binder removal.

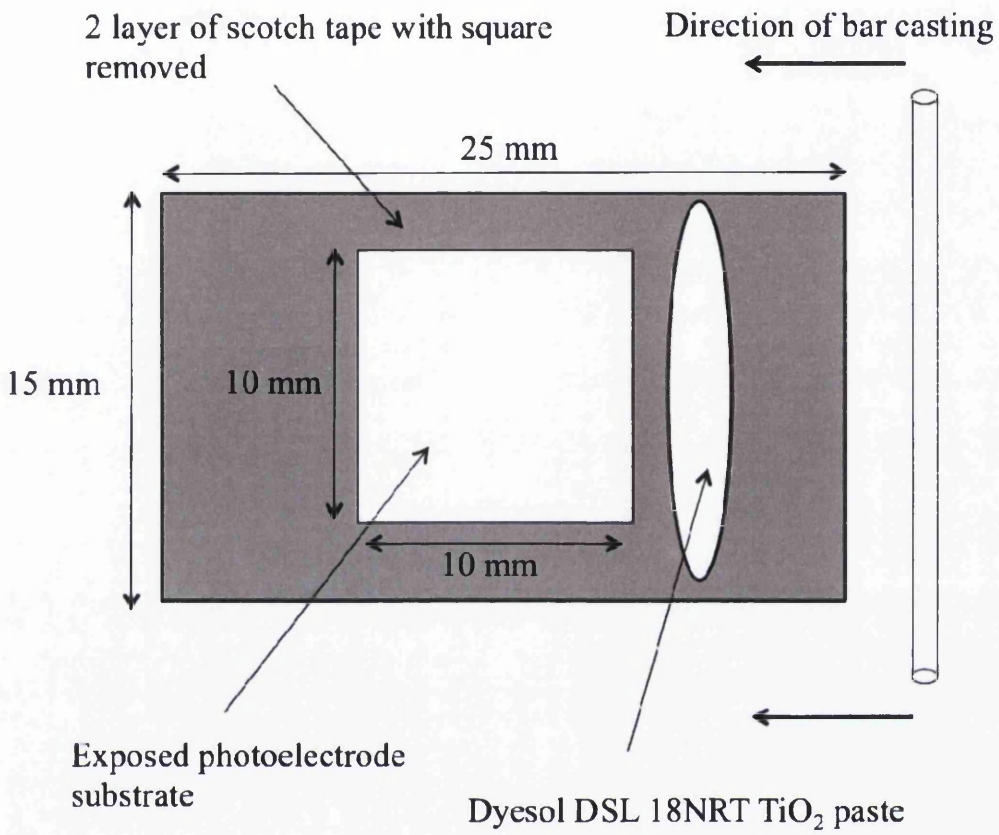

Figure 2.3: *A diagram to show TiO_2 photoelectrodes were prepared on metallic substrates*

4. Defining working area – A square metal template of side 10mm was placed over the TiO_2 coated area of the slide and any exposed titania was gently removed with a plastic scraper. A blower was used to remove any dust created.
5. Dye sensitisation – TiO_2 photoelectrodes were placed face up in a Petri dish at room temperature, which was then filled with sufficient dye solution to cover the TiO_2 layer. The Petri dish was then sealed and placed in the dark overnight.

2.4.3 Preparation of glass counter electrode

1. Cutting TEC 15 glass – Tec 15 glass slides of approximately 15mm x 25mm were cut from sheets of FTO coated TEC15 glass using a small tile cutter.
2. Drilling slides – One 0.5mm hole was drilled through each slide, inside the working cell area.
3. Cleaning – Slides were first cleaned using soapy water, then rinsed with deionised water, then isopropyl alcohol (IPA).
4. Platinisation – 5mM of chloroplatanic acid (H_2PtCl_6, Aldrich) in IPA was applied in small drops until the surface was wetted out. Slides were left to air dry for 30 minutes then heated to 400°C for a further 30 minutes.

2.4.4 Preparation of DSC electrolyte

In this experiment, a very simple DSC electrolyte solution was selected initially in order to isolate the effect of the iodide/tri-iodide redox couple without the interaction of the other electrolyte additives such as TBP or guanidinium thiocyanate as mentioned in Chapter 1. For this reason, unless otherwise stated, 0.1 M LiI and 0.05 I_2 dissolved in 3-methoxypropionitrile was prepared and introduced to each cell, respectively, by vacuum injection and the remaining hole sealed with Surlyn and a circular microscope coverslip.

2.4.5 Cell assembly

1. The dye-sensitised, titania coated primary electrodes were removed from the dye bath and excess dye rinsed form the surface using a tert-butanol / acetonitrile solution, then air dried.
2. A Surlyn® (DuPont) gasket was carefully placed on top of the primary electrode such that the $1cm^2$ cut out fitted around the sensitised titania layer exactly.

3. The pre-drilled and platinised counter electrode was then laid, conducting side down, on top of the Surlyn®.

4. The three items were moved in unison and placed on the lower platen of a one sided heat press (Model: Xpress). The heated upper platen (135°C) was then brought down and locked parallel to the lower platen, providing a constant pressure for 35 seconds, before being released. Heating the Surlyn® layer in this way causes the polymer to become tacky, the addition of pressure promotes adhesion of the primary and counter electrodes, whilst maintaining a gap between the two approximately equal to the Surlyn® layer thickness.

5. Once cooled, the sealed electrodes were placed in a small desiccator connected to a vacuum pump. A small O-ring was paced around the hole drilled in the counter electrode and a small volume of electrolyte placed in to the O-ring as shown in Figure 2.4. The desiccator was sealed and a partial vacuum, provided by the pump, drew air from the area enclosed between the two electrodes through the drop of electrolyte. After a few seconds the pump was turned off and as the pressure within the desiccator returned to ambient, the electrolyte was drawn into the void, thereby filling the cell.

6. The area around the drilled hole was wiped clean of residual electrolyte and the hole sealed using a piece of Surlyn® covered by a small disc of microscope cover glass which was heated using the tip of a soldering iron.

7. Finally the completed DSC had conducting silver paint, supplied by Sigma-Aldrich, applied along the exposed, conducting edges of the electrodes in order to facilitate more consistent electrical connection.

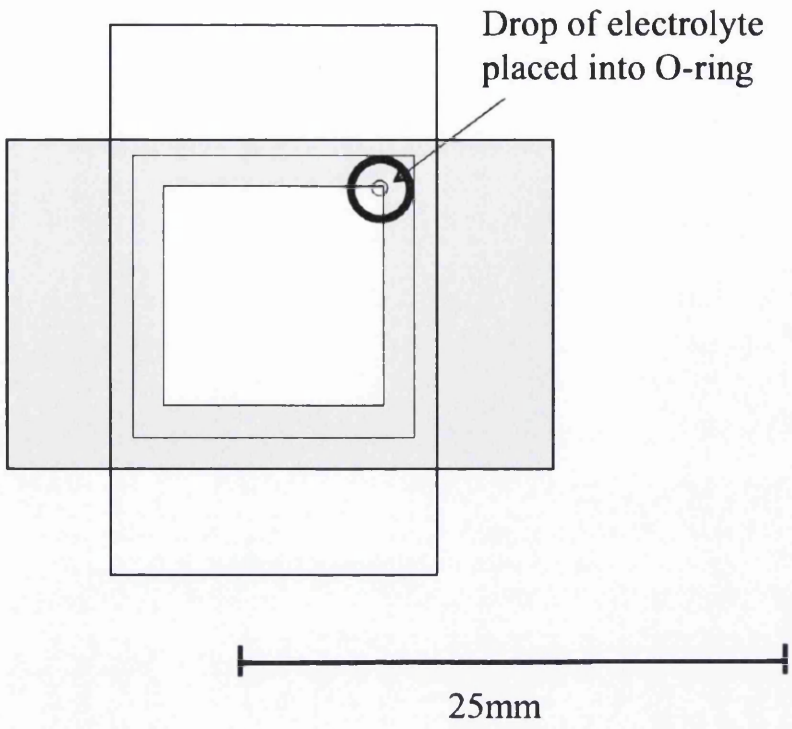

Figure 2.4: *Image to show how electrolyte was introduced to the dye-sensitised solar cells.*

2.4.6 DSC Current Voltage (I-V) Measurements

The current voltage characteristics of the cell were measured using an Oriel Sol3A (94023A) utilising a Xenon arc lamp (150 W), an AM1.5 filter and a Keithley 2400 source meter. A certified (Oriel 91150V) monocrystalline silicon reference cell traceable to the US dept. of energy National Renewable Energy Laboratory (NREL) was used to adjust the solar simulator to the standard light intensity of one sun, i.e. $1000W/m^2$.

2.5 DSC Corrosion Investigation – Electrolyte Encapsulation Cell Fabrication

The set up of an electrolyte encapsulation corrosion cell can be seen in Figure 2.5 and 2.6. Here, 2 mm thick metal substrate coupons of dimensions 50 mm × 50 mm,

were firstly abrasively polished using a coarse grade of silicon carbide paper, supplied by Fisher Scientific, washed in water and mild detergent, and then rinsed with ethanol and dried with pressurised air. The glass top layer used for corrosion cell construction had the same dimensions as the metal substrate, and was also washed in water and mild detergent, followed by rinsing with ethanol and drying using compressed air. In order to replicate the environment in which DSC electrolyte and a metal substrate interact within a DSC, encapsulation corrosion cells were produced on each metal substrate by the following procedure. A 25 mm × 25 mm × 25μm (approximately due to errors in experimental design) volume of electrolyte was exposed to the metal, through bonding the section of glass to the substrate using a 25μm thick Surlyn® (Dupont Ltd.) gasket that had been laser cut to required specifications. 0.5 mm diameter holes were conveniently drilled through the glass for the introduction of the redox electrolyte into the cell. The electrolyte solution (0.8 mol dm^{-3} 1-propyl-3- methylimidazolium iodide (PMII), 0.3 mol dm^{-3} benzimidazole, 0.1 mol dm^{-3} I_2 and 0.05 mol dm^{-3} guanidinum thiocyanate dissolved in N-methoxy propionitrile) was introduced to the cell by vacuum injection and the remaining hole sealed with Surlyn® and a circular microscope cover slip.

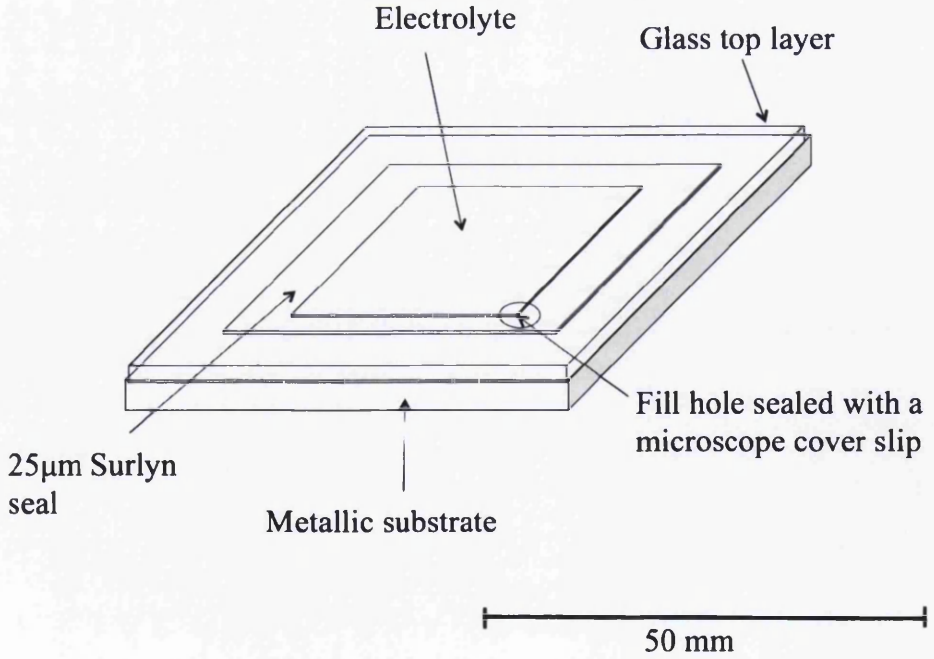

Figure 2.5: *Configuration of corrosion encapsulation test cell.*

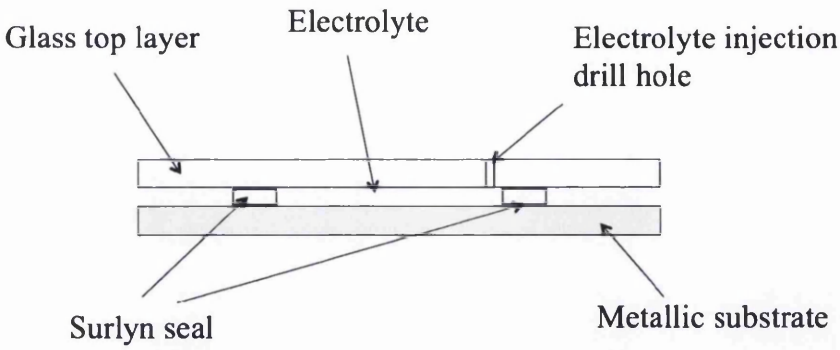

Figure 2.6: *A cross-sectional representation of an encapsulation cell design (not to scale).*

2.5.1 UV/Vis Diffuse Reflectance Spectrophotometry to monitor electrolyte-metal reaction

Corrosion activity was studied by using a Perkin Elmer Lambda 750S UV/Vis spectrophotometer to monitor the absorbance change of the I_3^- redox mediator over various periods of time, ranging from 24 hours to several months, when placed in contact with a metal substrate. The spectrophotometer was used in reflectance mode, with the various encapsulation cells placed so that a monochromatic light beam was able to pass through the glass top layer and the 25μm thick electrolyte medium and be reflected at the polished metal substrate. The encapsulation cells were angled with respect to the beam so that the reflected light was carried to the detector as shown by the schematic representation in Figure 2.7. Preliminary experiments were carried out in situ using a time-lapse setup, where absorption spectra over a wavelength range between 300 nm and 800 nm were recorded at 10 minute intervals for 24 hours, in order to capture any disappearance of I_3^-. Metals that had not corroded in this time period were subjected to further *ex-situ* tests for longer time periods thereafter. The absorption spectra was analysed, and rates of I_3^- disappearance for the various metal surfaces compared in order to draw up a ranking in terms of corrosion resistance.

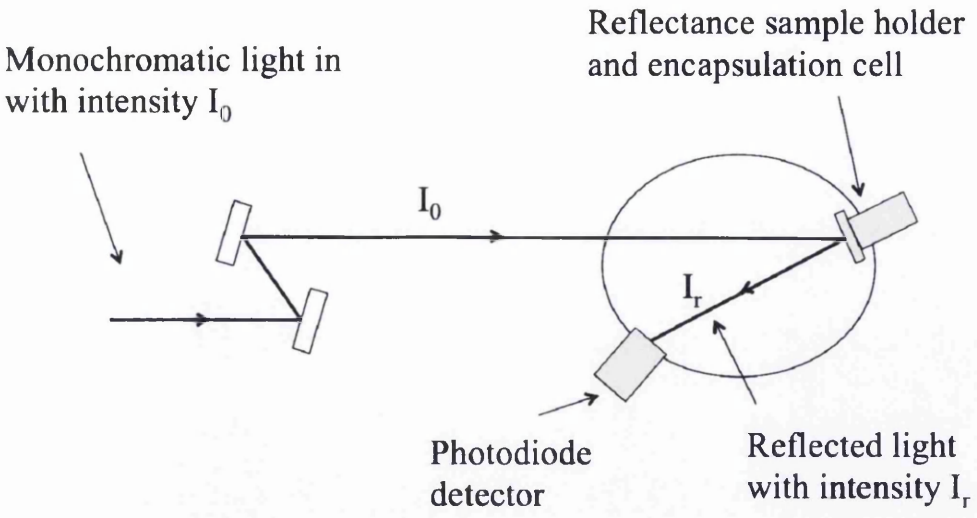

Figure 2.7: *Schematic representation showing the UV/Vis spectrophotometer setup when used in reflectance mode.*

2.5.2 Scanning Kelvin-Probe

The scanning Kelvin microprobe apparatus used in this work (Chapter 3) is shown schematically in Figure 2.8. The vibrating reference probe assembly was mounted in a fixed position above the moving test sample. The reference probe itself consisted of a 125 μm diameter gold wire, which was vibrated along the vertical axis using a moving coil electromechanical actuator. The probe vibration frequency was 280Hz and the vibration amplitude was 50 μm peak-to-peak [26,49]. Reference probe vibration amplitudes were checked using stroboscopic observation in conjunction with a travelling microscope. The experimental arrangement was such that the tip of the vibrating reference probe was held at earth potential and positioned inside a stainless steel environment chamber, which was also at earth potential. The electromechanical actuator and vibrator drive electronics were positioned outside the environment chamber in order to ensure effective electrostatic and magnetic shielding of both the reference probe and sample. Vibration was conducted to the probe tip through use of a 50 mm long glass push rod.

Positioning and scanning of the test sample was carried out using a micromanipulation stage consisting of three orthogonally arranged (x,y,z), stepper motor driven, linear bearings (Time and Precision Ltd.). The probe was held at a constant height of 100 μm above the sample surface and scanned in a raster of parallel lines 100μm apart. Kelvin probe measurements were made once every 100 μm to generate a regular array of values. To perform each measurement the A.C. current, T(t), generated in the external circuit connecting the sample and vibrating probe (see following section), was amplified and converted into an A.C. voltage signal, V(t), using a D.C. biased transconductance amplifier circuit. The V(t) signal was detected using a lock-in amplifier (EE&G model 7260). The D.C. output of the lock-in amplifier, V_{dc}, was transmitted to a feedback system based on an integrator circuit which controlled the D.C. bias, E, applied to the sample via the transconductance amplifier so as to automatically null I(t). The magnitude of the D.C. bias (equivalent to $-E_{kp}$ as defined in the following section) applied via the integrator, was digitised and logged. Probe scanning and data logging were all carried out automatically under microcomputer control. All scans were performed in ambient air (nominal temperature 22°C, R.H 45%).

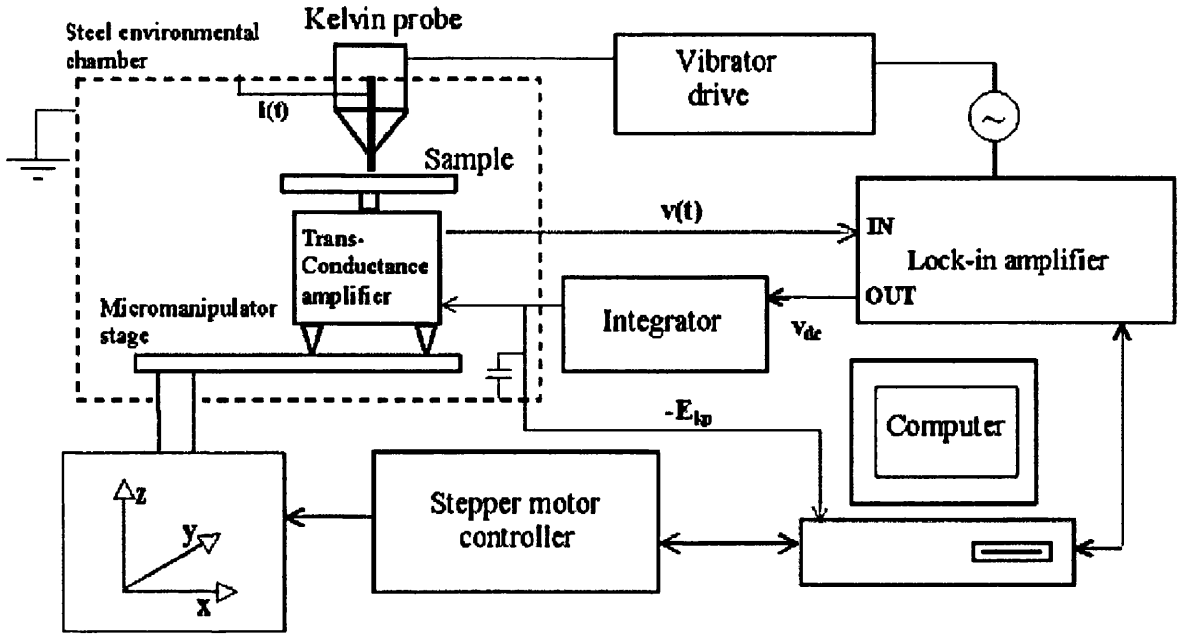

Figure 2.8: *A schematic of the scanning Kelvin microprobe apparatus that is a well established technique for the investigation of cathodic disbondment of organic coatings on iron.*

2.5.3 Kelvin Probe Calibration

The SKP was calibrated in terms of electrode potential using Ag/Ag^{+}, Cu/Cu^{2+}, Fe/Fe^{2+}, and Zn/Zn^{2+}, couples. Calibration cells were prepared by machining wells (8 mm diameter, 1 mm deep) in disks of the relevant metal (15 mm diameter, 5 mm thick). These wells were then filled with a 0.5 mol dm^{-3}, aqueous solution of the respective metal chloride salt (0.5 mol dm^{-3}, nitrate salt in the case of Ag) and E_{KP} values obtained with the vibrating reference probe positioned 100 μm above the electrolyte meniscus in the center of the well. The electrode potential of the metal was simultaneously measured *vs.* SCE using a Solartron 1280 potentiostat. The influence of the PVB polymer on SKP calibration was determined by placing a 30 μm thick self-supporting PVB film over each calibration disk and in contact with the electrolyte meniscus. The polymer film was then allowed to equilibrate with the electrolyte for 6 hours and E_{KP} values obtained as before [26,49].

2.6 Using a 4 Point Probe to Measure Sheets Resistance

The four-point probe is a widely used instrument that is specifically designed to measure the sheet resistance of a semiconductor material. It can measure a bulk or thin film specimen; the mathematics behind its operation is shown below.

In this thesis, an in-house 4 point probe was constructed to reduce cost that consisted of four equally spaced metal probes with tips each having a finite radius. Each probe has a spring-loaded tip so that damage to the sample was kept to a minimum during probing. A high impedance current source is used to provide current to the two outer probes whilst the potential difference between the two inner probes was measured. Utilizing Ohm's law, the sheet resistivity can therefore be determined. Figure 2.9 shows the configuration of a typical four point probe that was built in-house. In the diagram S represents the probe spacing, which was approximately 2mm. V represents the measured voltage drop across the two inner probes and I represents the current applied to the two outer probes. The symbols x_2, x_1 and 0 are the positions of each corresponding probe which is used in the next section to help derived equations for determining bulk resistivity and thin sheet resistance.

Ohm's per square is the unit of measurement when measuring the resistance of a thin film of a material using the four point probe technique. It is equal to the resistance between two electrodes on opposite sides of a theoretical square.

2.6.1 Derivation of bulk specimen:

In the derivations for this section, it will be assumed that the metal tips used are $\Delta R = \rho\left(\frac{dx}{A}\right)$ infinitesimal and samples are semi-infinite in lateral dimension. For bulk samples where the sample thickness t is much greater than s, the probe spacing, we assume a spherical protrusion of current emanating from the outer probe tips [54]. The differential resistance is:

$$\Delta R = \rho\left(\frac{dx}{A}\right) \tag{2.1}$$

Integrating between the inner probe tips we get:

$$R = \int_{x_1}^{x_2} \rho \frac{dx}{2\pi(x)^2} = \left[\frac{\rho}{2\pi}\left(-\frac{1}{x}\right)\right]_{s}^{2s} = \frac{\rho}{4s\pi} \tag{2.2}$$

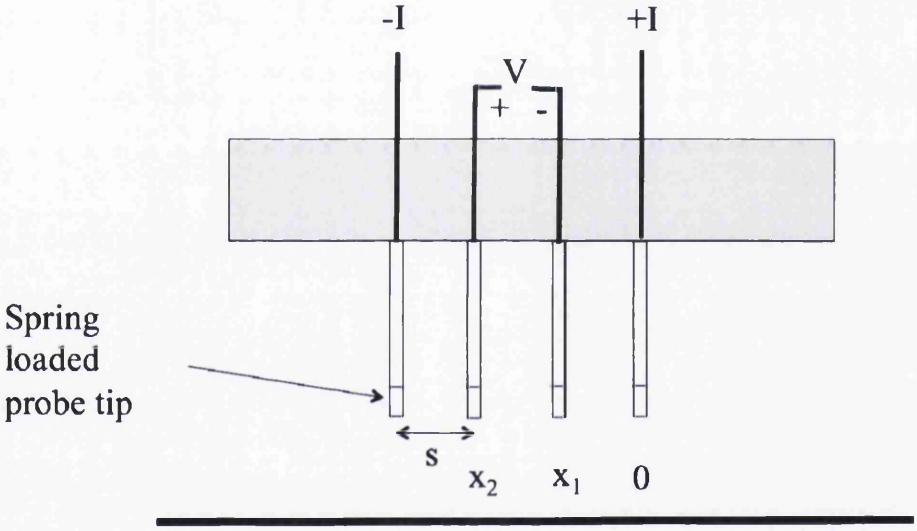

Figure 2.9 *Configuration of a typical in-house built 4 point probe*

Due to the superposition of current at the two outer tips R=V/2I, therefore we get the relation for bulk resistivity:

$$\rho = 2\pi s\left(\frac{V}{I}\right) \tag{2.3}$$

2.6.2 Derivation for thin film:

For a very thin sheet it can be assumed that the current flows in a circular manner rather than spherically due to the vertical constraints of the film. The thickness of the sheet can be seen as being very much smaller than the probe spacing s. The area is then equal to $2\pi xt$ [54].

So,

$$R = \int_{x_1}^{x_2} \rho\left(\frac{dx}{2\pi xt}\right) = \frac{\rho}{2\pi t}\int_{s}^{2s}\left(\frac{dx}{x}\right) = \frac{\rho}{2\pi t}\left(\ln(2s) - \ln(s)\right) = \frac{\rho}{2\pi t}\ln 2 \tag{2.4}$$

For R=V/2I, thin sheet resistivity is:

$$\rho = \frac{\pi t}{\ln 2}\left(\frac{V}{I}\right) \tag{2.5}$$

So sheet resistance can be expressed as:

$$R_s = \frac{\rho}{t} = k\left(\frac{V}{I}\right) \tag{2.6}$$

Notice that sheet resistance, R_s is not reliant upon the probe spacing s. The probe spacing has been set at 2mm to allow a design that can accommodate measurement of sheet resistances on smaller samples.

$$k = \frac{\pi}{\ln 2} = 4.53 \tag{2.7}$$

This implies that the raw data value of measured voltage, divided by the applied current, must be multiplied by 4.53, in order to arrive at the correct value of sheet resistance.

2.6.3 Construction of the In-house Built 4 Point Probe

2 probes were constructed using a pointed probe tip and a spherical probe tip shown below in figure 2.8.

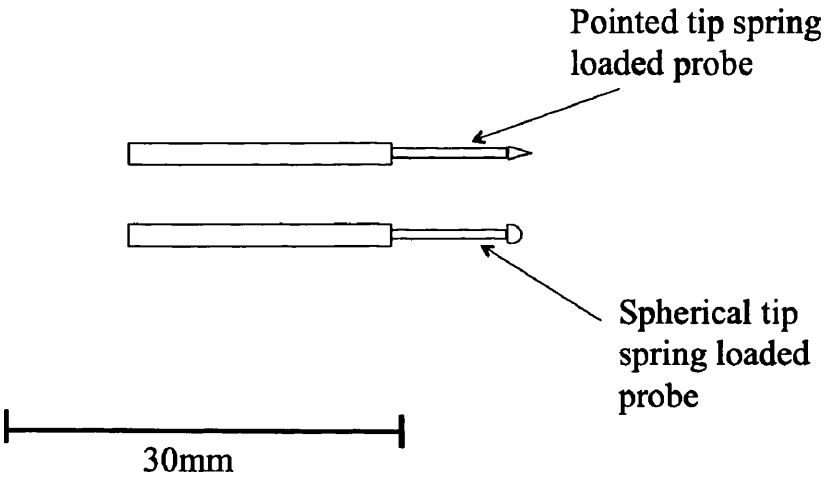

Figure 2.10: *Diagram representing the dimensions of the probes used in the construction of in-house built 4 point probes.*

Holes were drilled in the bottom of a small plastic box that would act as a case for the probe as shown in Figure 2.10. Four 1mm diameter spring loaded probes were set into a 4 input connector block at separation distance of 2mm.

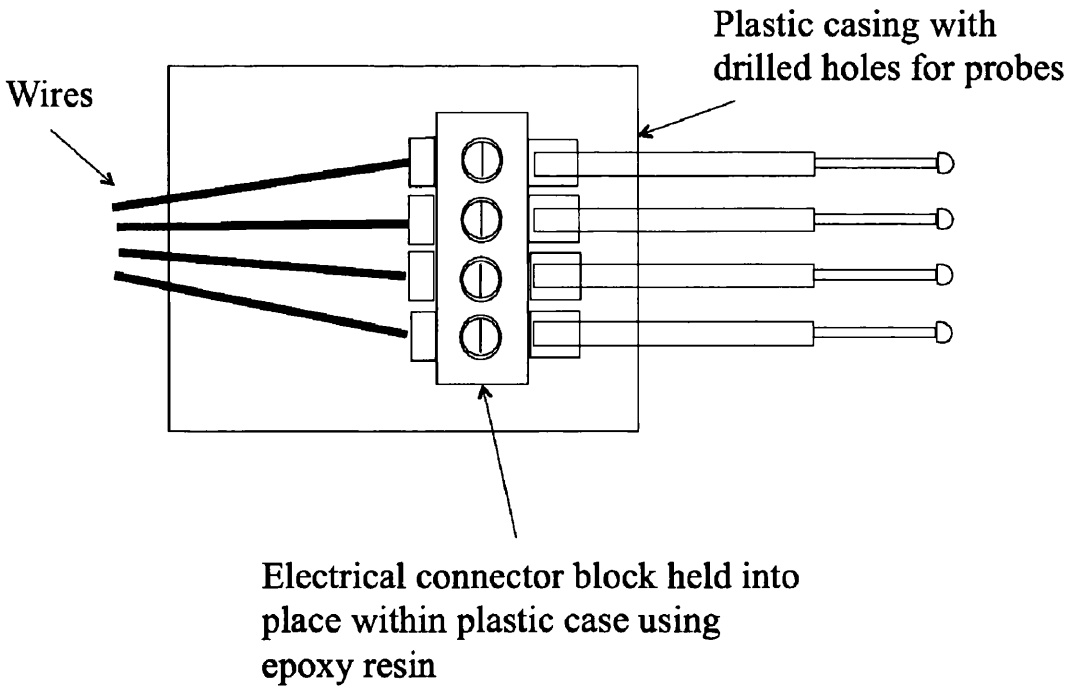

Figure 2.11: A schematic representation of the construction of an in-house built 4 point probe.

The probes were slotted through the drilled holes in the plastic casing, positioned correctly, and then epoxy resin was applied to the arrangement and left to set in order to hold the connector block in place. Low resistance wire was connected to each probe using the connection block. Test plugs were attached to the ends of the wires, and the system was then ready for use.

The tips were also be interchangeable, by unscrewing probes from the connector block and replacing with different style probes. This allowed a comparison of measurements taken using different tip types for a single device. As a variation to the design in Figure 2.11, a switch was also integrated into one version of the probe as seen in Figure 2.12. Although not essential to the operation of the probe, the switch was utilised in order to be able to position to probe on the surface of a sample before any resistance readings were measured. Once in position the switch could be pressed

and a reading of sheet resistance taken. This resulted in a reduction in damage to the surface of the sample.

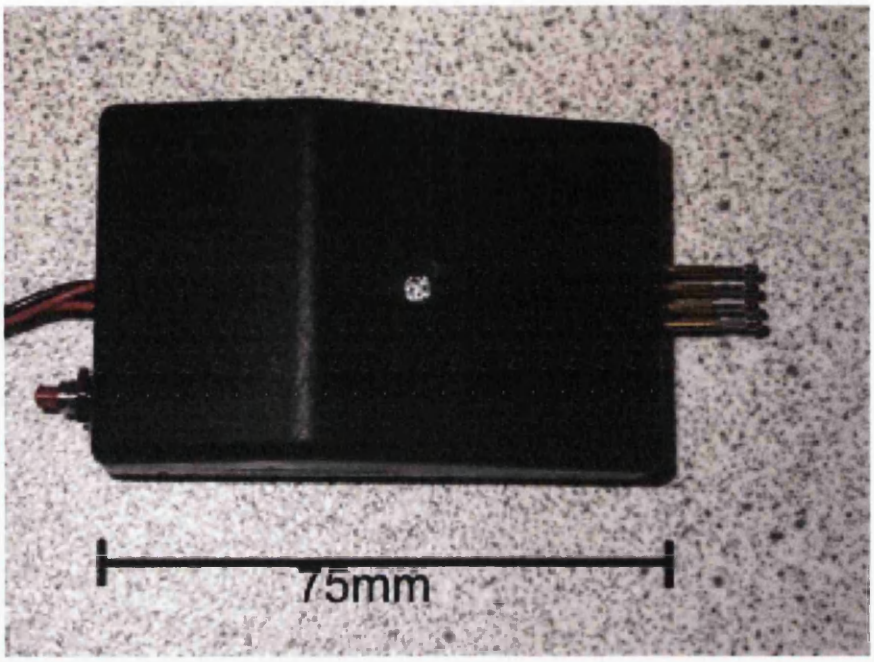

(a)

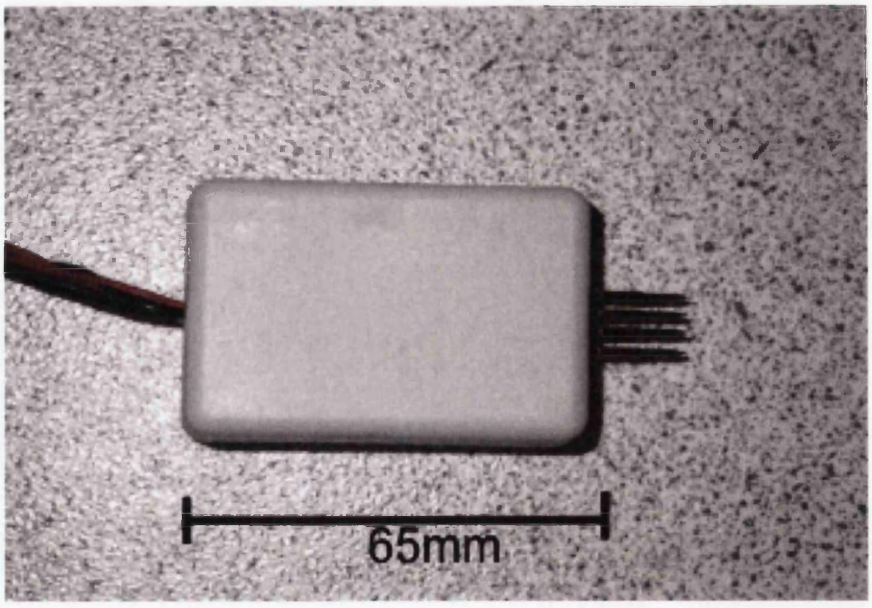

(b)

Figure 2.12: *Photos of the probes constructed for sheet resistance measurements. (a) Spherical tip four point probe. (b) Pointed tip four point probe*

2.7 DC Magnetron Sputtering Procedure

A schematic of the PVD processes used can be seen in Figure 2.13. All thin metallic coated films were produced in house through the use of a Kurt J. Lesker PVD 75 magnetron sputtering equipment. Samples to be sputter coated were firstly cleaned with ethanol to remove any organic contamination on the surface. Samples were left for around 10 minutes to dry in air at room temperature. Samples were placed and fixed onto the substrate holder using small grub screws. The substrate holder was then mounted into the Kurt J. Lesker deposition chamber. The target material was loaded into the source and the chamber was then evacuated. Once the chamber has reached a stable vacuum of around 1 x 10^{-3} Torr, argon gas was introduced to the chamber and power was supplied to the PVD source through a D.C. power supply. Argon plasma was created in the vicinity of the source and argon ions were attracted towards the surface of the target by a magnetron within the PVD source and sputtering was under way. The argon ions dislodged the target species atoms that were then transported towards the samples at the substrate holder where they form a mechanical bond with the surface of the sample. Once a suitable thickness, monitored through the use of a piezoelectric crystal, had been deposited, the power/argon flow is zeroed and the chamber is returned to atmospheric pressure by venting with nitrogen gas. Samples are then removed for analysis.

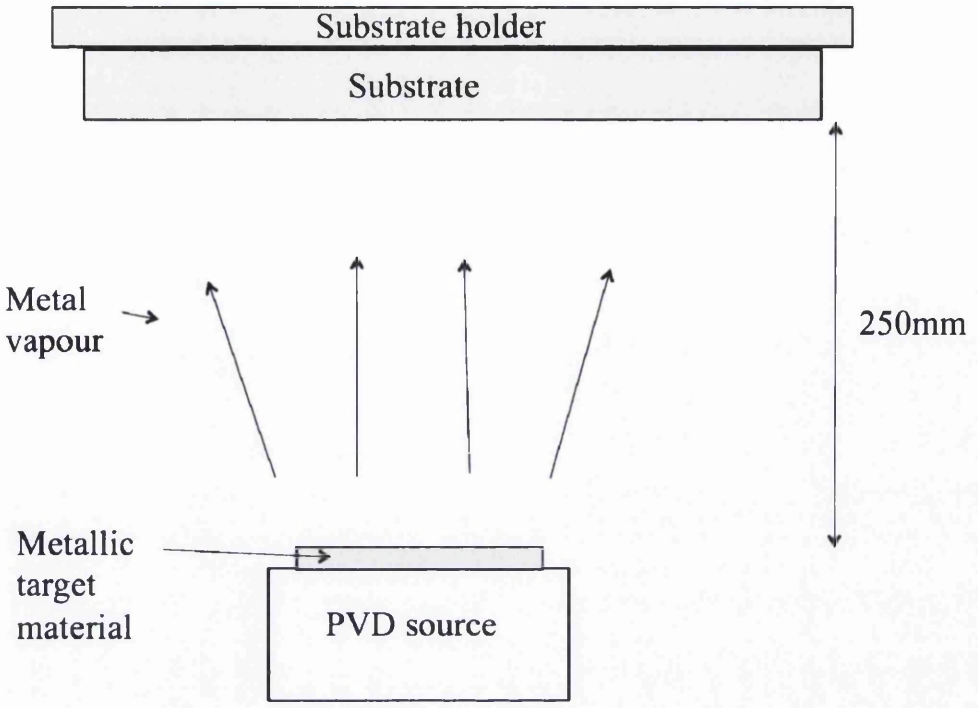

Figure 2.13: *A diagram to represent the deposition chamber for PVD coating.*

2.7.1 Deposition of Titanium Films

A Ti target with 99.995% purity was used. The deposition chamber was evacuated by equilibrating the chamber to a pressure of 1 x 10^{-3} Torr. Films were deposited using an argon flow rate of 30 cubic centimetres per second, and 250 watts of D.C. power. Film thicknesses were controlled using a piezoelectric crystal thickness monitor within the PVD equipment. A deposition rate of 1 $\overset{o}{A}$ s^{-1} was achieved.

2.7.2 Deposition of Aluminium Films

An Al target with 99.998% purity was used. The deposition chamber was evacuated by equilibrating the chamber to a pressure of 1 x 10^{-3} Torr. Films were deposited using an argon flow rate of 30 cubic centimetres per second, and 250 watts of D.C.

power. Film thicknesses were controlled using a piezoelectric crystal thickness monitor within the PVD equipment. A deposition rate of 2.5 $\overset{o}{A}\ s^{-1}$ was achieved.

2.7.3 Deposition of Aluminium – Titanium bilayer Films

Aluminium – titanium bilayer films were deposited in one procedure through the use of two separate PVD sources upon polyimide coated ECCS samples. Aluminium was deposited firstly and thicknesses were held constant at 500nm. Following the deposition of the aluminium film, various thicknesses, 500,1000 and 2000nm of titanium were then deposited on top of the aluminium under the same vacuum. Deposition parameters were consistent with those mentioned in section 2.7.1 and 2.7.2.

2. 8 Experimental Details of Work in Chapter 3

2.8.1 Materials

Pure iron foil of 1.5 mm thickness (99.99%, Goodfellow Metals Ltd) was cut into 60 × 60 mm coupons, with countersunk holes drilled into each corner. Pre existing surface contamination was removed by low pressure (20 psi) bead blasting using soda lime glass beads of 106 – 212 μm diameter (Guyson International Ltd). The sample surface was cleaned using aqueous detergent solution followed by rinsing with water. Any remaining contamination was removed by a 10 minute acetone degrease in an ultrasonic bath, followed by an ethanol rinse and drying in a pressurised stream of air.

2.8.2 Deposition of a PVD Aluminium Wedge

Figure 2.14 shows the details of how a PVD wedge of Al was produced on an iron substrate. The Kurt J Lesker PVD75 Physical Vapour Deposition system as detailed in section 2.7 was used to deposit a wedge of Al on an iron substrate, however a slight variation to the procedure explained is detailed here. The Al "wedge" was achieved by integrating a sliding shutter arrangement within the PVD apparatus. This allowed the deposition a thin film Al "wedge" of progressively increasing thickness over a single iron substrate as indicated in Figure 2.14, with the thickness-distance profile being controlled by the rate of retraction of the shutter which was set at 0.063mm s^{-1}. A piezoelectric crystal thickness monitor was used to measure the coating thickness. Deposition parameters were consistent with those detailed in section 2.7.2.

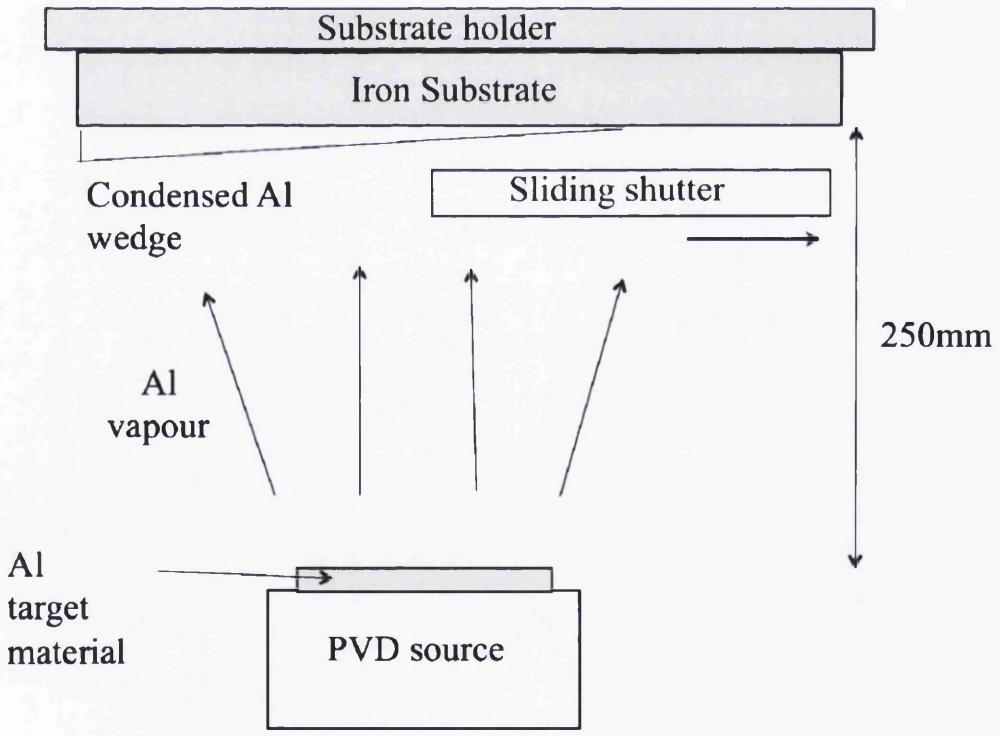

Figure 2.14: *Schematic diagram showing the principle of physical vapour deposition of a thin film wedge of condensed aluminium on an iron substrate.*

The sample was prepared in such a way that it could be attached to a stainless steel sample holder using four countersink head machine screws. The purpose of mounting the sample in this way was to ensure that it was held flat and that the method of fixing did not interfere with the sliding shutter used during the subsequent deposition process. Vacuum compatible polyimide tape (CHR K250 Saint-Gobain Performance Plastics) was used to mask all areas of the sample where aluminium deposition was not required as shown in Figure 2.15 (part i). The sample holder complete with sample was then loaded into the vacuum chamber of a Kurt J Lesker PVD75 Physical Vapour Deposition system. Using the process parameters given in section 2.7.1 along with the shutter retraction rate of 0.063mm s^{-1}, an aluminium film, varying linearly in thickness from 0 to 110 nm, was deposited in the unmasked area using a sliding shutter arrangement in the following way. Prior to beginning deposition, the sliding shutter was positioned as shown in Figure 2.15 (part ii), such that all the unmasked area was covered. During the subsequent deposition phase, the shutter was withdrawn at a constant rate of 0.063mm s^{-1}, thereby progressively exposing a greater portion of the unmasked sample surface. The shutter transfer rate was calculated as a function of the deposition time required to lay down the thickest portion of the film and the distance over which it must travel. The deposition was stopped when all the unmasked area was exposed. A schematic diagram of the final sliding shutter position and the coating cross section is given in figure 2.15 (part iii), while full details of the various parameters employed to deposit thin film Al are shown in Table 1.

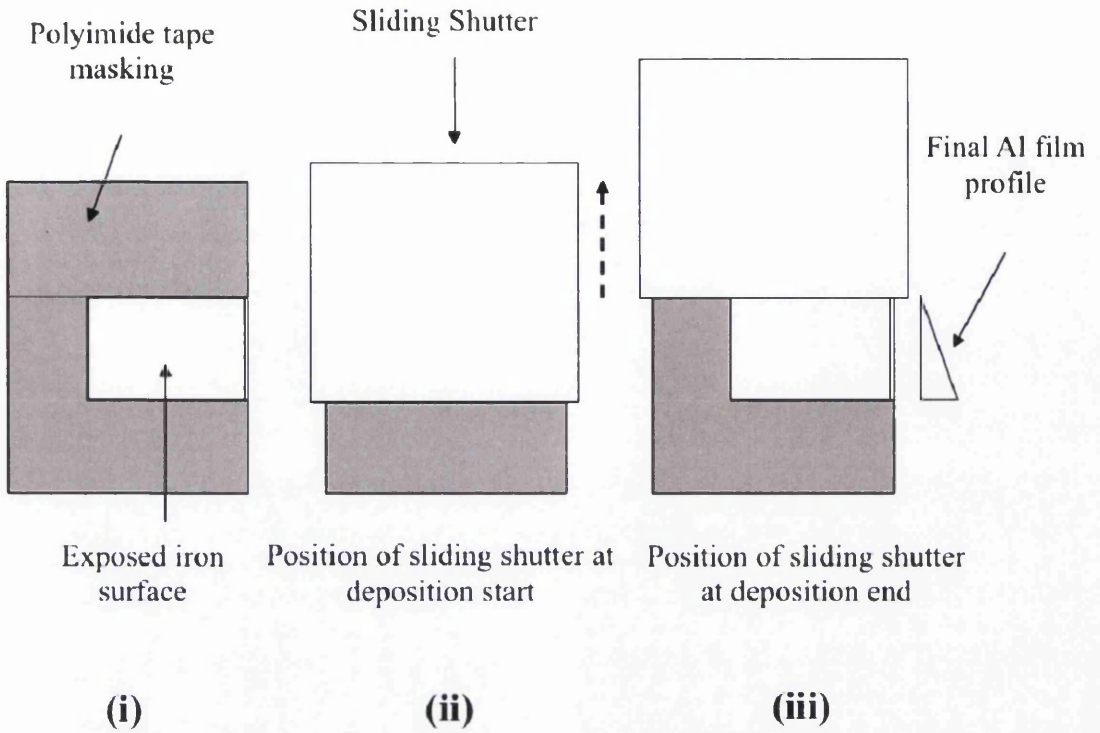

Figure 2.15: *Plan view diagram showing, i) exposed area of Fe substrate demarked by polyimide tape masking, ii) Sliding shutter position at start of aluminium deposition and iii) Sliding shutter position at end of aluminium deposition and resulting aluminium film thickness profile.*

2.8.3 Preparation of Organic Coated Al PVD "Wedge" on Iron Sample

Polyvinyl butyral (PVB) coatings were applied to the prepared substrate as shown in Figure 2.16a. Polyvinyl butyral-*co*-vinyl alcohol-*co*-vinyl acetate (PVB), mol weight 70,000 – 100,000, was obtained from the Aldrich Chemical Company. Prior to coating, a 60 × 15 mm strip of clear adhesive tape was placed over an area close to one edge of the coupon. The strip ran parallel with the thin Al wedge and was positioned so that its inner edge was *ca.* 4 mm distant from the interface with the wedge so that a 4 × 36 mm area of iron was left exposed. Two parallel strips of insulating tape (60 × 10 mm) were then laid down at right angles to the adhesive tape, leaving a 40 × 45 mm area comprising the Al wedge and adjacent 4 mm wide strips of exposed iron at mutual right angles as shown in Fig 2.16a. An ethanolic

PVB solution of 16 wt% was bar cast onto this region, using the insulating tape as a height guide for the casting bar, and air-dried to give a strongly adherent film of 30 μm thickness, as determined using a micrometer screw gauge. Following the approach of Stratmann *et al* [24, 25] a coating defect was then created by cutting and lifting the clear adhesive tape to reveal a 40 × 15 mm area of bare metal to which corrosive electrolyte was subsequently applied. A schematic diagram of the PVB-coated test specimen comprising the penetrative coating defect is given in Figure 2.16b. The residual lip of clear adhesive tape and overcoated PVB formed a convenient barrier between the intact polymer coated metal surface and the electrolyte applied to the defect area. Non-corrosive silicone rubber was applied to the remaining edges of the defect to form a reservoir sufficient to contain a 2 cm^3 volume of corrosive electrolyte.

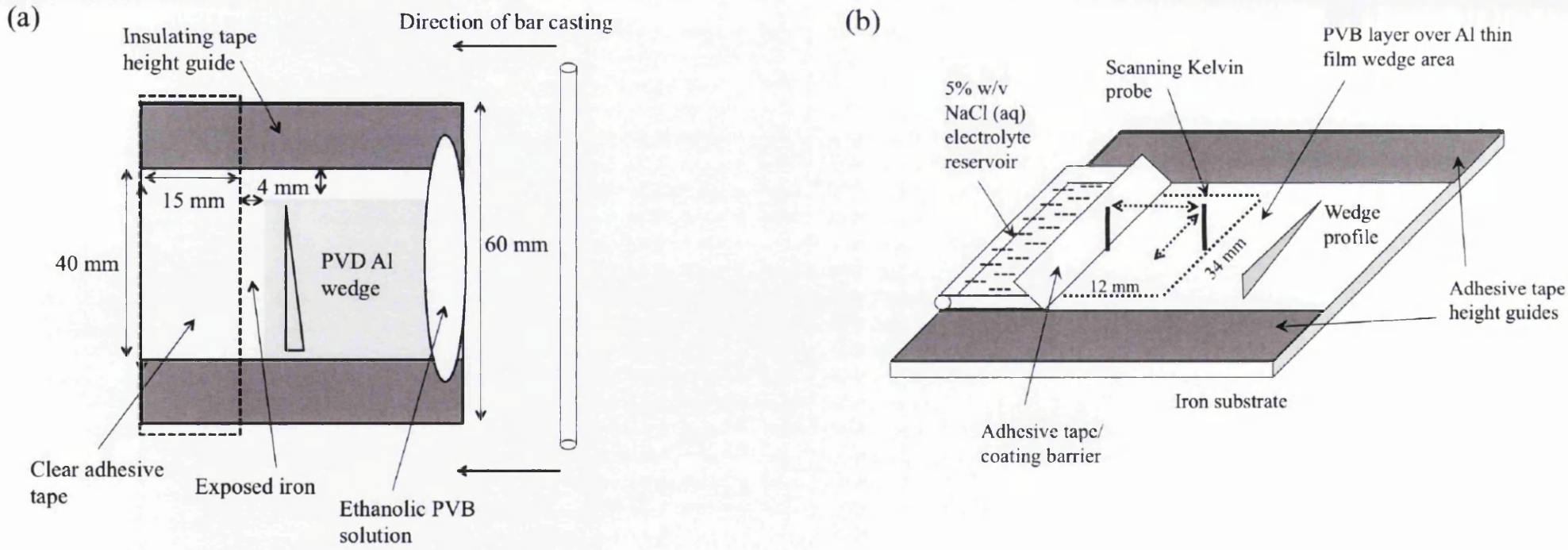

Figure 2.16: *Schematic representation of (a) sample orientation and arrangement of masking tapes employed during PVB coating procedure, and (b) sample configuration used for in-situ SKP analysis of corrosion-driven organic coating delamination via a cathodic disbondment mechanism.*

2.9 References

1. B. Navinsek, P. Panjan, I. Milosev, "PVD coatings as an environmentally clean alternative to electroplating and electroless processes", *Surface and Coatings Technology*, 1999, 116–119, p. 476–487.
2. B. Schuhmacher, W. Muschenborn, M. Stratmann, B. Schultrich, C.-P. Klages, M. Kretschmer, U. Seyfert, F. Forster, H.-J. Tiller, "Novel coating systems and surface technologies for continuous processing of steel sheet", *Advanced Engineering Materials*, 2001, 3, p. 681-689.
3. B. Schuhmacher, C. Schwerdt, U. Seyfert, O. Zimmer, "Innovative steel strip cotings by means of PVD in a continuous pilot line: process technology and coating development", *Surface and Coatings Technology*, 2003, 163–164, p. 703–709.
4. E. Reinhold, J. Richter, U. Seyfert, C. Steuer, "Metal strip coating by electron beam PVD-industrial requirements and customized solutions", *Surface and Coatings Technology*, 2004, 188–189, p. 708–713.
5. L. Baptiste, N. van Landschoot, G. Gleijm , J. Priede, J. Schade van Westrum , H. Velthuis, T. Y. Kim, "Electromagnetic levitation: A new technology for high rate physical vapour deposition of coatings onto metallic strip", *Surface and Coatings Technology*, 2007, 202, p. 1189–1193.
6. E. Reinhold, J. Faber, "Large area electron beam physical vapor deposition (EB-PVD) and plasma activated electron beam (EB) evaporation - Status and prospects", *Surface and Coatings Technology*, 2011, 206, p. 1653–1659.
7. C. Metzner, B. Scheffel, "Special aspects concerning the electron beam deposition of multicomponent alloys", *Surface and Coatings Technology*, 2001, 146–147, p. 491-497.
8. B. Scheffel, C. Metzner, O. Zywitzki, J Faber, "High-rate physical vapour deposition in combination with plasma processes for metal strip coating", *Galvatech 2001: 5th International Conference on Zinc and Zinc Alloy Coated Steel Sheet; Brussels; Belgium; June 2001. pp. 35-41.*

9. N. C. Hosking, M. A. Strom, P. H. Shipway, C. D. Rudd, "Corrosion resistance of zinc-magnesium coated steel", *Corrosion Science*, 2007, 49, p. 3669–3695.

10. M. H. Fathi, M. Salehi, A. Saatchi, V. Mortazavi, S. B. Moosavi, "In vitro corrosion behaviour of bioceramic, metallic and bioceramic metallic coated stainless steel implants", *Dental Materials*, 2003, 19, p. 188-198.

11. S. Maeng, L. Axe, T.A. Tyson, L. Gladczuk, M. Sosnowski, "Corrosion behaviour of magnetron sputtered α- and β-Ta coatings on AISI 4340 steel as a function of coating thickness", *Corrosion Science*, 2006, 48, p. 2154-2171.

12. I. Suzuki, Corrosion Resistant Coatings, Marcel Dekker, New York, (1989).

13. H. Dafydd, D. A. Worsley, H. N. McMurray, "The kinetics and mechanism of cathodic oxygen reduction on zinc and zinc–aluminium alloy galvanized coatings", *Corrosion Science*, 2005, 47, p. 3006-3018.

14. V. Jovancicevic, J. O'M. Bockris, "The Mechanism of Oxygen Reduction on Iron in Neutral Solutions", *Journal of the Electrochemical Society*", 1986, 133, p. 1797-1807.

15. E. L. Koehler, "The influence of contaminants on the failure of organic protective coatings on steel", *Corrosion*, 1977, 33, p. 209-213.

16. H. Leidheiser Jr, "Corrosion of Painted Metals-A Review", *Corrosion*, 1982, 38, p. 374-383.

17. H. Leidheiser Jr, M. W. Kendig, "Mechanism of Corrosion of Polybutadiene-Coated Steel in Aerated Sodium Chloride", *Corrosion*, 1979, 32, p. 69-76.

18. H. Leidheiser Jr., W. Wang, "Some substrate and environmental influences on the cathodic delamination of organic coatings", *Journal of Coatings Technology*, 1981, 53, p. 77–84.

19. H. Leidheiser Jr., "Cathodic delamination of polybutadiene from steel", *Journal of Adhesion Science Technology*, 1987, 1, p. 79–98.

20. J. J. Ritter, "Ellipsometric Studies on the Cathodic Delamination of Organic Coatings on Iron and Steel", *Journal of Coatings Technology*, 1982, 54, p. 51-57.

21. H. Leidheiser, W. Wang, L. Igetoft, "The mechanism for the cathodic delamination of organic coatings from a metal surface", *Progress in Organic Coatings*, 1983, 11, p. 19-40.

22. E. J. Koehler, "The Mechanism of Cathodic Disbondment of Protective Organic Coatings-Aqueous Displacement at Elevated pH.Corrosion", 1984, 40, p. 5-8.

23. M. Stratmann, H. Streckel, R. Feser, "A new technique able to measure directly the delamination of organic polymer films", *Corrosion Science*, 1991, 32, p. 467-470.

24. M. Stratmann, R. Feser, A, Leng, Corrosion protection by organic films, Electrochim. Acta, 1994, 39, p. 1207-1214,

25. A. Leng, H. Streckel, M. Stratmann, "The delamination of polymeric coatings from steel. Part 1: Calibration of the Kelvinprobe and basic delamination mechanism", *Corrosion Science*, 1991, 41, p. 547-578.

26. G. Williams and H. N. McMurray, "Chromate inhibition of corrosion driven organic coating delamination studied using a scanning Kelvin probe technique", *Journal of the Electrochemical Society*, 2001, 148, p. B377-B385.

27. S. A. Katz and H. Salem, "The toxicology of chromium with respect to its chemical speciation: a review", *Journal of Applied Toxicology*, 1993, 13, p. 217-224.

28. S. Langard and T. Norseth, "A cohort study of bronchial carcinomas in workers producing chromate pigments", *British Journal of Industrial Medicine*, 1975, 32, p. 62-65.

29. J. J. Caprari, A. R. Di Sarli, B. del Amo, "Zinc phosphate as corrosion inhibitive pigment of waterborne epoxy paints used for steel protection", *Pigment & Resin Technology*, 2000, 29, p. 16-22.

30. S. V. Lamaka, M. L. Zheludkevich, K. A. Yasakau, R. Serra, S. K. Poznyak, M. G. S. Ferreira, "Nanoporous titania interlayer as reservoir of corrosion inhibitors for coatings with self-healing ability", *Progress in Organic Coatings*, 2007, 58, p. 127-135.

31. D. Snihirova, S. V. Lamaka, M. Taryba, A. N. Salak, S. Kallip, M. L. Zheludkevich, M. G. S. Ferreira, M. F. Montemor, "Hydroxyapatite Microparticles as Feedback-Active Reservoirs of Corrosion Inhibitors", *ACS Applied Materials and Interfaces*, 2010, 2, p. 3011–3022.

32. J. Carneiro, J. Tedim, S. C. M. Fernandes, C. S. R. Freire , A. J. D. Silvestre , A. Gandini, M. G. S. Ferreira, M. L. Zheludkevich, "Chitosan-based self-healing protective coatings doped with cerium nitrate for corrosion protection of aluminum alloy 2024", *Progress in Organic Coatings*, 2012, 75, p. 8-13.

33. G. Williams, H. N. McMurray and D. A. Worsley, "Ce(III) inhibition of corrosion driven organic coating studied by a scanning Kelvin probe technique", *Journal of the Electrochemical Society*, 2002, 149, p. B154-B162.

34. G. Williams, H. N. McMurray and M. J. Loveridge, "Inhibition of Corrosion-Driven Organic Coating Disbondment on Galvanised Steel by Smart Release Group II and Zn(II)-Exchanged Bentonite Pigments", *Electrochimica Acta.*, 2010, 55, p. 1740-1748.

35. G. Williams, S. Geary and H. N. McMurray, "Smart Release Corrosion Inhibitor Pigments based on Organic Ion-Exchange Resins", *Corrosion Science*, 2012, 57, p. 139-147.

36. S. P. V. Mahajanam, R. G. Buchheit, "Characterization of Inhibitor Release from Zn-Al-$[V_{10}O_{28}]^{6-}$ Hydrotalcite Pigments and Corrosion Protection from Hydrotalcite-Pigmented Epoxy Coatings", *Corrosion*, 2008, 64, p. 230-240.

37. M. L. Zheludkevich, S. K. Poznyak, L. M. Rodrigues, D. Raps, T. Hack, L. F. Dick, T. Nunes, M. G. S. Ferreira, "Active protection coatings with layered double hydroxide nanocontainers of corrosion inhibitor", *Corrosion Science*, 2010, 52, p. 602–611.

38. J. M. Vega, N. Granizo, D. de la Fuente, J. Simancas, M. Morcillo, "Corrosion inhibition of aluminum by coatings formulated with Al–Zn–vanadate hydrotalcite", *Progress in Organic Coatings*, 2011, 70, p. 213-219.

39. G. Williams and H. N. McMurray, "Inhibition of Filiform Corrosion on Organic-Coated AA2024-T3 by Smart-Release Cation and Anion-Exchange Pigments", *Electrochimica Acta*, 2012, 69, p. 287-294.

40. W. G. Ji, J. M. Hu , L. Liu, J. Q. Zhang, C. N. Cao, "Improving the corrosion performance of epoxy coatings by chemical modification with silane monomers", *Surface Coatings Technology*, 2007, 201, p. 4789-4795.

41. P. Wang, D. W. Schaefer, "Why does Silane Enhance the Protective Properties of Epoxy Films?", *Langmuir*, 2008, 24, p. 13496-13501.

42. T. Titz, F. Hörzenberger, K. Van den Bergh, G. Grundmeier, "Correlation of interfacial electrode potential and corrosion resistance of plasma polymer coated galvanized steel. Part 1: Ultra-thin plasma polymer films of varying thickness", *Corrosion Science*, 2010, 52, p. 369–377.

43. T. Titz, F. Hörzenberger, K. Van den Bergh, G. Grundmeier, "Correlation of interfacial electrode potential and corrosion resistance of plasma polymer coated galvanized steel. Part 2: Influence of forming induced defects", *Corrosion Science*, 2010, 52, p. 378–386.

44. G. Williams and H. N. McMurray, "The mechanism of group (I) chloride initiated filiform corrosion on iron", *Electrochemistry communications*, 2003, 5, p. 871 -877.

45. G. Williams and H. N. McMurray, "The kinetics of chloride-induced filiform corrosion on aluminium alloy AA2024-T3", *Journal of the Electrochemical Society*, 2003, 150, p. B380 – B388.

46. G. Williams and R. Grace, "Chloride-induced filiform corrosion of organic coated magnesium", *Electrochimica Acta*, 2011, 56, p. 1894-1903.

47. G. Grundmeier, M. Stratmann, "Adhesion and de-adhesion processes at polymer/metal interfaces", *Annual Review in Materials Research*, 2005, 35, p. 571–615.

48. G. Grundmeier, W. Schmidt, M. Stratmann, "Corrosion protection by organic coatings: electrochemical mechanism and novel methods of investigation", *Electrochimica Acta*, 2005, 45, p. 2515–2533.

49. G. Williams, H. N. McMurray, D. A. Worsley, "Latent fingerprint detection using a scanning Kelvin microprobe", *Journal of Forensic Science*, 2001, 46, p. 1085-1092.

50. O. Ozkanat, B. Salgin, M. Rohwerder, J. M. C. Mol, J. H. W. de Wit and H. Terryn, "Scanning Kelvin Probe Study of (Oxyhydr)oxide Surface of Aluminum Alloy", *Journal of Physical Chemistry C*, 2012, 116, p. 1805-1811.

51. D. A. Jones, N. R. Nair, "Electrochemical corrosion studies on zinc coatings on steel", *Corrosion*, 1985, 41, p. 357-362.

52. R. Vera, D. Delgado, B. M. Rosales, "Effect of atmospheric pollutants on the corrosion of high power electrical conductors: Part 1. Aluminium and AA6201 alloy", *Corrosion Science*, 2006, 48, p. 2882-2900.

53. Yong-Ji Song, Shuang_He Meng, Fu-Dong Wang, Cai-Xia Sun, Zhi-Cheng Tan, "Thermochemical study on the properties of polyimide BPADA-m-PDA", *Thermochimica Acta*, 2002, 389, p. 19-24.

54. J. C. Li, Y. Wang, D. C. Ba, "Characterization of semiconductor surface conductivity by using microscopic four-point probe technique", *Physics Procedia*, 2012, 32, p. 347-355.

Chapter 3

Preventing Cathodic Disbondment of Organic Coatings on Iron Substrates

This chapter describes a combinatorial investigation of the influence of physical vapour deposited aluminium thin films on the kinetics of organic coating cathodic delamination from iron. The principal aim of this body of work was to evaluate the use of in-situ SKP in conjunction with an organically-coated, thin Al wedge-deposited Fe sample, as a high-throughput method of studying the influence of varying thickness of a cathodic blocking film on underfilm corrosion rates. A second aim was to establish a threshold film thickness of PVD Al which would, under atmospheric corrosion conditions, halt the progress of a cathodic disbondment front by stopping interfacial oxygen reduction at the metal-coating interface. Work described here gives a successful insight in to slowing organic underfilm disbondment through the use of very small thicknesses of PVD Al deposited on iron substrates. However, this work describes a potential problem that may occur even in situation where cathodic disbondment of the organic film has been halted. Anodic disbondment has been reported through the observation of filliform corrosion progressing beneath the organic coating due to the presence of chloride anions within a defect electrolyte.

3.1 Introduction

Of the various technologies currently available, physical vapour deposition (PVD) [2,3] and its high deposition rate variant Electron Beam (EB) PVD [4 - 6] are considered to be the most promising and economically viable method of depositing thin coatings on an industrial scale via a clean process. This is largely because PVD

technology allows a sufficiently high deposition rates to enable the application of thin film coatings to strip products *via* a continuous or semi-continuous process [2 – 4]. In contrast, other rival methods such as magnetron sputtering or chemical vapour deposition cannot produce layers of sufficient thickness in the timescales required for coil coating-type production [1,3]. Although large scale EB-PVD technologies have been used successfully to deposit decorative and functional metallic or ceramic films on steel-based surfaces [4 - 6], it is the potential of a thin metallic PVD layer to provide corrosion protection to the underlying substrate which is of interest to the work described here.

The subject of PVD based coatings as direct replacements for traditional galvanic (zinc or cadmium) or barrier-type (nickel) corrosion resistant metallic layers has been reviewed comprehensively elsewhere [1]. It is not the intention here to re-tread the same ground, hence only recent developments since the 1999 publication date of this review [1] will be discussed here. In the intervening period the focus has shifted from single metal films to alloy systems [7,8], or single metals which can subsequently be thermally interdiffused with the substrate, to form an alloyed surface layer, such as magnesium on zinc-coated (galvanised) steel [9]. In addition, highly efficient, corrosion-resistant thin coatings based on metals such as titanium [10] and tantalum [11], which develop highly protective passive films, have also been demonstrated on surfaces such as stainless and carbon steels respectively.

The work described here employs a different approach to these previous studies, where the PVD coating served directly as a corrosion resistant or sacrificial layer in a corrosive environment, typically a chloride containing solution [1,9 – 11]. In this study, the PVD layer has been over-coated with a polyvinyl butyral (PVB) protective barrier layer, to replicate the action of a paint film in providing corrosion protection to a metal substrate. The inclusion of the PVD layer is explored as a method of de-activating the surface of an underlying iron (Fe) substrate to underfilm corrosion processes. Aluminium has been selected as the PVD layer, since it is known to be a poor electrocatalytic surface for oxygen reduction [12,13], whereas Fe is an excellent oxygen reduction electrocatalyst [14]. As such, one of the major modes of failure of

organic coated Fe surfaces is *via* corrosion-driven delamination by a cathodic disbondment mechanism. Here an oxygen concentration cell is established in which a thin layer of electrolyte, ingressing beneath the delaminated coating, couples anodic metal dissolution at a penetrative defect to cathodic oxygen reduction occurring near sites of coating disbondment. [15 - 25]. The alkaline environment, which forms at the cathode, promotes coating disbondment from the underlying iron through polymer degradation and the hydrolysis of interfacial bonds [15 - 25].

The conventional approach to preventing corrosion-driven organic coating failure is to disperse corrosion-inhibiting pigments within the polymer solution prior to paint application. The most effective anti-corrosion pigment technologies are those based upon sparingly soluble salts of chromium (VI) anions, such as zinc or strontium chromate, which have been demonstrated to profoundly inhibit the cathodic disbondment process due to the fact that these salts react in preference with any oxygen present to prevent it reaching the underlying metal [26]. However, the known toxicity [27] and carcinogenic nature of chromium (VI)-containing compounds [28] has resulted in increasing pressure to develop practical alternatives. Although non-chromate pigments based on phosphate technologies are in common use, they are considered to provide an inferior level of corrosion protection [29]. Recent developments in the field of chromate-based pigment replacements include the use of nano-container [30 - 32] and ion exchange [33 - 39] technologies as intelligent-release delivery systems of inhibitor ions within organic coatings. The use of such an approach has allowed promising corrosion inhibitors species, such as trivalent cerium [30 - 33] and divalent calcium cations [34,35] or vanadate anions [36 - 39], to be incorporated within organic coatings and assessed with regard to their efficiency of protection. In addition, recent work has also demonstrated that alternative additives to the organic coating, such as silane coupling agents [40,41] can also bestow improved corrosion protection of the underlying metal substrate.

An alternative approach to halting or slowing organic coating failure via cathodic disbondment has recently been demonstrated by Grundmeier *et al*, using a plasma deposition technique to create thin, electrically insulating silica-like layers on a steel

surface, prior to the application of an organic coating [42,43]. The silica-like layers were shown to depress underfilm corrosion potential and act as a barrier to underfilm electron transfer, thus disfavouring cathodic oxygen reduction and halting the progress of a cathodic delamination front [42]. A similar methodology is used in this present work, although the emphasis here was to employ physical vapour deposition of thin aluminium layers to block underfilm cathodic oxygen reduction on organic coated iron substrates. Even though aluminium is not electronically insulating, the thick protective oxide present on the surface of PVD may act as a barrier to oxygen reaching the surface of the aluminium-iron interface, establishing a poor cathode system for cathodic oxygen reduction, hence halting progress of a cathodic delamination front. A further innovation described here is to use a high-throughput approach to investigate the influence of Al film thickness on the kinetics of the underfilm cathodic disbondment process. This was achieved by integrating a sliding shutter arrangement within the PVD apparatus, as detailed in section 2.8.2.

The iron substrate, complete with thin film Al wedge is subsequently overcoated with a model polyvinyl butyral (PVB) organic coating, as detailed in section 2.8.3, which has been employed in several recent works as a model "paint" system allowing the efficiency of novel corrosion inhibitor pigments to be evaluated [33–35, 39] and local underfilm corrosion mechanisms to be investigated [44 - 46]. In this work, the organic coated substrate was prepared by incorporating a well-defined coating defect in such a way that coating delamination proceeds by a cathodic disbondment mechanism, once initiated by application of corrosive electrolyte to the defect.

In the work reported here, an *in situ* scanning Kelvin probe (SKP) technique was used to follow the delamination kinetics of the model organic coating adherent to the Al film wedge-deposited iron substrate. The technique is now a firmly established method of measuring free corrosion potentials (E_{corr}) of organic coated metals held in humidified air [23-26, 44-48]. By following changes in spatially resolved E_{corr} distributions which mark the onset of an underfilm disbondment front, the kinetics of delamination were conveniently monitored [23-26]. In this work aerated 5% w/v

aqueous sodium chloride (NaCl) has been used as the experimental electrolyte in order to reflect standard accelerated corrosion test conditions.

3.2 Experimental Methods

The procedures adopted in the sample production and preparation, for the organic coating delamination studies, are detailed in section 2.8. All delamination experiments were carried out at 20°C using 5% w/v (0.86 mol dm^{-3}) aqueous NaCl at pH 6.5 and a constant relative humidity of 95 %. A scanning Kelvin probe (SKP) reference electrode was scanned over the coated surface along 12 mm lines normal to, and adjacent with the defect-coating boundary enabling profiles of free corrosion potential versus distance to be obtained on regions of the PVB-coated surface comprising varying thicknesses of thin-film Al at the metal-coating interface. The sample orientation and location of the scanned area with respect to the coating defect region are shown in Figure 3b. Kelvin probe scans were conducted immediately after the addition of electrolyte and thereafter at hourly intervals over a 24 h period using a reference probe-to-sample air gap of 100 μm and recording 20 free corrosion potential (E_{corr}) data points per mm along individual lines. Scans were conducted in order to reveal information of corrosion activity beneath the surface of the organic coating. Full details about the SKP instrumentation and calibration procedure employed in this work are given elsewhere and are detailed in section 2.5.3 [26,49].

Samples used to investigate the susceptibility of organic coated, thin-Al deposited iron substrates to underfilm corrosion *via* an anodic disbondment mechanism were prepared in a different way. A 100 nm thick Al film was deposited by PVD onto a cleaned Fe substrate without employing the sliding shutter arrangement. The surface was subsequently coated with an ethanolic solution of PVB as described above, but the coating defect was created by a scribing a central region of the coated surface (10 mm) using a scalpel. Underfilm corrosion was initiated by applying a 1 μL quantity of 1 mol dm^{-3} HCl (aq) to the coating defect by means of a microlitre syringe. The sample was subsequently maintained in air at 20°C and 95% relative humidity for periods of up to 4 days. *In situ* SKP scanning of the corroded surface was carried out

on a sample which comprised 2 parallel coating defect scribes leaving a *ca.* 12 mm distance between. SKP scanning was carried out on a 10 mm square area in between the 2 coating defects, thus alleviating problems of instrument overload caused when the reference probe was scanned directly over the defect region.

3.3 Results and Discussion

3.3.1 High-throughput investigation of coating delamination on a thin film Al wedge on iron

Figure 3.1 shows a series of SKP-derived E_{corr} distribution maps for a PVB-coated Fe substrate comprising a PVD wedge of thin film at the metal-organic coating interface. The E_{corr} distributions, shown as spatially resolved surface maps, were recorded at different intervals following initiation of corrosion-driven coating delamination by applying 5% w/v NaCl (aq) to the artificially produced defect and holding in air at 95% RH. Figure 3.1a, recorded 1h after application of $NaCl_{(aq)}$ but before the onset of underfilm corrosion, shows the location of the thin film Al wedge in relation to the artificial defect and areas of exposed iron at mutual right angles, included in order to establish baseline coating delamination kinetics. The regions of exposed iron are shown as areas of significantly higher E_{corr} (typically between 0 to +0.1 V vs SHE) than the thin-film Al covered section. The progressive increase in the wedge thickness of the Al wedge, in the direction indicated by the direction of the arrow in Figure 3.1a, is marked by a slight decrease in E_{corr} from *ca.* 0 V vs SHE to -0.25 V vs SHE at the point where the wedge is thickest (*ca.* 100 nm). After the onset of underfilm corrosion, Figure 3.1b shows that a cathodic disbondment front has traversed the area of iron adjacent to the defect-coating edge as significantly lower E_{corr} values were observed in this zone. E_{corr} values were up to 0.4V more negative than previously established in Figure 3.1a.

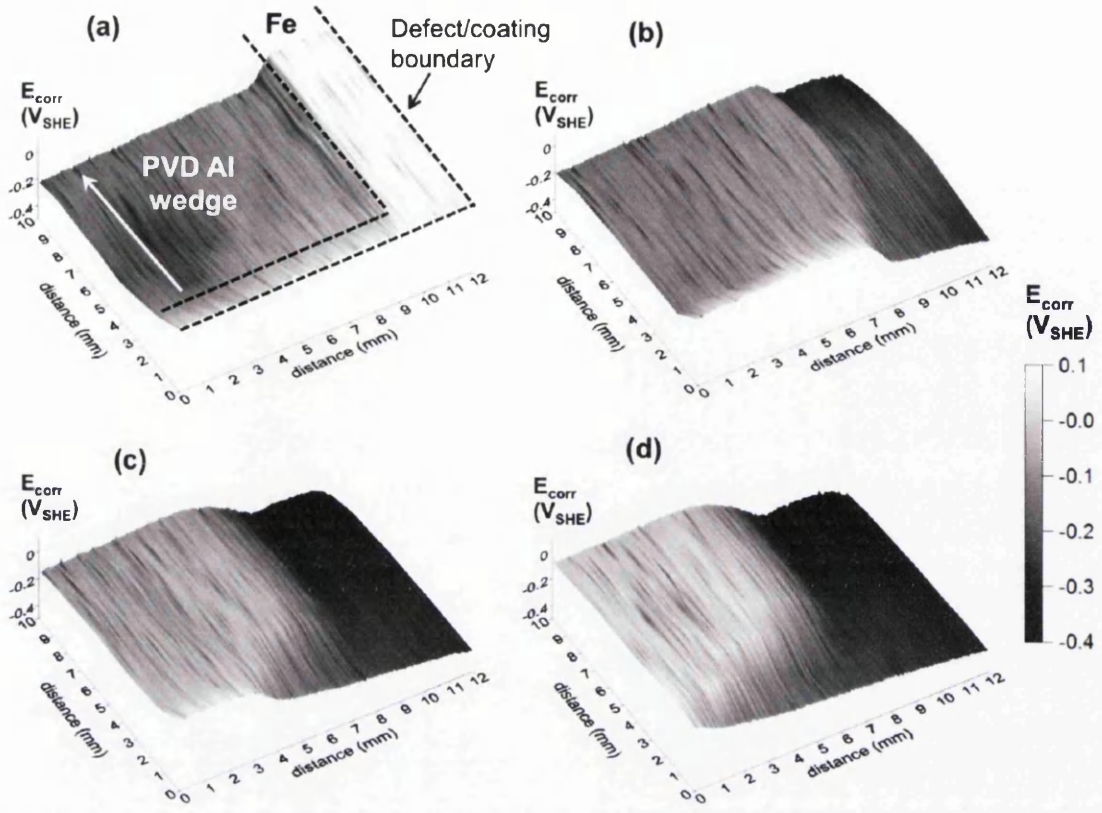

Figure 3.1: *Surface maps showing E_{corr} distributions, measured by in situ SKP, taken over a PVB-coated, thin film Al-wedge deposited Fe substrate following initiation of corrosion by applying 5% w/v NaCl (aq) electrolyte to the coating defect region. Time key: (a) 2h, (b) 7h, (c) 14h and (d) 24h following initiation and holding at a constant relative humidity of 95%.*

The inflection in E_{corr} with distance observed on the bottom edge of the scan area, where a thin strip of iron was also left exposed during Al depositions, indicates the position of the delamination front [23 - 26], confirming previous observations of others who have SKP to establish kinetics of corrosion driven cathodic disbondment on coated steel (iron) surfaces. Further scans recorded at longer holding times of 14 and 24h (Figures 3.1c and 3.1d respectively) show that the point of E_{corr} inflection, and hence the disbondment front, moves further away from the defect region with time. However, in contrast, the potentials in the area occupied by the Al thin film wedge remain largely unaffected. The exception is the bottom right corner of the Al

wedge at its thinnest point, close to the boundaries with exposed iron, where some evidence of more negative E_{corr} values is observed.

Figure 3.2 shows the physical appearance of the corroded specimen following 24h held in air at 95% relative humidity. The defect region, to which an aliquot of 5% w/v NaCl (aq) was initially applied, is seen on the far right of the specimen and shows significant quantities of red rust on the electrolyte covered bare iron surface. Although in-situ SKP measurements have indicated that organic coating delamination has take place on the regions of organic coated iron, in this case the 4 mm strip adjacent to the defect and the 3 mm wide region running along the bottom of the PVB coated area, there is no visible evidence of any underfilm corrosion product. This is consistent with previous observations [25, 44] about the nature of iron in contact with the thin layer of electrolyte which ingresses beneath the organic coating during cathodic disbondment, which will be discussed at length later. Figure 3.2 also indicates the lines along which E_{corr} versus distance profiles were recorded, enabling the influence of Al film thickness on both disbondment rate and local E_{corr} values to be established in a single experiment. Thus in Figure 3.2, line 1 corresponds with a region of the specimen where the PVB organic coating is in direct contact with the underlying iron substrate, while line 10 represents a zone where a 100 nm Al layer is present at the substrate-organic coating interface. Lines 2 – 10 therefore represent zones of progressively increasing Al layer thickness, where the actual thickness value can be calculated from the known wedge thickness profile and the distance of the line from position 1.

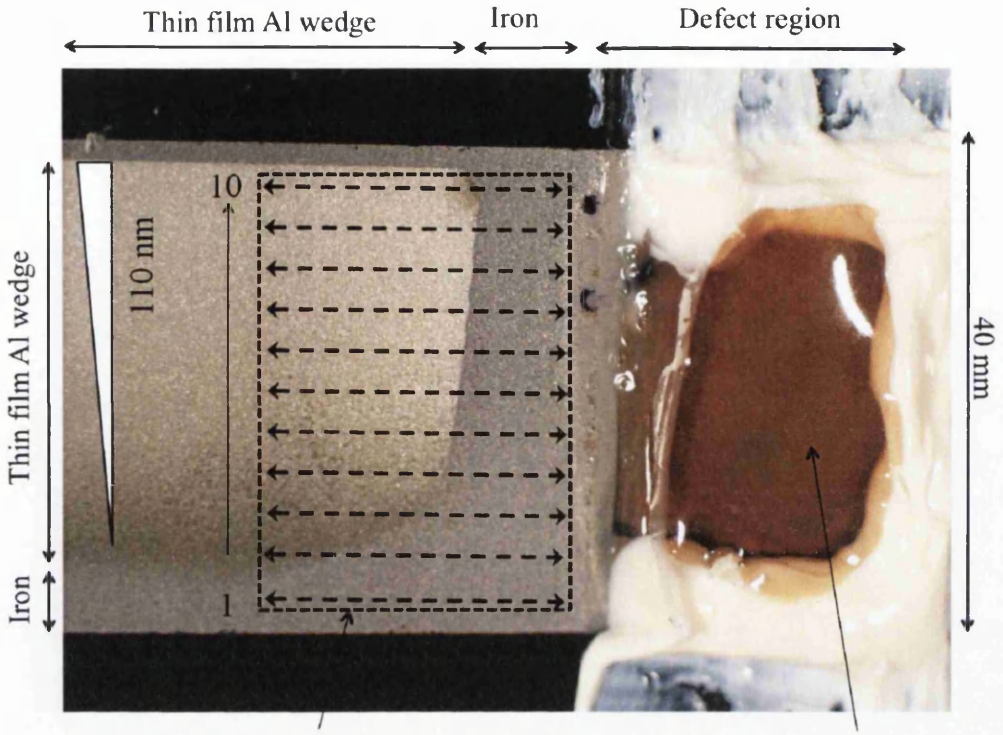

Figure 3.2: *Photographic image of a PVB-coated, thin film Al-wedge deposited Fe sample held at 24h at 95% relative humidity following initiation of corrosion using 5% w/v NaCl (aq). The arrows show the locations where E_{corr} versus distance profiles were recorded.*

The relationships of E_{corr} with distance from the coating defect can perhaps be better understood in Figure 3.3, where individual time-resolved profiles recorded by in-situ SKP at positions 1, 2, 4 and 7 (corresponding to Al layer thicknesses of 0, 4, 14 and 72 nm respectively) are presented. For the sample region where the organic coating was in direct contact with the underlying substrate (see Figure 3.3a), E_{corr} values over the intact coating surface were uniformly high, following equilibration with the humid experimental atmosphere, and similar to the uncoated iron surface under the same conditions, i.e. *ca.* 0 to +0.1 V vs. SHE. Upon addition of 5% w/v NaCl (aq) to the defect area, the bare metal surface, within the vicinity of the defect, became visibly corroded within minutes. Coating delamination typically became initiated within 2 hours of electrolyte contact. As delamination proceeded, distinctive time-

dependent E_{corr} – distance (x) profiles became established as shown in Figure 3.3a. It may be seen from Figure 3.3a that a sharp potential drop of *ca.* 0.2 V occurs in the immediate vicinity of the delamination front. A more gradual, approximately linear, drop in potential then links the delamination front to the region adjacent to the coating defect, where potentials ultimately fall to between –0.3 and –0.4 V vs SHE. It has been shown elsewhere [24 - 26] that during corrosion driven cathodic coating delamination cathodic O_2 reduction (reaction (3.1) below), occurs primarily in the region of the delamination front. Conversely, anodic metal dissolution, reaction (3.2), is constrained to the region of the coating defect.

$$O_2 + 2H_2O + 4e^- \longrightarrow 4OH^- \qquad (3.1)$$

$$Fe \longrightarrow Fe^{2+} + 2e^- \qquad (3.2)$$

Ionic current passes along the thin layer of electrolyte, which becomes ingressed beneath the delaminated coating, to link the cathodic and anodic processes. It has also been shown that in the absence of inhibition this ionic current, and hence the rate of delamination, is limited by the mass transport of cations (in this case Na^+) from the external electrolyte to the delamination front. Thus, in Figure 3.3a, the sharp potential drop at the delamination front may be understood to arise from the ingress of ions, loss of coating adhesion, and the onset of reaction (3.1). Similarly, potentials in the defect region ultimately approximate those anticipated for the reaction (3.2) where the equilibrium potential is -0.44 V *vs.* SHE. The approximately linear potential gradient linking the defect and delamination front regions arises ohmically, as a consequence of the finite ionic conductivity of the underfilm electrolyte layer. The composition of this underfilm electrolyte layer is proposed to be principally dilute sodium hydroxide, with the OH^- derived from reaction (3.1). The ingress of chloride ions from the defect region is disfavoured, since the underfilm cathode is a site of net negative charge generation and consequently the "passivity" of the iron surface is not disrupted, resulting in the observation of very little tarnishing in the underfilm delaminated zone.

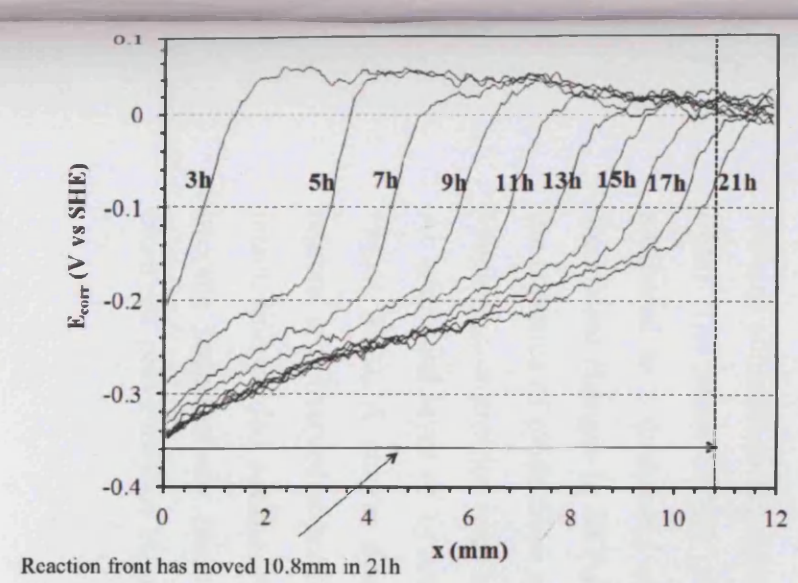

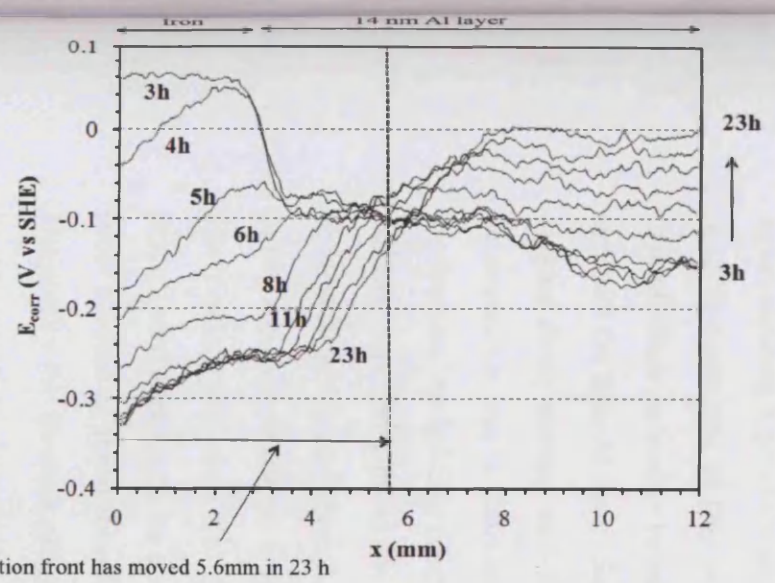

(b) 4 nm Al

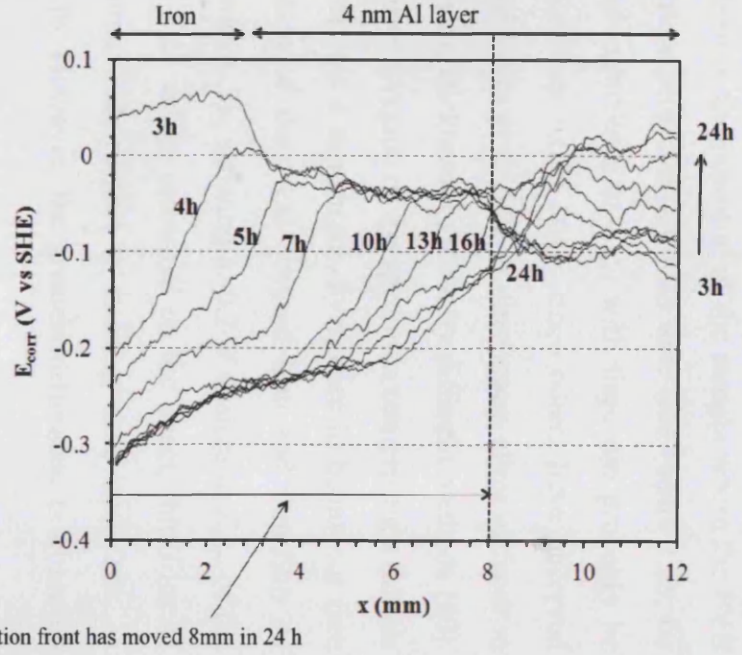

(d) 72 nm Al

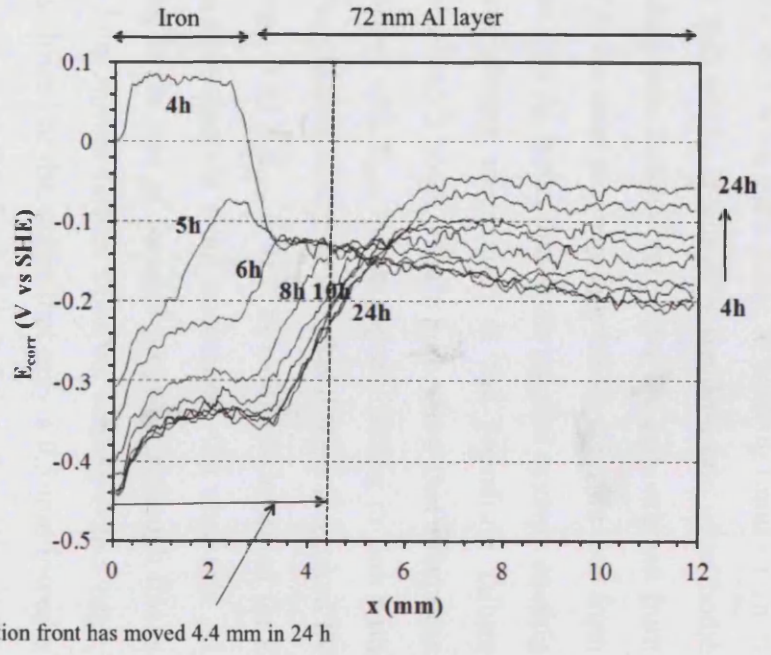

Figure 3.3: *E_{corr} versus distance profiles extracted from a high-throughput, cathodic disbondment experiment carried out using a thin film Al-wedge deposited Fe substrate coated using a 30 μm PVB layer. Data is shown for Al thin film thicknesses of (a) 0 nm, (b) 4 nm, (c) 14 nm and (d) 72 nm.*

The influence of an ultra-thin 4 nm Al layer on E_{corr} *versus* distance profiles associated with the delamination cell on PVB coated iron is shown in Figure 3.3b. A 3 mm wide zone between the defect region and the area occupied by the thin film Al layer, where the underlying iron surface is in direct contact with the organic coating, again exhibits a potential in the 0 - +0.1 V vs SHE range at holding times of 3h or less. The purpose of this zone is that firstly, it allows a baseline rate of cathodic delamination on iron to be established prior to the point where the disbondment front contacts the thin-Al layer. Secondly, the zone prevents aggressive chloride ions from making direct contact with the thin-film Al layer, thus ensuring that organic coating delamination *via* a cathodic disbondment mechanism is the prevailing failure mechanism. At holding times greater than 3 hours, Figure 3.3b, show that a cathodic disbondment front traverses this zone, with E_{corr} values rapidly falling in line with the results given in Figure 3.3a. The position of the Al interfacial layer is marked by more negative potentials in the range $-0.05 \geq E_{corr} \geq -0.1$, as would be expected for a less noble metal than Fe. As the delamination front encounters the ultra-thin Al layer, there appears to be a slowing in the rate of forward progress, although this is most evident as the disbondment front moves further from the coating-defect edge. Eventually the forward progress is slowed to the extent that only a 0.5 mm increase in delamination distance is observed over the final 8 h holding duration of the experiment. It is also evident that the thin Al film surface is affected by long term exposure to a humid environment, since the potential of the sample where the PVB remains adherent to the substrate rises progressively with time (see Figure 3.3b, far right). The cause of this progressive increase in E_{corr} with time can probably be attributed to a thickening of the surface oxide layer, since others have observed significant changes in SKP-derived Volta potentials of aluminium alloy surfaces in the presence of oxide films of varying thicknesses grown by different methods [50]. When E_{corr} -x profiles were taken over a region of the specimen comprising a thicker Al interfacial layer of 14 nm, there was a significant divergence in behaviour (see Figure 3.3c). A clearer demarcation of the PVB covered iron and thin-film Al regions are observed at holding times $\leq$ 3h, showing a -0.2 V change in E_{corr} of the intact, uncorroded surface. Again E_{corr} values measured on the intact, thin film Al become progressively more positive with respect to holding time over 24h, as observed previously in Figure 3.3b. However, the greatest difference is observed

when the delamination front encounters the 14 nm Al film, where a marked slowing of the forward progress of the front is observed, to such an extent that electrolyte ingress in limited to only *ca.* 1 mm over the final 16h of the experiment. A significantly greater Al film thickness of 72 nm is shown to further retard the progress and eventually halt the forward movement of the cathodic disbondment front, as can be seen in Figure 3.3d, where the position of the $E_{corr} - x$ inflection remains constant at holding times of > 10h.

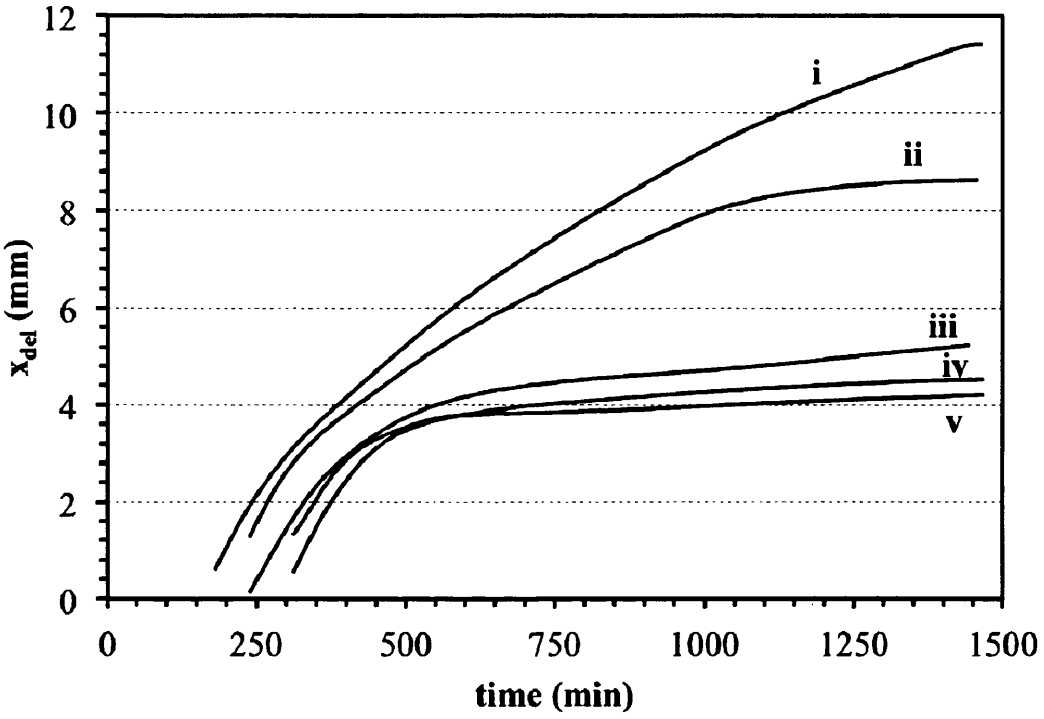

Figure 3.4: *Delamination front distance (x_{del}) plotted as a function of holding time at 95% relative humidity. Data was obtained for a thin film Al-wedge deposited on an Fe substrate coated using a 30 μm PVB layer for regions corresponding with an Al film thickness of (i) 0 nm, (ii) 4 nm, (iii) 14 nm, (iv) 26 nm and (v) 72 nm.*

The influence of Al layer thickness on delamination kinetics is best represented by the plots of time-dependent delamination front distance from the coating-defect edge (x_{del}) given in Figure 3.4, for a range of different Al thicknesses. For any given time (t_{del}) after addition of electrolyte to the defect, x_{del} was obtained by locating the peak

in the first derivative of the E_{corr} - x profile obtained at that time. Since all plots in Figure 3.4 involve delamination over a zone of exposed iron adjacent to the defect region, all plots are characterised by similar initial rates of disbondment. However, for values of $x_{del} > 4$ mm, when the disbondment front encounters the iron-Al edge, there is a progressive decrease in rate observed for curves (i) through to (v), with the greatest change observed for Al film thicknesses between 4 and 14 nm (curves (ii) and (iii)). Curves (iv) and (v) confirm that when film thicknesses of ≥ 26 nm are employed, x_{del} increases only very marginally with respect to time, and to all intents and purposes the delamination rate tends to zero at holding times of greater than 16h.

Previous work has shown that under conditions similar to our own, the overall rate of delamination is controlled by the migrational mass transport of electrolyte cations (here Na^+) from the defect region to the principal underfilm site of reaction (3.1) [25]. Under these circumstances x_{del} and t_{del} are related by,

$$x_{del} = k_d (t_{del} - t_i)^{1/2} \qquad (3.3)[45]$$

where t_i is the time required for the delamination cell to become initiated following electrolyte addition and k_d is the delamination rate constant. Figure 3.5 shows plots of x_{del} *vs.* $(t_{del} - t_i)^{1/2}$ obtained from the data shown in Figure 3.4, where it can be seen that the plot of the control experiment data, for PVB-coated iron in the absence of an Al layer (curve (i)), is a straight line, consistent with delamination proceeding under migrational control or fixed concentration. However, curves (iii) – (v) obtained in the presence of thin Al films of varying thickness display a marked inflection in the x_{del} *vs.* $(t_{del} - t_i)^{1/2}$ relationship at $x_{del} > 4$ mm. For curve (ii), corresponding with a film thickness of 4 nm, the inflection is not so evident at the same point, but occurs when the delamination front has traversed *ca.* 4 mm further from the defect-coating boundary.

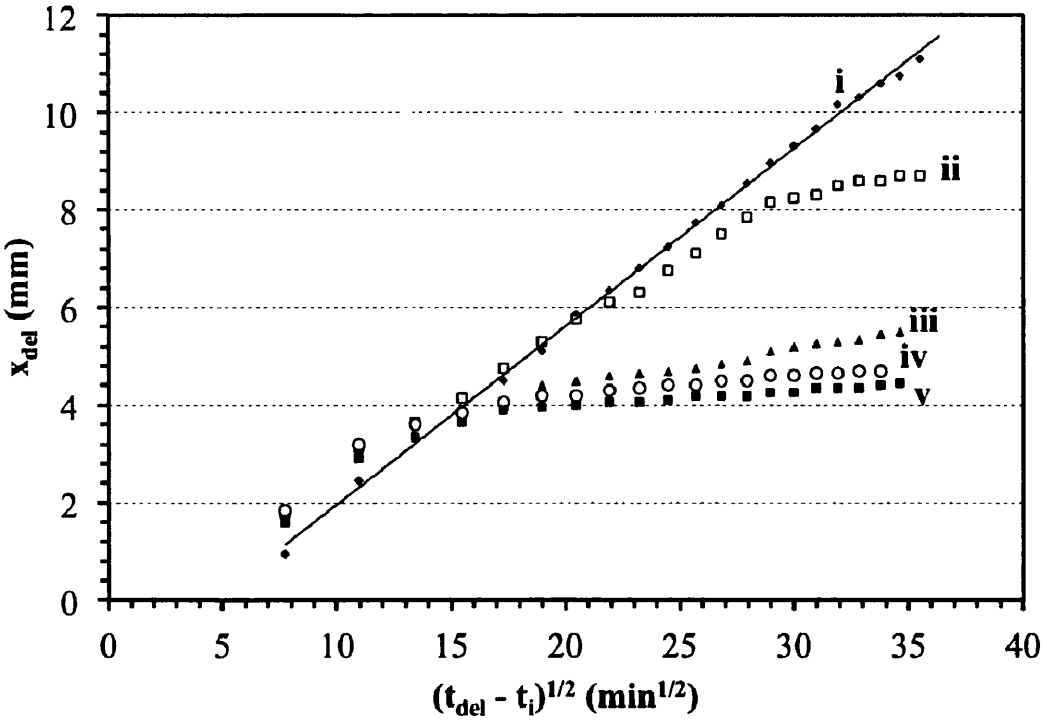

Figure 3.5: *Delaminated front distance (x_{del}) plotted as a function of the square root of holding time at 95% relative humidity, where t_i is the time taken for delamination to become initiated Plots i – v were obtained from the same Al thicknesses given in Fig 3.4.*

A final summary of the kinetics data, showing the relationship of the delamination rate constant with Al film thickness is given in Figure 3.6. In this case the rate constant (k_{del}) is calculated from the initial rate of delamination (dx_{del}/dt), rather than using expression (3.3), for which only PVD-coated iron shows a straight line relationship. For delamination kinetics established in the presence of Al thin films, the initial rate is taken at the point where the disbondment front encounters the Al-coated section of the substrate. Again the summary plot in Figure 3.6 confirms that an Al film thickness of between 4 and 15 nm marks a threshold, where a profound inhibition of the underfilm cathodic disbondment process taken place.

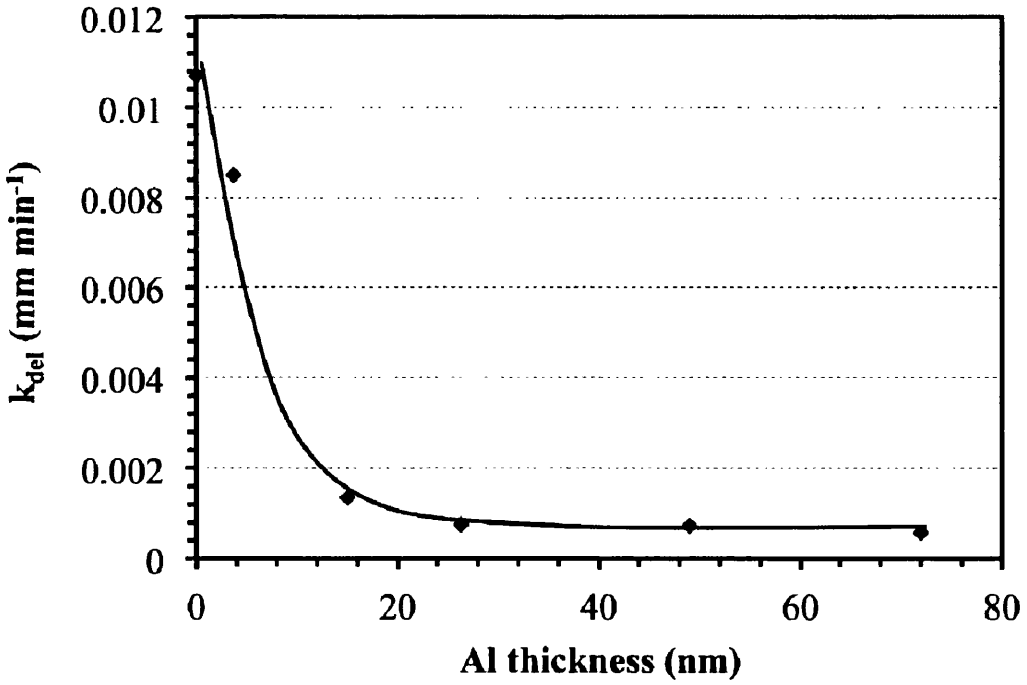

Figure 3.6: *Summary plot of delamination rate constant (k_{del}) versus Al PVD layer thickness.*

Questions therefore arise about why such a threshold value of Al film thickness is observed, and why increasing thickness by a further order of magnitude over and above this threshold gives relatively little extra benefit in terms of a reduced organic coating delamination rate, *via* a cathodic disbondment mechanism. To address these, the action of the Al layer, existing at the iron-PVB interface must first be discussed. Figure 3.7 shows a schematic diagram of the delamination cell existing on an organic coated iron substrate, along with a typical SKP-derived E_{corr}-distance profile, reconciling the main features of the profile with the principal processes occurring within the localised cell. High E_{corr} values measured for the intact region to the far right hand side are consistent with metal dissolution being strongly inhibited by the limited amount of bulk electrolyte present and the Al surface being covered with a passive oxide layer. In the defect region the presence of aqueous chloride electrolyte at pH 6.5 removes inhibition of reaction (3.2), leading to dissolution of a passive oxide layer, and consequently E_{corr} falls to values observed for bare iron freely corroding chloride containing electrolyte. Corrosion rates in the

defect region, covered by a several mm thick electrolyte layer, are likely to be limited by O_2 mass transport [51] and the defect region therefore becomes a site of net anodic activity.

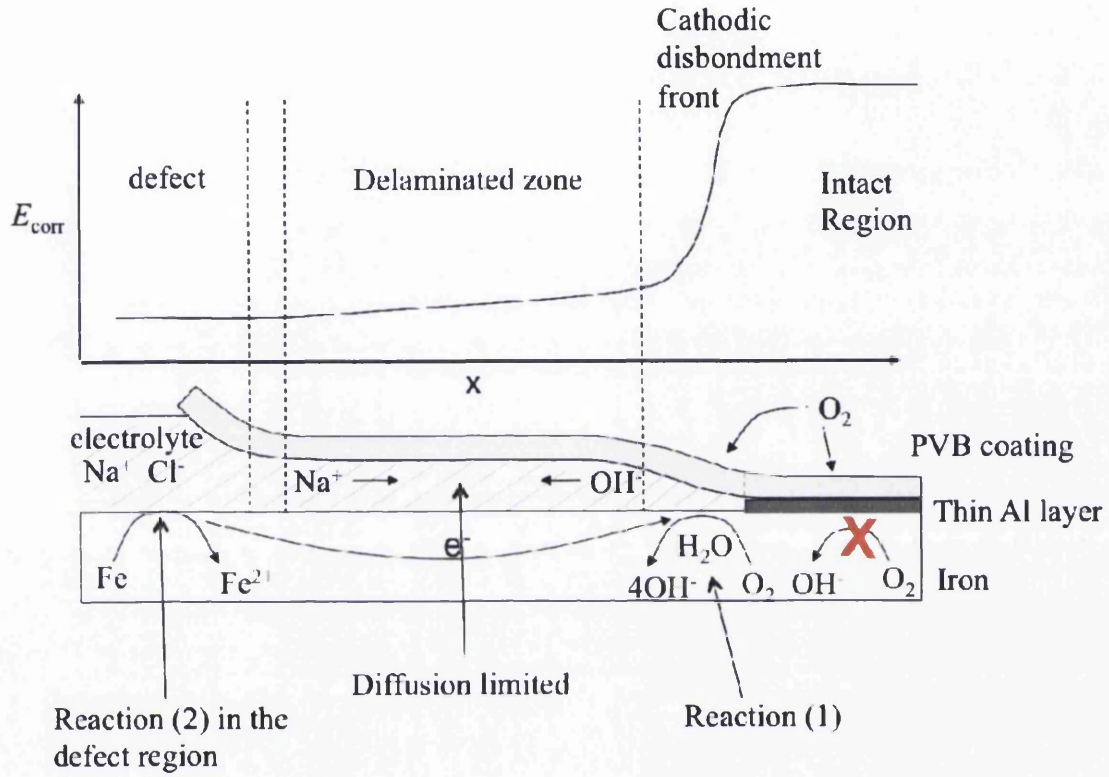

Figure 3.7: *Schematic representation of the process of organic coating delamination from an iron substrate via a cathodic disbondment mechanism and the proposed influence of the thin Al layer at the coating-iron interface. The diagram also reconciles a typical SKP-derived E_{corr} vs distance profile with the main features of the delamination cell.*

In the region of cathodic disbondment, electrolyte penetration, and rapid through-polymer O_2 diffusion allow an increase in the rate of reaction (3.1), causing E_{corr} to decrease significantly. The persistence of the passive film in a chloride-free alkaline underfilm electrolyte, following polymer disbondment, results in this region being a site of net cathodic activity and keeps E_{corr} values higher than in the defect region, but lower than those measured in the intact region. The high local pH, comparable to

that of sodium hydroxide, resulting from reaction (3.1) will promote base catalysed hydrolysis of vinyl acetate functions in the PVB coating and will tend to bring about de-adhesion by increasing the hydrophilicity of the PVB film. Furthermore, generation of OH^- *via* reaction (3.1) and the consequent migration of charge balancing Na^+ to the cathodic front will exert an (electro)osmotic pressure tending to delaminate partially disbonded PVB. In the delaminated zone, ionic current flux along the under-film layer of electrolyte linking the defect and cathodic disbondment front produces an approximately linear ohmic potential drop.

However, once the cathodic front encounters an interfacial Al layer, several factors may influence the rate of cathodic oxygen reduction at the disbondment front. Firstly, the rate of reaction (3.1) may be reduced significantly or even halted by the poor electrocatalytic properties of Al towards oxygen reduction, compared with iron [12,13] as indicated in Figure 3.7. Secondly the high pH existing at the cathodic front would tend to promote the dissolution of the aluminium (hydroxide surface layer on the Al thin film (equation (3.4)) and could in turn also anodically activate the underlying Al *via* equation (3.5). The exposed iron immediately adjacent to the boundary with the thin film Al would act as the corresponding site of reaction (3.1), coupling with reaction (3.5) at the Al-organic coating interface.

$$Al(OH)_3(s)+OH^-(aq)\rightarrow\left[Al(OH)_4\right]^-(aq) \tag{3.4}$$

$$Al(s)+4OH^-(aq)\rightarrow\left[Al(OH)_4\right]^-(aq)+3e^- \tag{3.5}$$

However, it should be noted that both reactions in equations (3.4) and (3.5) consume hydroxide ions, depending on time and concentration, and will therefore tend to limit underfilm pH at the disbondment front. Therefore, a second possible cause of a slowing of cathodic disbondment kinetics may be a reversal of polarity at the delamination front, where a net cathode on iron is transformed to a net anode, according to reaction (3.5), coupled with cathodic oxygen reduction on the iron

surface immediately adjacent. This would therefore lead to a slower, film-thickness dependent anodic undercutting of the organic coating *via* Al dissolution.

A closer look at the disbondment kinetics as a function of Al thickness (Figure 3.6) allows the possibility of distinguishing between the 2 effects, described above, thus enabling the predominant influence of the Al to be identified. Although the relatively rapid rate of organic coating disbondment observed on the ultra-thin 4 nm Al layer (see Figure 3.3b) can probably be ascribed to reactions (3.4) and (3.5), the reduction in delamination rate observed for thicker Al layers would be expected to be directly proportional to film thickness if option 2 were in operation. The fact that this linear relationship is not determined empirically (see Figure 3.6) suggests therefore that the slowing of disbondment rate is not determined by the amount of available Al to be consumed via reaction (3.5), but rather by disfavouring reaction (3.1) at the thin film Al interface with the organic coating.

3.3.2 Organic coating delamination on thin film Al-deposited iron via an anodic disbondment mechanism

The apparent susceptibility of an ultra-thin (< 15 nm) Al coated Fe substrate to anodic disbondment, *via* activation of the Al by elevated pH, raises a question about what might occur should more aggressive underfilm ions, such as chloride, come into contact with the Al deposited on iron. To test possible organic coating failure mechanisms in a situation where chloride ions make direct contact with Al-deposited Fe at on organic coating defect, a technique developed previously to initiate filiform corrosion on organic coated aluminium alloys was employed [45]. In this method a controlled quantity of aqueous $HCl_{(aq)}$ was applied to a scribed coating defect, with the coated specimen subsequently maintained in air at high humidity and constant temperature.

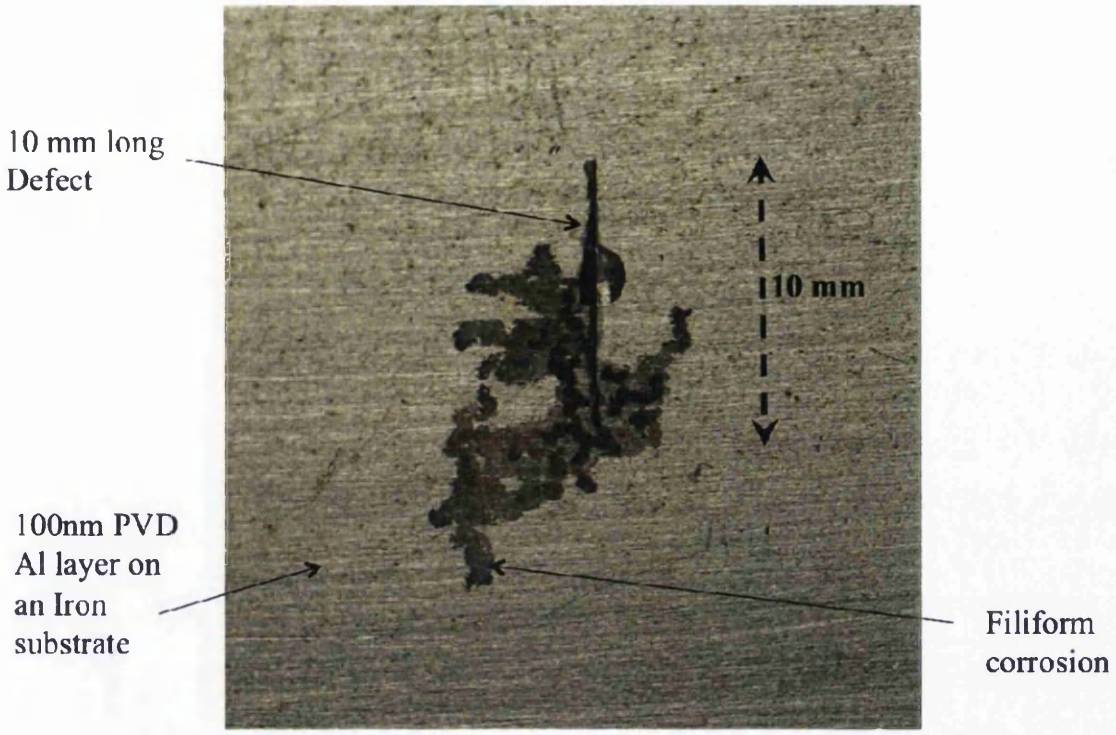

Figure 3.8: *Photographic image of a PVB coated Fe substrate, comprising a 100 nm Al thin film layer at the Fe-coating interface, following initiation of corrosion by the application of $HCl_{(aq)}$ to a penetrative coating defect and holding at 95% RH for 12 hours.*

Figure 3.8 shows the appearance of a PVB coated Fe substrate, comprising a 100 nm thick Al layer at the organic coating-metal iron interface, following hydrochloric acid initiation of underfilm corrosion and subsequent holding in air at 95% relative humidity for 12 hours. The nature of the corrosion features observed differ markedly from those observed for the specimens described in section 3.3.1 and are consistent with the occurrence of filiform corrosion (FFC), suggesting the presence of an anodic disbondment process [33]. The tips of the filaments which emanate from the scribed region are dark, with the tail region immediately behind appearing slightly tarnished. A time-lapse study of underfilm corrosion, where the positions of the filament front edges were monitored with respect to time, gave an average filament velocity of 0.4 mm/h, a value of underfilm corrosion rate which is significantly more rapid than the progress of cathodic disbondment fronts over Al thin-film surfaces discussed previously in 3.3.1. When comparing the filament kinetics observed for

the PVD Al film on iron to those mentioned in the literature it is only possible to compare to the kinetics of filiform corrosion on bulk aluminium and aluminium alloy substrates [39]. On pure Al substrates it has been reported that a filament velocity of 0.078mm/h has been observed, which is approximately five times less than the velocities for 100nm of PVD Al on iron.

In situ SKP analysis of the organic coated surface, following the initiation of corrosion was used to measure the local E_{corr} distributions associated with the propagation of filiform-like features. Figure 3.9 shows a series of greyscale E_{corr} distribution maps obtained at progressively greater times following application of HCl to the coating defect. It may be seen from Figure 3.9 that, initially, the intact (uncorroded) PVB coated Al deposited on Fe surface exhibits an E_{corr} value of approximately – 0.15 V *vs.* SHE. This E_{corr} value is therefore typical of a situation in which anodic metal dissolution is strongly disfavoured by the presence of a passive oxide layer [33]. The first surface maps recorded following initiation shows several dark areas of low E_{corr} close to the left hand edge of the scan area (Figure 3.9a). These regions of decreased E_{corr} are consistent with localised oxide dissolution of the aluminium thin film surface and active anodic metal dissolution *via* reaction (3.6) below occurring during the initiation of corrosion filament heads in the coating defect area. The occurrence of reaction (3.6) is also favoured by the low pH which derives from the initiating electrolyte.

$$Al \longrightarrow Al^{3+} + 3e^{-} \qquad (3.6)$$

For holding times ≥7 hours, corrosion filament heads having potentials as low as -0.7 V *vs.* SHE may be observed to move away from the coating defect at the left hand side of the scan area (Figure 3.9b). Regions lying in the wake of the advancing filament heads passivate significantly with time, exhibiting E_{corr} values of up to – 0.05 V *vs.* SHE. As the filaments move further from their points of initiation the length of the head region characterised by low E_{corr} values decreases, from *ca.* 2 mm at a 14h holding time (Figure 3.9c) to *ca.* 0.5 mm at ≥ 24 hours. The observations are wholly consistent with previous observations of E_{corr} distributions associated with

actively propagating filiform corrosion on both iron and aluminium alloy samples coated with PVB [44, 45], again suggesting that the underfilm corrosion on the specimen studied is *via* an anodic disbondment mechanism in the context of initiation through HCl.

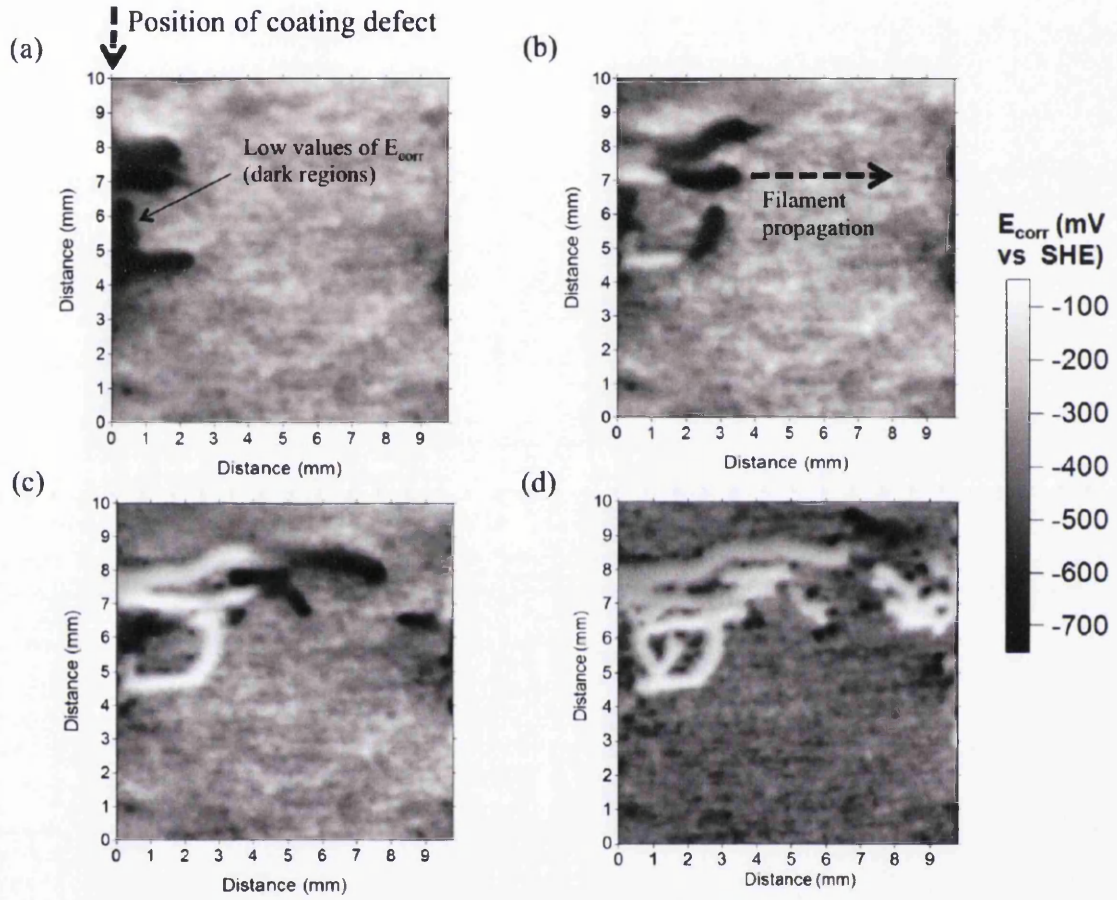

Figure 3.9: *Greyscale image maps showing changes in E_{corr} distributions observed for a PVB coated Fe substrate, comprising a 100 nm Al thin film layer at the Fe-coating interface, following initiation of corrosion by the application of HCl (aq) to a penetrative coating defect and holding at 95% r.h. for (a) 2h, (b) 7h, (c) 14h. The coating defect is situated on the left hand side of the scanned area.*

The digital nature of the E_{corr} data in Figure 3.9 allows detailed spatial analysis of the instantaneous E_{corr} distributions observable in individual SKP scans. Figure 3.10 shows the time-dependent variation of E_{corr} along the long axis of a filament

indicated in Figure 3.9b, moving from right to left. The active head is evidenced as a 2 mm long region of E_{corr} = -0.5 V *vs.* SHE, again consistent with the aluminium thin film surface becoming substantially depassivated within the head region. E_{corr} values are shown to rise significantly to *ca.* 0 V vs SHE in the tail region, left in the wake of the advancing head, therefore becoming significantly more positive than the original intact thin Al-polymer interface.

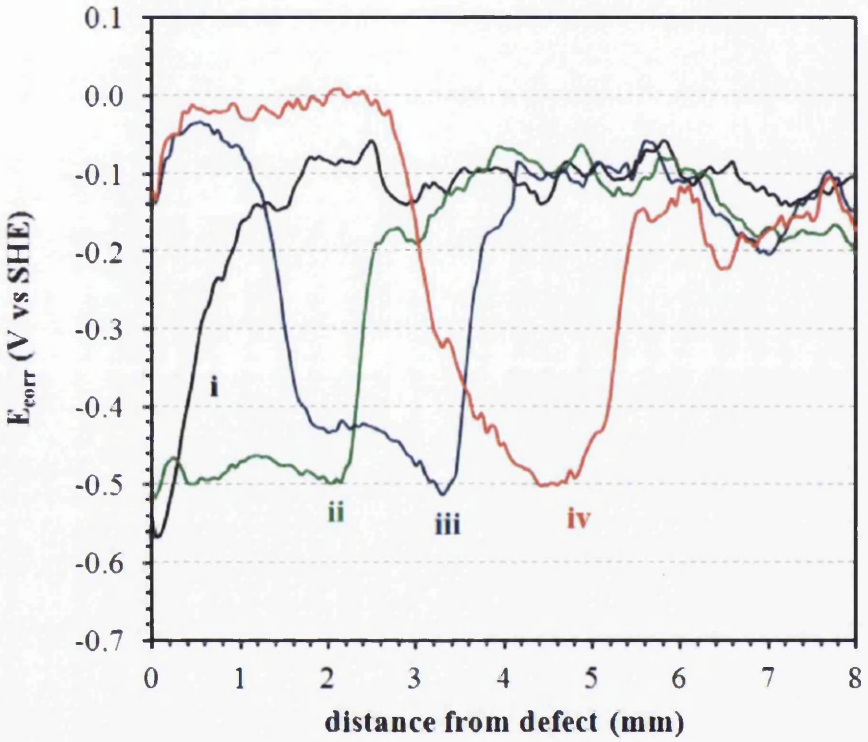

Figure 3.10: *Profiles of E_{corr} versus distance, taken along the length of a propagating filament on a PVB coated Fe substrate, comprising a 100 nm Al thin film layer at the Fe-coating interface. The profiles were recorded at holding times of (i) 2 hours, (ii) 10 hours, (iii) 16 hours and (iv) 21 hours.*

The E_{corr}-distance profiles in curves (iii) and (iv) (Figure 3.10) may be interpreted in terms of the thin film Al layer being consumed *via* reaction (3.6) over a length of *ca.* 1 – 2 mm within the active head region, leaving a zone immediately behind where the underlying Fe substrate is exposed. The rather positive E_{corr} values observed in the tail regions of curves (iii) and (iv) towards the left hand side of Figure 3.10 suggest that not only is the underlying Fe exposed, but that surface is largely passive.

If chloride ions were to remain in contact with Fe is this zone, E_{corr} values close to the active potential of iron, according to reaction (3.2) should be observed, i.e. -0.44 V *vs.* SHE. The actual values of *ca.* 0 V *vs.* SHE suggest that chloride ions are conserved within the electrolyte-filled head region and are drawn along by the need to preserve electroneutrality at the leading edge of the head, presumed to be the principal site of reaction (3.6). The forward progress of the head is driven by a local cathode, proposed to exist towards the rear of the head, where exposed iron provides an efficient electrocatalytic surface for cathodic oxygen reduction *via* reaction (3.1).

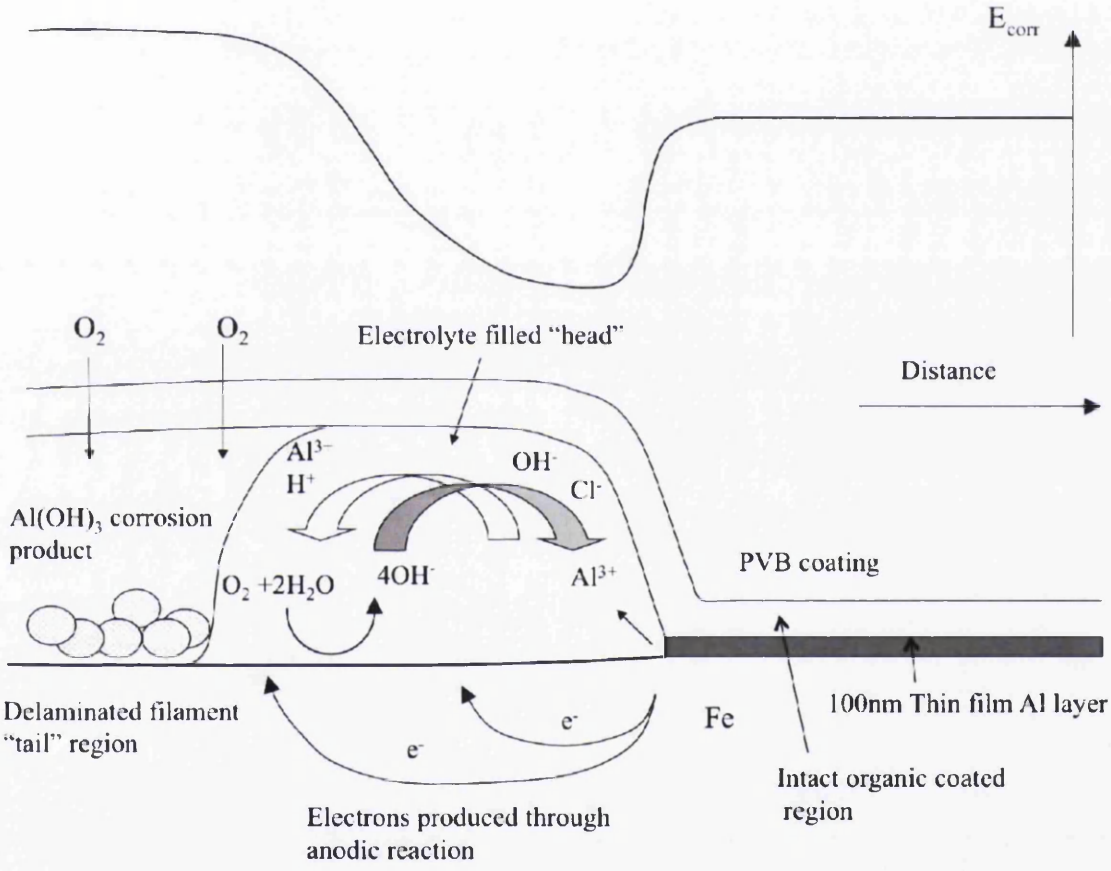

Figure 3.11: *Schematic representation of filiform corrosion affecting an organic coated Fe substrate in the presence of a thin Al film at the coating-substrate interface.*

A schematic diagram of the proposed anodic disbondment mechanism, where a characteristic E_{corr}-distance profile recorded along a propagating "filament" is reconciled with the main features of the delamination cell, is shown in Figure 3.11. Filiform corrosion on organic-coated aluminium and iron substrates is known to be driven by differential aeration, arising from facile mass transport of gaseous O_2 through the filament-tail. The oxygen concentration cell formed directs anodic metal dissolution towards the leading-edge of the filament-head, while the principal site of cathodic oxygen reduction lies towards the trailing-edge of the active head. Aggressive anions (Cl^-) and water are conserved in the filament head electrolyte and are drawn along by electro-osmotic action. The organic coating disbondment arises as a consequence of anodic undercutting by either reaction (3.2) or (3.6). A low pH is maintained in the filament head electrolyte by the hydrolysis of hexa-aquo Al^{3+} (or Fe^{3+}) cations produced by anodic attack near the leading edge of the head region. The proposed mechanism for thin-Al deposited iron (Figure 3.11) is largely similar, but a greater driving force for filament propagation is derived from electrocatalytic activation of the rear of the electrolyte filled head to reaction (3.1), when the underlying iron substrate becomes exposed. The high potentials measured in the tail region, some 3 - 4 mm behind the anodic disbondment edge, confirm that chloride ions are no longer in contact with the iron surface in this region and have been conserved in the head electrolyte.

Therefore, whilst the findings presented in section 3.3.1 suggest that the presence of thin Al films at the iron-organic coating interface can profoundly limit delamination by a cathodic disbondment mechanism, the preliminary findings discussed in section 3.3.2 confirm a susceptibility to underfilm attack via an anodic disbondment process. This in turn arises from a galvanic couple which is set-up in the presence of underfilm chloride ions, where anodic dissolution of the Al thin film is coupled with cathodic oxygen reduction on exposed iron. Therefore, it appears unlikely that the use of thin cathodic blocking Al films at an iron-organic coating interface will be a practicable method of improving resistance to corrosion driven delamination. Nevertheless, this work has demonstrated in principle that, with careful selection of the metallic "cathodic blocking" layer to avoid galvanic mismatch with the substrate in the presence of chloride ions, the approach described here holds considerable

promise as a means of preventing organic coating failure via a cathodic disbondment route. In addition, the deposition of the blocking layer in the form of the wedge, combined with in-situ SKP analysis of a Stratmann-type delamination sample, provides a rapid method of establishing the influence of layer thickness on the rate of coating disbondment.

3.4 Conclusions

Thin PVD-deposited layers of Al on an iron substrate have been investigated as a means of slowing corrosion-driven organic coated delamination by a cathodic disbondment mechanism. A novel high-throughput method involving the deposition of a PVD Al thin wedge of graded thickness enabled the influence of Al layer thickness on the kinetics of organic coating disbondment to be studied on a single specimen in one 24 h experiment. An *in situ* scanning Kelvin probe was used to monitor time-dependent changes associated with underfilm corrosion on a model PVB coated, iron substrate comprising a thin film Al "wedge" at the substrate-coating interface. Experiments were carried out in such a way that cathodic disbondment front propagation was allowed to occur on PVB coated iron, prior to encountering a region comprising a thin Al interfacial layer. For all Al layer thicknesses $\geq$ 15 nm, derived from Figure 3.6, the Al layers were shown to profoundly limit further progress of a organic coating delamination front. The persistence of organic coating delamination on thin Al layers of $<$ 15 nm was ascribed to the activation of the Al by the high underfilm pH, leading to anodic dissolution coupled with cathodic oxygen reduction on the previously delaminated iron surface. Thicker Al layers remained unaffected by the high underfilm pH and provided a effective blocking layer to further cathodic oxygen reduction at the disbondment front.

However, although Al proved highly effective in the inhibition of organic coating failure *via* a cathodic disbondment mechanism, experiments carried out on chloride-initiated specimens, through use of small quantities of HCL, showed that the Al layers rendered organically coated Fe substrates susceptible to delamination *via*

anodic disbondment. Initiation of underfilm corrosion by applying HCl to an organic coating defect on Al-deposited iron gave rise to filiform corrosion, characterised by propagating thread-like tracks which lengthened with time when held in a humid environment. *In situ* SKP potentiometry was used to monitor the corrosion potentials associated with the observed propagating corrosion feature, demonstrating that the active filament tip was a region of active aluminium dissolution. The principal driving force for filament propagation is proposed to derive from a differential electro-catalytic activation of the region immediately behind the filament tip. In this region the anodic dissolution of Al has produced exposure of underlying iron, providing a significantly more efficient surface for cathodic oxygen reduction than aluminium. The findings of this investigation demonstrate, in principle, that the use of a thin cathodic blocking film at metal-organic coating interface can stop coating failure by cathodic disbondment. However, the selection of blocking layer material composition should be carefully considered, as the inclusion of the extra interfacial film can lead to organic coating failure by other mechanisms.

3.5 References

1. B. Navinsek, P. Panjan, I. Milosev, "PVD coatings as an environmentally clean alternative to electroplating and electroless processes", *Surface Coatings Technology,* 1999, 116–119, p. 476–487.
2. B. Schuhmacher, W. Muschenborn, M. Stratmann, B. Schultrich, C.-P. Klages, M. Kretschmer, U. Seyfert, F. Forster, H.-J. Tiller, "Novel coating systems and surface technologies for continuous processing of steel sheet", *Advanced Engineering Materials,* 2001, 3, p. 681-689.
3. B. Schuhmacher, C. Schwerdt, U. Seyfert, O. Zimmer, "Innovative steel strip coatings by means of PVD in a continuous pilot line: process technology and coating development", *Surface Coatings Technology*, 2003, 163 –164, p. 703–709.
4. E. Reinhold, J. Richter, U. Seyfert, C. Steuer, "Metal strip coating by electron beam PVD-industrial requirements and customized solutions", *Surface Coatings Technology*, 2004, 188–189, p. 708–713.

5. L. Baptiste, N. van Landschoot, G. Gleijm , J. Priede, J. Schade van Westrum , H. Velthuis, T. Y. Kim, "Electromagnetic levitation: A new technology for high rate physical vapour deposition of coatings onto metallic strip", *Surface Coatings Technology*, 2007, 202, p. 1189–1193.

6. E. Reinhold, J. Faber, "Large area electron beam physical vapor deposition (EB-PVD) and plasma activated electron beam (EB) evaporation - Status and prospects", *Surface Coatings Technology*, 2011, 206, p. 1653–1659.

7. C. Metzner, B. Scheffel, "Special aspects concerning the electron beam deposition of multicomponent alloys", *Surface Coatings Technology*, 2001, 146 –147, p. 491-497.

8. B. Scheffel, C. Metzner, O. Zywitzki, J. Faber, "High-rate physical vapour deposition in combination with plasma processes for metal strip coating", *Galvatech 2001: 5th International Conference on Zinc and Zinc Alloy Coated Steel Sheet; Brussels; Belgium; June 2001*, p. 35-41.

9. N. C. Hosking, M. A. Strom, P. H. Shipway, C. D. Rudd, "Corrosion resistance of zinc-magnesium coated steel", *Corrosion Science*, 2007, 49, p. 3669–3695.

10. M. H. Fathi, M. Salehi, A. Saatchi, V. Mortazavi, S. B. Moosavi, "In vitro corrosion behaviour of bioceramic, metallic and bioceramic metallic coated stainless steel implants", *Dental Materials*, 2003, 19, p. 188-198.

11. L. A. Maeng, T. A. Tyson, L. Gladczuk, M. Sosnowski, "Corrosion behaviour of magnetron sputtered α- and β-Ta coatings on AISI 4340 steel as a function of coating thickness", *Corrosion Science,* 2006, 48, p. 2154-2171.

12. I. Suzuki, *Corrosion Resistant Coatings*, Marcel Dekker, New York, (1989).

13. H. Dafydd, D. A. Worsley, H. N. McMurray, "The kinetics and mechanism of cathodic oxygen reduction on zinc and zinc–aluminium alloy galvanized coatings", *Corrosion Science*, 2005, 47, p. 3006-3018.

14. V. Jovancicevic, J. O'M. Bockris, "The Mechanism of Oxygen Reduction on Iron in Neutral Solutions", *Journal of the Electrochemical Society*, 1986, 133, p. 1797-1807.

15. E. L. Koehler, "The influence of contaminants on the failure of organic protective coatings on steel", *Corrosion*, 1977, 33, p. 209-213.

16. H. Leidheiser Jr, "Corrosion of Painted Metals-A Review", *Corrosion*, 1982, 38, p. 374-383.

17. H. Leidheiser Jr, M. W. Kendig, "Mechanism of Corrosion of Polybutadiene-Coated Steel in Aerated Sodium Chloride", *Corrosion*, 1979, 32, p. 69-76.

18. H. Leidheiser Jr., W. Wang, "Some substrate and environmental influences on the cathodic delamination of organic coatings", *Journal of Coatings Technology*, 1981, 53, p. 77–84.

19. H. Leidheiser Jr., "Cathodic delamination of polybutadiene from steel", Journal of Adhesion Science Technology, 1987, 1, p. 79–98.

20. J. J. Ritter, "Ellipsometric Studies on the Cathodic Delamination of Organic Coatings on Iron and Steel", *Journal of Coatings Technology*, 1982, 54, p. 51-57.

21. H. Leidheiser, W. Wang, L. Igetoft, "The mechanism for the cathodic delamination of organic coatings from a metal surface", *Progress in Organic Coatings*, 1983, 11, p. 19-40.

22. E. J. Koehler, *The Mechanism of Cathodic Disbondment of Protective Organic Coatings-Aqueous Displacement at Elevated pH.Corrosion*, 1984, 40, p. 5-8.

23. M. Stratmann, H. Streckel, R. Feser, "A new technique able to measure directly the delamination of organic polymer films", *Corrosion Science,* 1991, 32, p. 467-470.

24. M. Stratmann, R. Feser, A. Leng, "Corrosion protection by organic films", *Electrochima Acta*, 1994, 39, p. 1207-1214.

25. A. Leng, H. Streckel, M. Stratmann, "The delamination of polymeric coatings from steel. Part 1: Calibration of the Kelvinprobe and basic delamination mechanism", *Corrosion Science*, 1999, 41, p. 547-578.

26. G. Williams and H. N. McMurray, "Chromate inhibition of corrosion driven organic coating delamination studied using a scanning Kelvin probe technique", *Journal of the Electrochemical Society*, 2001, 148, p. B377-B385.

27. S. A. Katz and H. Salem, "The toxicology of chromium with respect to its chemical speciation: a review", *Journal of Applied Toxicology*, 1993, 13, p. 217-224.

28. S. Langard and T. Norseth, "A cohort study of bronchial carcinomas in workers producing chromate pigments", *British Journal of Industrial Medicine*, 1975, 32, p. 62-65.

29. J. J. Caprari, A. R. Di Sarli, B. del Amo, "Zinc phosphate as corrosion inhibitive pigment of waterborne epoxy paints used for steel protection", *Pigment & Resin Technology*, 2000, 29, p. 16-22.

30. S. V. Lamaka, M. L. Zheludkevich, K. A. Yasakau, R. Serra, S. K. Poznyak, M. G. S. Ferreira, "Nanoporous titania interlayer as reservoir of corrosion inhibitors for coatings with self-healing ability", *Progress in Organic Coatings*, 2007, 58, p. 127-135.

31. D. Snihirova, S.V. Lamaka, M. Taryba, A. N. Salak, S. Kallip, M. L. Zheludkevich, M. G. S. Ferreira and M. F. Montemor, "Hydroxyapatite Microparticles as Feedback-Active Reservoirs of Corrosion Inhibitors", *ACS Applied Materials and Interfaces*, 2010, 2, p. 3011–3022.

32. J. Carneiro, J. Tedim, S. C. M. Fernandes, C. S. R. Freire , A. J. D. Silvestre , A. Gandini, M. G. S. Ferreira, M. L. Zheludkevich, "Chitosan-based self-healing protective coatings doped with cerium nitrate for corrosion protection of aluminum alloy 2024", *Progress in Organic Coatings,* 2012, 75, p. 8-13.

33. G. Williams, H. N. McMurray and D. A. Worsley, "Ce(III) inhibition of corrosion driven organic coating studied by a scanning Kelvin probe technique", *Journal of the Electrochemical Society*, 2002, 149, p. B154-B162.

34. G. Williams, H. N. McMurray and M. J. Loveridge, "Inhibition of Corrosion-Driven Organic Coating Disbondment on Galvanised Steel by Smart Release Group II and Zn(II)-Exchanged Bentonite Pigments", *Electrochimica Acta.*, 2010, 55, p. 1740-1748.

35. G. Williams, S. Geary and H. N. McMurray, "Smart Release Corrosion Inhibitor Pigments based on Organic Ion-Exchange Resins", *Corrosion Science*, 2012, 57, p. 139-147.

36. S. P. V. Mahajanam, R. G. Buchheit, "Characterization of Inhibitor Release from Zn-Al-$[V_{10}O_{28}]^{6-}$ Hydrotalcite Pigments and Corrosion Protection from Hydrotalcite-Pigmented Epoxy Coatings", *Corrosion*, 2008, 64, p. 230-240.

37. M.L. Zheludkevich, S.K. Poznyak, L.M. Rodrigues, D. Raps, T. Hack, L.F. Dick, T. Nunes, M.G.S. Ferreira, "Active protection coatings with layered double hydroxide nanocontainers of corrosion inhibitor", *Corrosion Science,* 2010, 52, p. 602–611.

38. J. M. Vega, N. Granizo, D. de la Fuente, J. Simancas, M. Morcillo, "Corrosion inhibition of aluminum by coatings formulated with Al–Zn–vanadate hydrotalcite", *Progress in Organic Coatings*, 2011, 70, p. 213-219.

39. G. Williams and H. N. McMurray, "Inhibition of Filiform Corrosion on Organic-Coated AA2024-T3 by Smart-Release Cation and Anion-Exchange Pigments", *Electrochimica Acta,* 2012, 69, p. 287-294.

40. W. G. Ji, J. M. Hu , L. Liu, J. Q. Zhang, C. N. Cao, "Improving the corrosion performance of epoxy coatings by chemical modification with silane monomers", *Surface Coatings Technology*, 2007, 201, p. 4789-4795.

41. P. Wang, D. W. Schaefer, "Why does Silane Enhance the Protective Properties of Epoxy Films?", *Langmuir*, 2008, 24, p. 13496-13501.

42. T. Titz, F. Hörzenberger, K. Van den Bergh, G. Grundmeier, "Correlation of interfacial electrode potential and corrosion resistance of plasma polymer coated galvanized steel. Part 1: Ultra-thin plasma polymer films of varying thickness", *Corrosion Science*, 2010, 52, p. 369–377.

43. T. Titz, F. Hörzenberger, K. Van den Bergh, G. Grundmeier, "Correlation of interfacial electrode potential and corrosion resistance of plasma polymer coated galvanized steel. Part 2: Influence of forming induced defects", *Corrosion Science*, 2010, 52, p. 378–386.

44. G. Williams and H. N. McMurray, "The mechanism of group (I) chloride initiated filiform corrosion on iron", *Electrochemistry communications*, 2003, 5(10), p. 871 -877.

45. G. Williams and H. N. McMurray, "The kinetics of chloride-induced filiform corrosion on aluminium alloy AA2024-T3", *Journal of the Electrochemical Soc*iety, 2003, 150(8), B380 – B388.

46. G. Williams, R. Grace, "Chloride-induced filiform corrosion of organic coated magnesium", *Electrochimica Acta*, 2011, 56, p. 1894-1903.

47. G. Grundmeier, M. Stratmann, "Adhesion and de-adhesion processes at polymer/metal interfaces", *Annual Review of Material Research*, 2005, 35, p. 571–615.

48. G. Grundmeier, W. Schmidt, M. Stratmann, "Corrosion protection by organic coatings: electrochemical mechanism and novel methods of investigation", *Electrochimica Acta*, 2005, 45, p. 2515–2533.

49. G. Williams, H. N. McMurray, D. A. Worsley, "Latent fingerprint detection using a scanning Kelvin microprobe", *Journal of Forensic Science*, 2001, 46, p. 1085-1092.

50. O. Ozkanat, B. Salgin, M. Rohwerder, J. M. C. Mol, J. H. W. de Wit and H. Terryn, "Scanning Kelvin Probe Study of (Oxyhydr)oxide Surface of Aluminum Alloy", *Journal of Physical Chemistry C*, 2012, 116, p. 1805-1811.

51. D. A. Jones, N. R. Nair, "Electrochemical corrosion studies on zinc coatings on steel, *Corrosion*, 1985, 41, p. 357-362.

Chapter 4

Corrosion Mechanisms of DSC Technology Fabricated on Metallic Substrates

In order to set the scene for the focus of the rest of this thesis, at this stage in my doctoral research programme, the sponsor, Tata Steel, had proposed a change in the direction of study. It became apparent that the sustainability of steel strip products, produced by Tata Steel, was becoming of ever increasing importance. Research into the possibility of fabricating a novel photovoltaic process, Dye-sensitised Solar Cell technology (DSC), onto pre existing Tata produced steel products began and became a major interest by the company. I was offered the opportunity to be integrated into a research team known as the 'PV', photovoltaic team, who were mainly based at Swansea University and Tata Colours at Shotton Works in North Wales. The team began investigating the possibility of producing steel roofing and cladding products with light harvesting capabilities, to produce a sustainable solution for the construction sector. My area of interest in this challenging venture started off by studying the suitability of a range of different metals as potential DSC substrates. Although the prime focus was for a pre-existing, organically coated, corrosion resistant steel product to act as a substrate, it had quickly become apparent that there were many implications of this regarding corrosion activity at DSC electrolyte-metal substrate interface. This posed major compatibility issues and due to these implications it was suggested that a range of metal substrates should be investigated for chemical suitability when in contact with DSC technology with the idea that this separate system could then be adhered or mounted on to a current steel roofing and cladding product. This chapter of work has studied the corrosion resistance of metallic substrates for the fabrication of dye-sensitised solar cells.

4.1 Introduction

With reference to the review compiled in section 1.3.4.3, the work reported here seeks to address this deficiency by describing a new method of characterising the reaction kinetics of triiodide with a wide range of potential metal substrates for DSC applications. Time-resolved UV/Vis spectrophotometry has been employed in order to monitor colour change within the electrolyte solution, enabling even very subtle changes to be detected over considerable timescales. The principal aim of these studies is both to gain insight into the mechanisms by which metals undergo triiodide-induced corrosion and identify suitable metals for use as stable and cost-effective DSC substrates.

4.2 Results and Discussion

4.2.1 Preliminary screening of the corrosion performance of potential metal DSC substrates

Details of the metallic substrates used in this section of work can be found in Table 2.1. Details of the fabrication of corrosion encapsulation cells can be found in section 2.5. Details of the technique used to monitor the interaction of DSC electrolyte and metallic substrates can be found in section 2.5.1.

Of the metals evaluated in the various encapsulation cells prepared in this study, zinc (Zn) substrates by far showed the most rapid interaction with the DSC electrolyte layer. At the instant the I_3^- containing electrolyte was introduced to the Zn encapsulation cells, a visible loss of dark brown colour, characteristic of the DSC electrolyte, was detected.

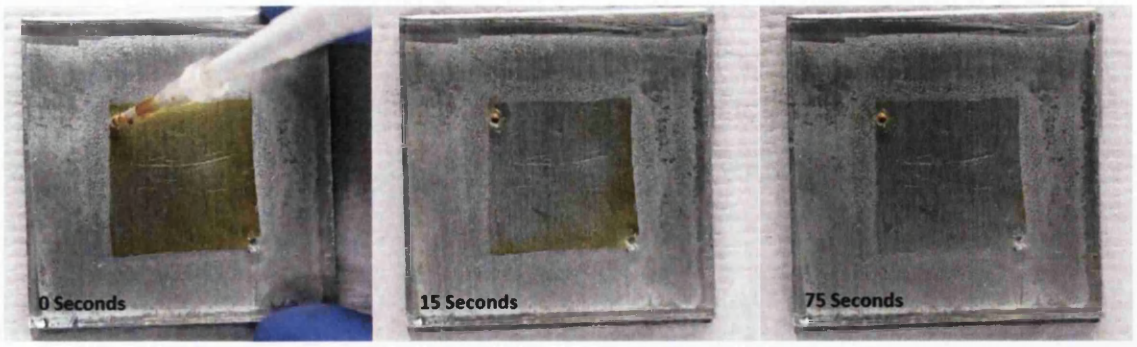

Figure 4.1: *Photographic evidence to show the visible loss of colour when an I_3^- containing electrolyte was introduced to a Zn substrate encapsulation cell.*

From Figure 4.1 it was evident that within 75 seconds, the electrolyte layer had become colourless, signifying the complete reduction of I_3^- to I^- according to reaction (4.1) and the subsequent oxidation of metallic zinc to release Zn^{2+} ions. The overall reaction is represented by equation (4.2) below.

$$I_3^- + 2e^- \rightarrow 3I^- \qquad (4.1)$$

$$Zn + I_3^- \rightarrow Zn^{2+} + 3I^- \qquad (4.2)$$

As a consequence of the speed of the above reaction, no quantitative analysis using diffuse reflectance spectrophotometry could be produced for a Zn substrate. The poor corrosion resistance of Zn observed here confirms the findings of Toivola *et al.* [2] using a method based on the immersion of metal coupons in millilitre quantities of DSC electrolyte. Although these authors state that the reaction takes place over a series of days, their findings are not inconsistent with the speed of reaction observed in this present study as the absolute quantity of I_3^- used here in the encapsulation cells will be several orders of magnitude less and will consequently be completely consumed significantly more rapidly through measurement of colour loss. The findings therefore suggest that any metal strip product incorporating a galvanizing technology, as corrosion protection would also be wholly unsuitable as a potential

substrate for direct fabrication of DSCs. For cells prepared using aluminium (Al) at two different purity levels (Table 2.1) and iron (Fe), both commonly employed as architectural cladding sheet materials, improved corrosion performance was observed. However, although the longevity of the I_3^- was superior in comparison with Zn, both types of metallic substrate had undergone reaction giving complete I_3^- disappearance within hours of introducing the electrolyte to the encapsulation cells. The changes in the absorption spectra recorded at different holding times for both Al (99%) and iron substrates are shown in Figure 4.2.

For the aluminium substrates at both purity levels, a reaction of I_3^- with the Al surface was detected from the point of electrolyte introduction albeit at much lower rates than observed for Zn. Only Al (99%) has been displayed here as more pure Al (99.999%) produced nearly identical absorbance *vs* wavelength characteristics. On the whole the lower purity Al (99.0%) underwent a slightly more rapid reaction than the 99.999% sample, where complete disappearance of I_3^- was observed over 180 and 300 min holding durations, respectively. It is proposed that the increase in rate results from the greater availability of transition metal impurity phases, as those detailed in Table 2.1, which in turn will provide a greater number of sites of high electrocatalytic activity for the reduction of tri-iodide. The absorption spectra given in Figure 3a for the 99.0% Al substrate shows a blue shift in triiodide absorption wavelength (λ_{max}) as the I_3^- concentration decreases, eventually giving the expected λ_{max} of 390 nm when the reaction is approximately half complete.

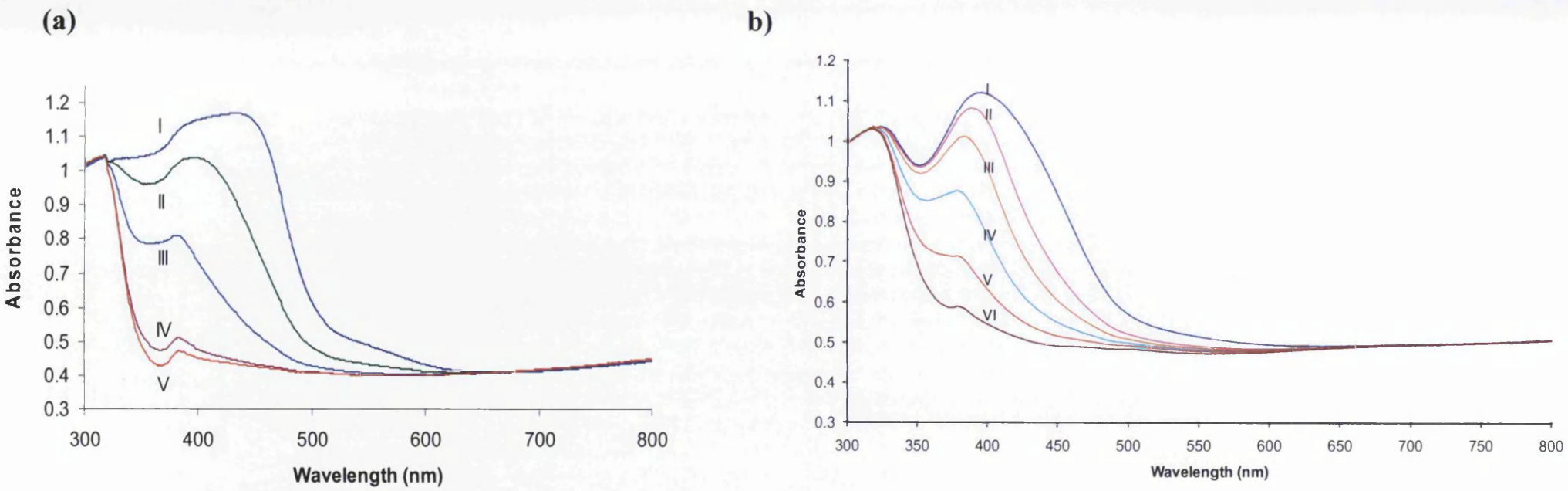

Figure 4.2: *UV/Vis Absorbance spectra of I_3^-, recorded in reflectance mode for encapsulation cells using an (a) aluminium (99.0%) and (b) and iron substrate in contact with DSC electrolyte. Time key (a): I) 0, II) 30, III) 60 min and at 30 min intervals thereafter. Time key (b): I) 0, II) 900, III) 920, IV) 940, V) 960 and VI) 1130 min.*

The reasons for this are unclear, although it may be that the spectrum at t = 0 min may include a contribution from a surface complex of aluminium oxide and tri-iodide which gives an apparent λ_{max} at a longer wavelength than expected. This behaviour appeared to be exaggerated on Al and only small spectral shifts were observed the case of Fe (see Figure 3b) or other metal substrates to be described later. Previously published work has suggested that iron or carbon steel surfaces show little evidence of degradation in the presence of DSC electrolyte [2]. For the encapsulation cell experiments carried out here, it was observed that no change in the I_3^- absorbance with respect to time occurred for the first 15 hours following the introduction of DSC electrolyte. However, after this induction time, a rapid decrease in the I_3^- concentration was observed, and over the ensuing 2 hour period a complete and irreversible disappearance of the I_3^- occurred as shown in Figure 4.2b. This finding again is not immediately consistent with prior observation of others, using coupons of carbon steel immersed in significantly larger volumes of DSC than the estimated 0.015 cm^3 quantity introduced to the encapsulation cells employed here [2]. However, for the same reasons explained above, the difference arises because of the considerably lower absolute quantity of I_3^- employed in this study. This result for Fe raises significant doubts about the suitability of carbon steel as a potential DSC substrate because the stability in the presence of I_3^- is temporary.

The exact reason for the delay observed before the onset of reaction involving Fe and I_3^- has not as yet been identified. One theory is that oxygen present in the DSC electrolyte can lead to an alternative cathodic reaction on the Fe surface, where the oxygen reduction occurs preferentially to reaction (1), up to a point where all the O_2 present is consumed, whereupon I_3^- reduction commences. However, when the DSC electrolyte was purged with nitrogen gas to remove any dissolved O_2, prior to its introduction to the Fe encapsulation cell, an entirely similar behaviour to that shown in Figure 3b was observed. An alternative reason may that Fe(III) species in the surface film are reduced to Fe(II) prior to any reaction with triiodide, and this may give rise to induction period prior to any observable loss of I_3^-. It is well known that cathodic oxygen reduction on oxide covered iron surfaces is mediated *via* Fe(II) species in the surface oxide layer [12,13], and therefore a similar type of process may be in operation for the reduction of triiodide.

The final group of metal substrates evaluated, including well known corrosion resistant surfaces such as stainless steel, titanium and molybdenum, showed significantly greater stability in the presence of DSC electrolyte. Both grades of stainless steel (304 and 316L) exhibited only very small changes in I_3^- within a 24 hour test period. Rates of change in absorbance, taken at λ_{max}, were of the order of 10^{-6} s^{-1} in magnitude for the 304 grade material. This can be considered as negligible compared to the metal surfaces discussed earlier. The 316L grade steel showed a similar rate of change, although interestingly the absorbance at λ_{max} increased rather than decreased. The reason for this behaviour is unclear, but again may signify that slow formation of a surface oxide complex with one or more of the constituents of the DSC electrolyte. Spectra for both stainless steel grades the encapsulation cells were taken at regular intervals over a 3 month period, with the result that relatively little (< 2%) change in the concentration of triiodide within the electrolyte solution was observed.

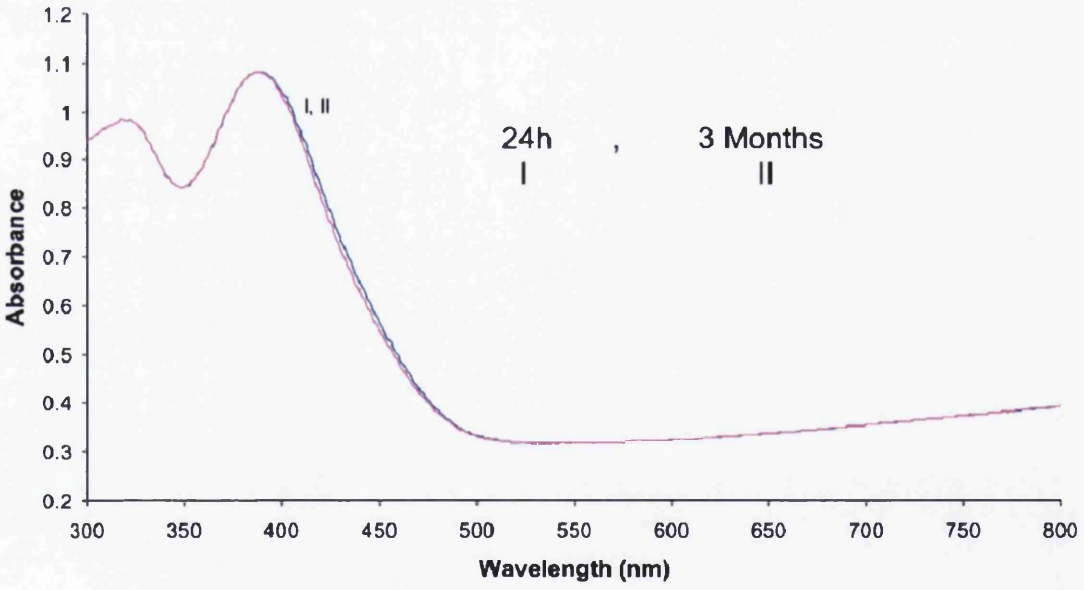

Figure 4.3: *UV/Vis Absorbance spectra of triiodide, recorded in reflectance mode for encapsulation cells using a titanium substrate in contact with DSC electrolyte.*

Encapsulation cells prepared on titanium (Ti) substrates were exceptionally stable, and as shown in Figure 4.3, no change in the absorption spectrum could be detected even over a 3 month holding time. In contrast, although molybdenum (Mo) appeared stable for the first 24h period following DSC electrolyte contact, over the ensuing 3 month holding period, a slow but measureable decrease in triiodide absorbance at 390 nm could be detected as shown in Figure 4.4. A comparison of the various metals evaluated in this study over a 24h holding period is given in Figure 4.5, while a summary of the longer term stability of encapsulation cells prepared using the most corrosion resistant metals over 3 months is shown in Figure 4.5.

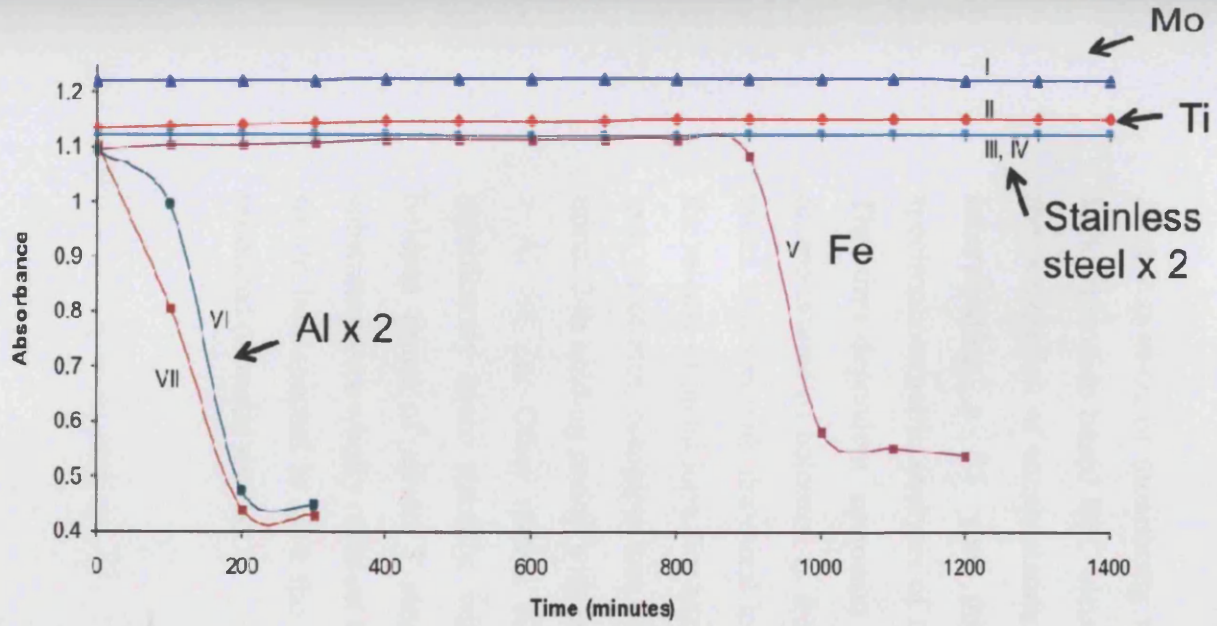

***Figure 4.4**: Absorbance values of I_3^- at λ_{max} vs time measured for each metal, tested over a period of up to 24h. The metal substrates employed were as follows: I) Molybdenum, II) Titanium, III) Stainless steel 316, IV) Stainless steel 304, V) Iron, VI) Aluminum 99.9%, VII) Aluminum 99.0%*

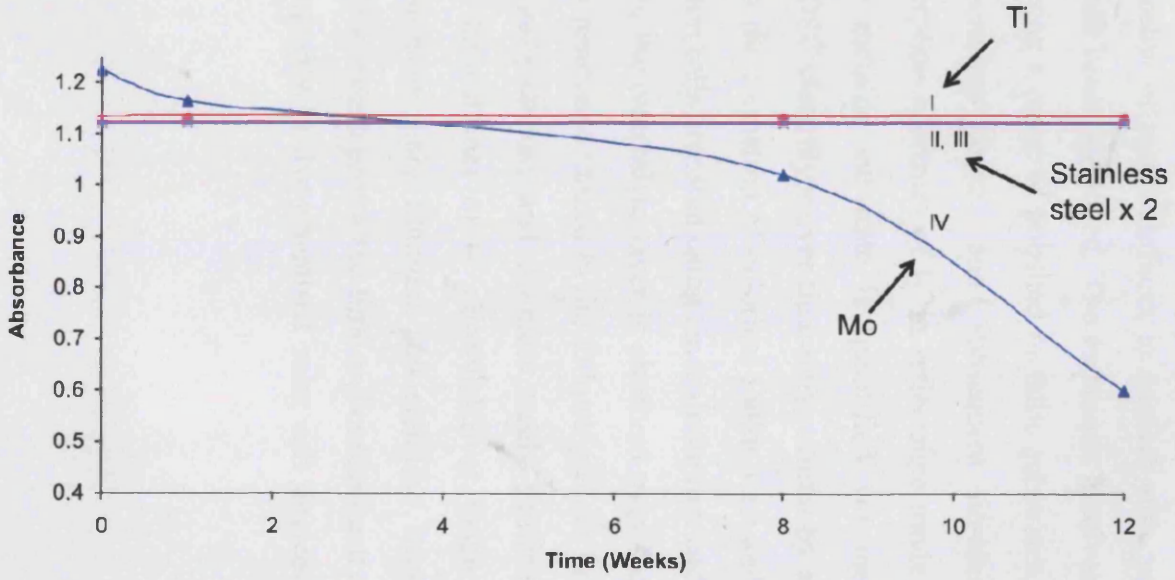

***Figure 4.5:** Absorbance values of I_3^- at λ_{max} vs time (weeks) measured over a 3 month period. I) Titanium, II) Stainless steel 316, III) Stainless steel 304, IV) Molybdenum*

The summary plot in Figure 4.4 shows clearly the delay observed before the Fe/I_3^- redox reaction commences and also allows the reaction rates for the least corrosion resistant surfaces to be conveniently compared. The result obtained for a Zn substrate is not included, since the rate of reaction was too rapid for a sufficient number of points to be obtained on the absorbance *vs* time axis. Figure 4.5 clearly shows the slow progressive loss of I_3^- from the electrolyte in contact with a Mo surface and the comparative stability of both Ti and stainless steel over a protracted holding time.

4.3 Conclusions

A new method of monitoring the corrosion of metal surfaces in contact with an iodide/triiodide based DSC electrolyte has been developed. The technique involves the preparation of encapsulation cells using a range of polished metallic substrates, incorporating a 25 μm thick electrolyte layer, and subsequent in-situ spectrophotometric analysis of the absorption spectrum of I_3^- in reflectance mode. The time-dependent corrosion of the metallic substrate is quantified *via* the disappearance of coloured I_3^- from the DSC electrolyte over time only, caused by a redox reaction with the metal leading to the formation of colorless iodide ions and the release of metal ions. For encapsulation cells prepared using zinc, aluminium and iron substrates, complete loss of I_3^- from the electrolyte layer is observed over the initial 24h holding period with corrosion resistance ranked in the following order Fe > Al >> Zn. Other metals such as molybdenum and stainless steels showed significantly more stability, with only limited loss of I_3^- observed over longer holding times of up to 3 months. However, only titanium and stainless steel substrates were wholly resistant to corrosion over a protracted time and consequently would be expected to give the best longevity in dye-sensitised solar cell devices produced on metal sheets.

4.4 References

1. B. O'Regan and M. Gratzel, "A low-cost, high-efficiency solar cell based on dye-sensitized colloidal TiO_2 films", *Nature*, 1991, 353, p. 737-740.

2. M. Toivola, F. Ahlskog, and P. Lund, "Industrial sheet metals for nanocrystalline dye-sensitized solar cell structures", *Solar Energy Materials and Solar Cells*, 2006, 90, p. 2881-2893.

3. X. M. Fang, T. L. Ma, M. Akiyama, G. Q. Guan, S. Tsunematsu, and E. Abe, "Flexible counter electrodes based on metal sheet and polymer film for dye-sensitized solarcells", *Thin Solid Films*, 2005, 472, p. 242-245.

4. M. Toivola, T. Peltola, K. Miettunen, J. Halme, K. Aitola, and P. D. Lund, Large area optimized thin film nano-solar cells on metal sheets", in *Clean Technology 2009: Bioenergy, Renewables, Storage, Grid, Waste and Sustainability*, M. Laudon, D.L. Laird, and B. Romanowicz, Editors, p. 25-28, CRC Press-Taylor & Francis Group, Boca Raton (2009).

5. M. Toivola, K. Miettunen, J. Halme, and P. Lund, "Thin nanostructured solar cells on metal sheets", in *Clean Technology 2008: Bio Energy, Renewables, Green Building, Smart Grid, Storage, and Water*, M. Laudon, B. Romanowicz, and D.L. Laird, Editors, p. 96-99, CRC Press-Taylor & Francis Group, Boca Raton (2008).

6. M. Toivola, T. Peltola, K. Miettunen, J. Halme, and P. Lund, "Thin film nano solar cells - from device optimization to upscaling", *Journal of Nanoscience and Nanotechnology*, 2010, 10, p.1078-1084.

7. K. Miettunen, X. L. Ruan, T. Saukkonen, J. Halme, M. Toivola, G. S. Huang, and P. Lund, "Stability of Dye Solar Cells with Photoelectrode on Metal Substrates", *Journal of the Electrochemical Society*, 2010, 157, B814-B819..

8. K. Miettunen, J. Halme, and P. Lund, "Segmented Cell Design for Improved Factoring of Aging Effects in Dye Solar Cells", *Journal of Physical Chemistry C*, 2009, 113, p. 10297-10302

9. K. Miettunen, J. Halme, M. Toivola, and P. Lund, "Initial performance of dye solar cells on stainless steel substrates", *Journal of Physical Chemistry C*, 2008, 112, p. 4011-4017.

10. T. L. Ma, X. M. Fang, M. Akiyama, K. Inoue, H. Noma, and E. Abe, "Properties of several types of novel counter electrodes for dye-sensitized solar cells", *Journal of Electroanalytical Chemistry*, 2004, 574 , p. 77-83.

11. A. Kay, "Solar cells based on dye-sensitized nanocrystalline TiO_2 electrodes, PhD thesis", Ecole Polytechnique Federale de Lausanne, Switzerland, (1994).

12. A. Kuch, "Investigations of the reduction and re-oxidation kinetics of iron(III) oxide scales formed in waters", *Corrosion Science*, 1998, 28, p. 221-231.

13. M. Stratmann and K. Hoffman, "In situ Möβbauer spectroscopic study of reactions within rust layers", *Corrosion Science*, 1989, 29, p. 1329-1352.

Chapter 5

Painted Steel mounted Dye-Sensitised Solar Cells

5.1 Introduction

As discussed earlier, the application of DSC to construction steel roofing and cladding materials is an exciting opportunity given the large areas of material installed globally. To illustrate, around 400 million square metres of painted steel roof and wall materials are installed in Europe each year, much of which on commercial buildings and large area warehouses. This provides a perfect opportunity for the application of photovoltaic technology to an existing continuous manufacturing process. This chapter studies the development of using painted steel mounted dye-sensitised solar cells using titanium metallisation by magnetron sputtering to create the working electrode contacts. This section of work was proposed as a consequence of the conclusions presented in Chapter 4 of this thesis. Of all the potential metal substrates investigated in Chapter 4, only titanium and stainless steel substrates showed to exhibit long-term stability when in contact with DSC electrolyte. As a result this provided us with the knowledge that if DSC technology were to be fabricated onto a metallic substrate, as an electron collector electrode, only these successful metals would provide a solution to the problem. Hence one option for manufacture of a coated steel product is the lamination of a functionalised metal foil such as Ti and stainless steel.

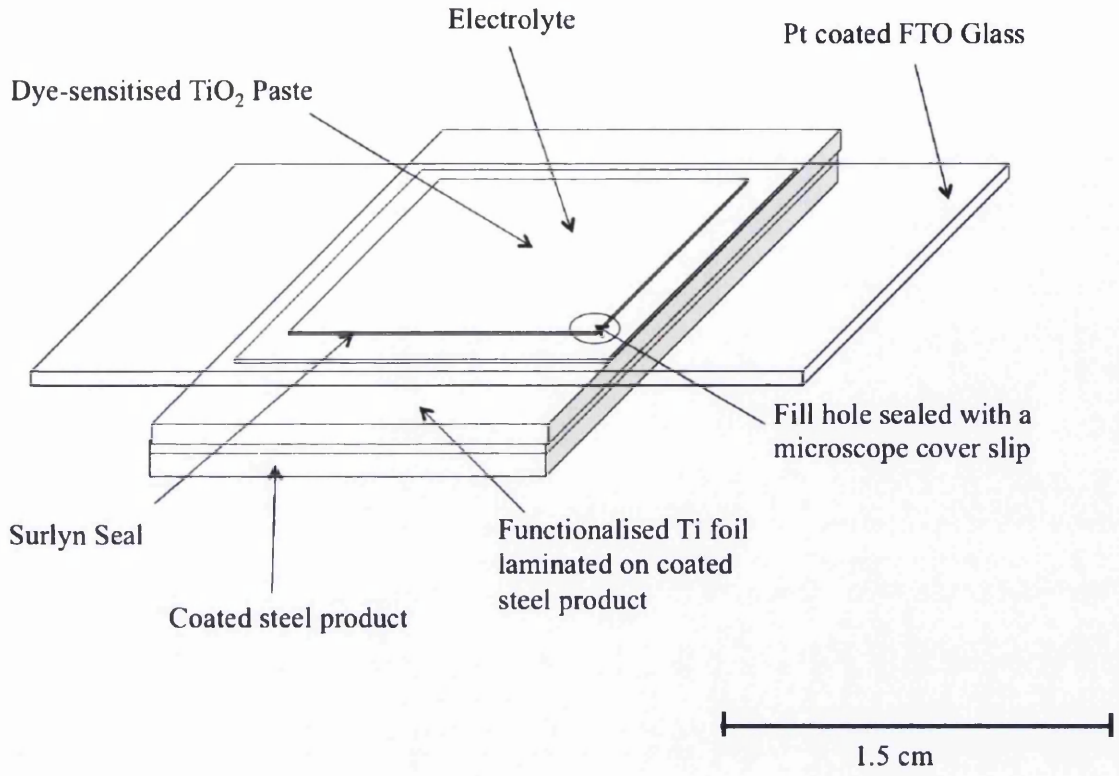

Figure 5.1: *A schematic representation of DSC technology that has been fabricated onto a Ti foil substrate and laminated onto a coated steel product.*

In Figure 5.1 the organically coated steel product, a building and cladding material, will act as a substrate for DSC technology. The organic layer is present to protect the underlying steel from corrosion. DSC technology fabricated onto a Ti foil substrate may then be laminated onto the coated steel product. The Ti foil acts as a collector electrode for injected electrons transported through a layer of titania within the device, and also resists any corrosion when in contact with the DSC electrolyte as reported in Chapter 4.

However, materials such as Ti foil and stainless steels have associated drawbacks if they were to be used on a large scale in this manner. From an economical point of view, due to the associated costs of such materials, it would be somewhat unfeasible to use such materials as collector electrode for DSCs. As well as cost, initial investigations were carried out on titanium and stainless steel substrates, regarding their compatibility with DSC technology, and only successful DSCs, giving an

electrical output, were witnessed on titanium substrates. Current technologies have shown that DSC can be applied to flexible titanium foil (typically >100 μm) in a roll to roll process [6]. DSCs built on stainless steel substrates produced no electrical output, removing this material from the list of potential metallic substrate materials. It was suggested through communication with members of the PV team and during progress review meetings at Tata Steel that the reason for the poor performance witness by stainless steel might have been linked to the lack of compatibility between the titania semiconductor and the oxide present on the surface of a stainless steel material. For this reason, titanium became the main focus in providing a solution to the fabrication of DSC technology on to metallic substrates. To bypass the issue of high the cost associated with using large area titanium as a collector electrode, work began on investigating a means of utilising lower quantities of titanium instead. The focus had now been placed on the possibility of rendering an organically coated steel product electrically conducting, and for use as a DSC collector electrode, through the application of a physical vapour deposited thin titanium film. By using this method, the application of titanium coatings on the micron scale onto pre existing organic coated steel products currently in production at Tata Steel, was deemed possible. This section of work details the success of this system and shows a promising insight into the development of DSC technology on a large-scale continual production process.

In this chapter we directly apply a Ti layer of (1.2 μm) to an existing painted steel substrate through magnetron sputter deposition. The reason for choosing an existing coated steel product is to prevent the need for the development of a novel coated steel product whilst those already available may be suitable.

This chapter describes the direct magnetron sputtering of metallic titanium onto a pre-painted steel substrate and subsequent assembly of a conventional DSC. The metallisation has the potential to act as a conduction layer and additional barrier to the corrosive effects of the tri-iodide electrolyte redox couple on the steel [14]. The assembly of such a cell in one embodiment without the need for inclusion of a metal

foil offers an exciting scale up potential for the technology for metal roofing products.

It was quickly evident from searching literature available on the industrialisation of DSC technology that there was no reports of sputter metallised organic coated steel products being investigated as DSC photoelectrodes. Magnetron sputtering has found application in the field of DSC for preparing the functional titania layer. Gomez showed in a series of papers that a TiO_2 layer can be deposited on top of conductive glass by reactive magnetron sputtering [8-13] as an alternative to titania paste deposition *via* screen printing or doctor blading. Resulting glass DSCs with forward illumination showed a typical 4 % efficiency using this TiO_2 deposition method [8]. Sputtering as also showed use in deposition of a Pt photcatalytic layer on glass counter electrode substrates [16].

5.2 Preliminary Developmental Work

Before investigations of thin Ti films produced on organically coated steel substrates began there was a requirement to assess the range of film thickness needed for use in the study. A range of thicknesses from 100nm to 1500nm at intervals of 100nm were deposited, using the PVD process explained in Chapter 2, on to the organic coated steel product, Bakeware coated steel which had been chosen by Tata Steel, to verify adhesion properties of the deposited films. It was evident that depositing Ti onto an organic coating was more complex than originally thought. Very poor adhesion was witnessed for films of less than a micron thick. The film virtually departed the surface of the sample during removal from the PVD facility. Film thicknesses of more than one micron proved to show much better adhesion properties. For this reason a film thickness of 1.2 μm was chosen to be the thickness used in the main study.

5.3 Experimental

5.3.1 Substrate material

For the purpose of this work a conventional sintering temperature of 450°C was selected for the titania layer. This was consistent with recommended sintering temperatures by the titania paste supplier Dyesol. The organic steel product used was a 0.7 mm gauge steel substrate protected from corrosion by a metallic coating of aluminium was used. Aluminium was used due to the fact that it develops a thick protective oxide on its surface, which deems the Al layer a poor cathode for oxygen reduction, preventing underfilm corrosion from occurring. The hot dip coated aluminised steel was obtained from Tata Steel. The aluminised coating itself contains *ca.* 10wt% Si (as an addition to the hot dip spelter) as this prevents large scale iron-aluminium intermetallic formation and leaves the coating very formable. An organic coating applied was a modified version of a proprietary formulation used to produce commercial bakeware, again chosen for its known resistance to degradation at higher temperatures [15]. The organic coating comprised of a thermosetting epoxy binder; exact details of the chemistry are protected by commercial confidentiality. The material was produced on a trial roll-to-roll coating line, using a process of reverse roller coating for the organic layer and conventional oven curing at a peak metal temperature (PMT of 240 °C) to produce the heavily cross linked polymer structure. The resulting pre-painted aluminised steel substrate was guillotined to shape prior to application of the sputtered Ti layer.

5.3.2 Sputtering of titanium

The titanium layer was deposited onto 20 x 30 mm coupons of the pre-painted aluminised steel substrate *via* a DC magnetron sputtering system (PVD 75 supplied by Kurt J Lesker) as described in Chapter 2. The coupons were wiped clean with ethanol to remove any surface contamination prior to sputtering. Sputtering was performed from a 2 inch diameter titanium target (99.995 % supplied by Kurt J

Lesker). The geometry of the system was such that the target was separated from the sample at a distance of 200 mm. The sample was earthed and the sputtering atmosphere (Argon 99.995%) was kept at 3.5mTorr and at room temperature. The power density applied to the target was 12 W/cm^2 and this achieved a deposition rate of 2 Å /s (~0.7μm/hour) as determined by an internal piezoelectric crystal. Ti was applied at a total thickness of 1.2 μm for the purpose of this initial study taking approximately two hours to complete. Blank samples were also included on glass substrates to evaluate certain thermal expansion issues. The thickness of Ti was controlled using a piezoelectric crystal monitoring system.

5.3.3 Preparation of TiO_2 photoelectrode

TiO_2 photoelectrodes were prepared as detailed in section 2.4.2, A Titania film thickness of 7 (±1)μm was achieved after sintering determined using stylus profilometry. In order to simplify the process steps, in this instance, a typical but not essential post treatment with $TiCl_4$, which can increase TiO_2 surface area was not attempted. In any case, it was felt that this process could result in delamination of the Ti layer through undercutting of the organic coating Ti interface.

5.3.4 Device fabrication

DSCs were fabricated as detailed in section 2.4. The geometry of the final cell design is shown schematically in Figure 5.2.

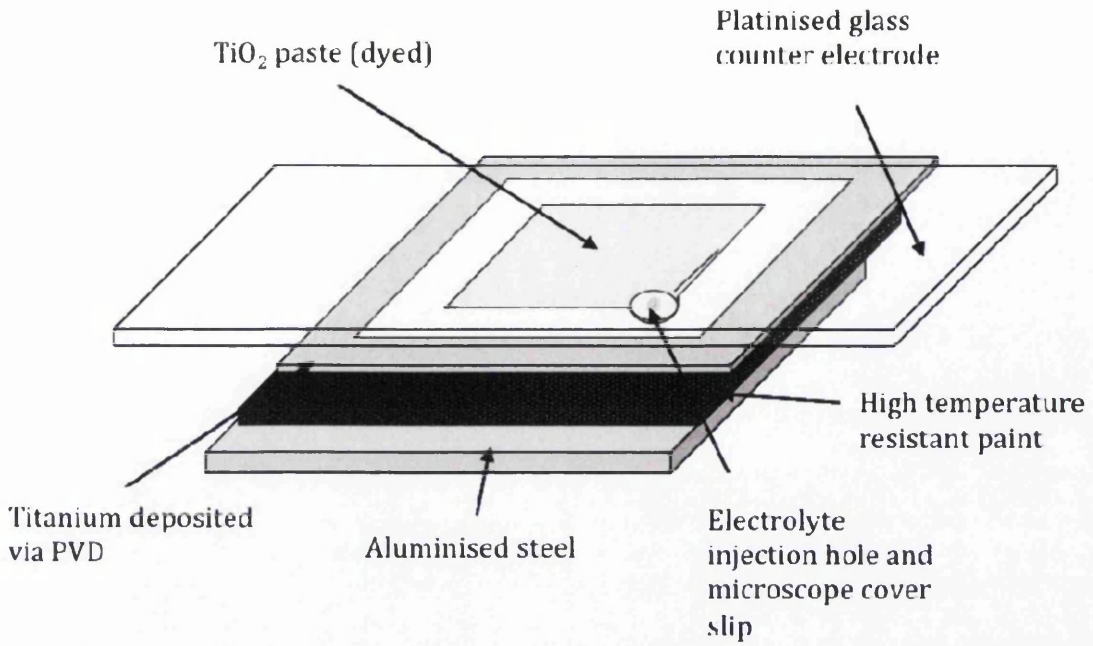

Figure 5.2: *Schematic illustration of the geometry of a DSC on an organically coated steel substrate*

5.4 Results and Discussion

The PVD deposited 1.2 μm Ti layer showed generally excellent adhesion to the organically coated steel substrate and could not be removed using industry standard tape pull off tests. The layer displayed an average sheet resistance of 6.7 ohm square as tested using a 4 point probe method (detailed in Chapter 2). This compared favourably to glass mounted 1.2 μm Ti layers (5.9 ohm square) prepared under identical deposition conditions. However, this is a higher resistance than displayed for 1 mm thick Ti coupons (as shown in Table 5.1) due to the relatively high resistance of the thin deposited film. In this respect the deposited layer seemed to be performing as would be expected for a micro-foil electrode.

Heating of the system at 450℃ for 30 minutes did however degrade the conductivity of the Ti layer applied to the pre-painted aluminised steel surface as shown in Table 5.1. This was not the case for either the Ti coupon or glass mounted PVD layer

where there was a slight improvement in conductivity following heating. The fall off in Ti layer conductivity in the pre-painted steel samples can be explained by considering the nature of the Ti layer post sinter. Figure 5.3 illustrates an optical micrograph of the sample post sintering (without a titania layer).

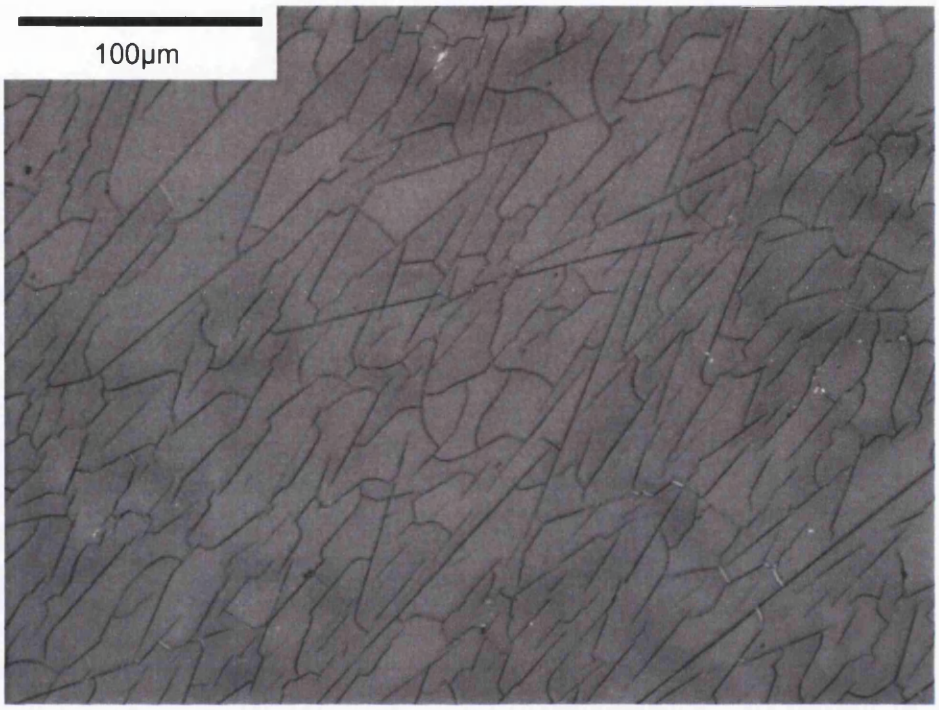

Figure 5.3: *Optical micrograph showing micro-cracking of the 1.2 µm PVD Titanium layer on pre-painted aluminised steel following heat treatment at 450 ℃ for 30 minutes*

It can be seen that there is considerable surface micro cracking (10-20µm between cracks) in the material. This may reflect a serious mismatch in thermal expansion properties between the trial high temperature epoxy organic binder and the PVD Ti layer. No cracking was observed on glass mounted Ti layers, as shown in Figure 5.4, of the same thickness (which is consistent with the improved conductivity in these systems shown in Table 5.1). This cracking leads to a large potential variability in post sinter sheet resistance as shown by the standard deviation in measurements for separate samples in Table 5.1.

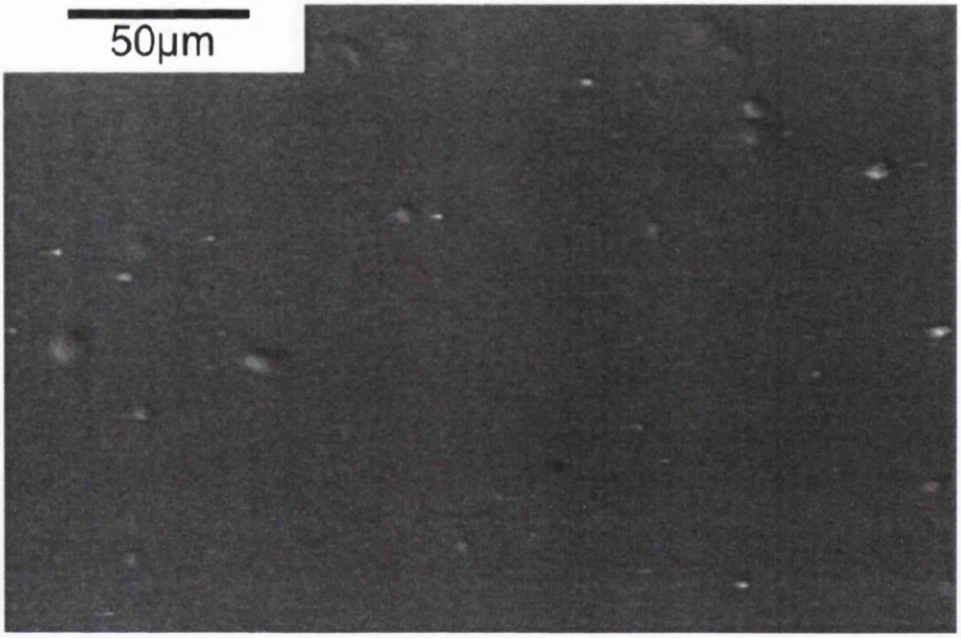

Figure 5.4: *Optical micrograph showing micro-cracking of the 1.2 µm PVD Titanium layer on glass following heat treatment at 450℃ for 30 minutes*

Table 5.1: *Four point probe determined sheet resistance values for Ti coupons (1mm) and PVD layers of Ti (1.2 µm) deposited on glass and pre-painted steel substrates before the sintering step and after application of a heating step at 450℃ for 30 minutes without prior titania deposition.*

Substrate	**Resistance before heating at 450℃ for 30 minutes Ohm square**	**Resistance after heating at 450℃ for 30 minutes Ohm square**
Ti coupons (1mm thick)	0.0063 (±0.0005)	0.0045 (±0.0005)
Ti PVD on glass (1.2 µm)	5.9 (±1.1	3.6 (±0.3)
Ti PVD on coated steel (1.2 µm)	6.7 (±1.9)	37 (±22)

Figure 5.5 shows the IV curves produced from a DSC on titanium sputtered organically coated steel compared to DSCs produced under identical conditions on 1 mm thick Ti. It can be seen from Figure 5.5 and the average cell performance data in Table 5.2 that the 1mm Ti sheet and 1.2 μm PVD Ti pre-painted aluminised steel mounted DSCs performances were reasonably comparable. In both cases the efficiency is lower than that obtained on glass since the cell is essentially in a reverse setup with light travelling through the iodide/tri-iodide electrolyte.

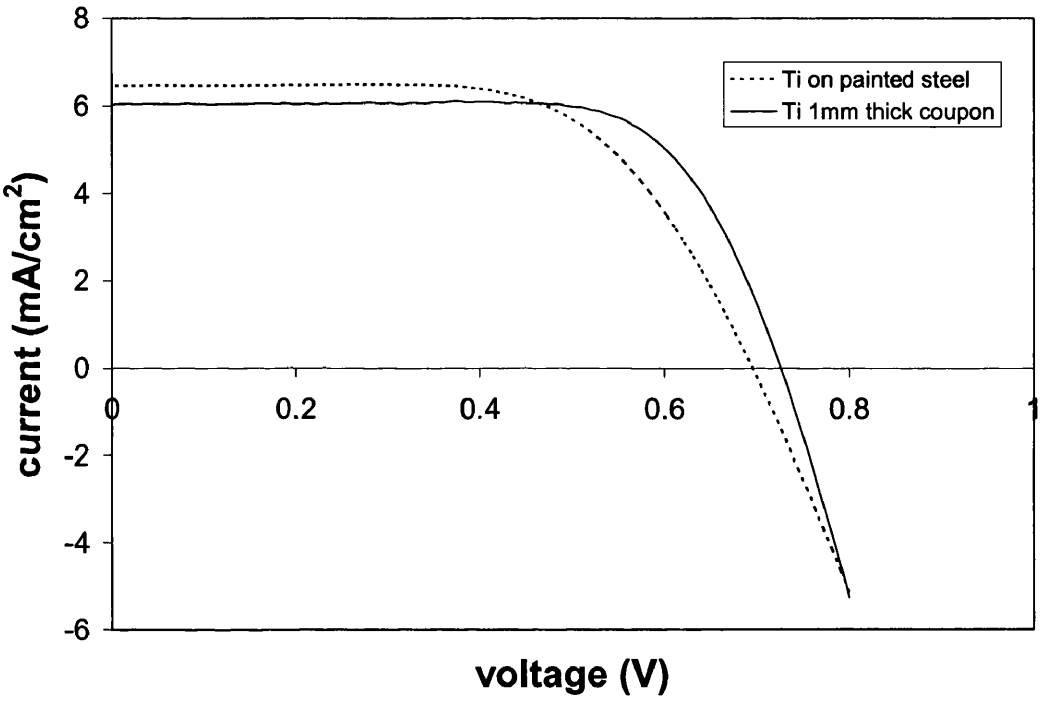

Figure 5.5: *Typical current voltage curves at one sun for DSCs prepared on 1mm thick Ti coupons (solid line) and Ti vapour deposited (1.2 μm) on pre-painted aluminised steel substrates.*

Table 5.2: *Efficiency data for 1cm^2 dye sensitised solar cells mounted on 1 mm titanium coupons and on 1.2 μm thick PVD titanium mounted on pre-painted steel substrates at one sun illumination. Values are based on an average of 5 cells produced for each cell type.*

Cell type	**Efficiency (%)**	**V_{OC} (V)**	**I_{SC} (mA/cm^2)**	**FF**
PVD Ti (1.2μm)	2.9 (±0.1)	0.69 (±0.01)	6.5 (±0.5)	0.64 (± 0.04)
Ti coupon (1mm)	3.2 (±0.1)	0.73 (±0.01)	6.0 (±0.1)	0.72 (± 0.02)

The 1 mm Ti coupon data presented shows that the organically coated steel cell still has some way to go to match a solid substrate. The lower fill factor suggests that the increased sheet resistance caused by Ti layer micro-cracking (illustrated in Figure 5.2) is the primary reason for the lowering in cell efficiency. There is clearly an effect upon the film from the underlying organic polymer layer. Whether it was a coefficient of thermal expansion (CTE) mismatch between the polymer and the Ti micro-layer or an effect of solvent removal during the sintering process that has an impact on the thin Ti film remained to be fully proved. Future work was aimed at matching the performance of the layers in heating steps and to further understand what role oxidation plays in changing the sheet resistance of micro layers of Ti on organic binders. Oxidation is evident through the creation of multi-coloured surface effects on the titanium surfaces on heating. Further efficiency gains could also be possible by secondary treatments such as $TiCl_4$ or through the inclusion of scattering particles in the titania paste material. In addition, the electrolyte used here has not been optimised for reverse cell set up (i.e. the high tri-iodide concentration reduces the photons reaching the sensitising layer whereas in forward set up the first layer the photons hit is the sensitising layer on glass). Nevertheless the 1.2 μm PVD titanium layer on pre-painted aluminised steel has been shown to be capable of

providing sufficient electron transport to sustain a dye sensitized solar cell at an efficiency of *ca.* 3%. Following paint curing, a metallisation unit could be incorporated to apply a Ti (or another metal layer) which would then form the basis of subsequent printed and roller coated dye cell components could now be a possibility. Furthermore given that deposition of TiO_2 *via* magnetron sputtering has already been demonstrated elsewhere [8-13] there is an opportunity to use this method to not only isolate and metallise the underlying substrate but also deposit the nanoporous TiO_2, entirely within one PVD operation. This proposal came with its challenges. Firstly, the Ti film deposition rates *via* our lab unit, for coating thicknesses of 1.2μm, are somewhat slow. Commercial industrial coating lines would need to operate at speeds of 20-120 m min^{-1}. With a coating time of two hours this is clearly a limiting factor. PVD is however a technology which is being explored for industrial application of micrometre scale metallic coatings. The major challenges are creating a roll-to-roll vacuum lock and ensuring consistent and fast deposition. The development of electron beam evaporation should assist with the latter and the former is already being addressed in work aimed at functionalising thin polymer films and in the development of galvanised products with a micrometre additional layer of elements such as magnesium. The second challenge is to address thermal mismatch. Firstly, what can be altered is the nature of the organic layer. The epoxy coating used in this work was chosen as it had known heat resisting properties and good adhesion to the aluminised substrate and so could be used to show potential in this early demonstration. The choice of a different polymer with a co-efficient of thermal expansion (CTE) closer to Ti would help reduce cracking. It is also the case that multi target PVD offers the opportunity of laying down several metal layers consecutively or creating an alloy material with a closer match to the CTE of the polymer. The third challenge links to the first two and that is to reduce the cracking and maintain both the corrosion barrier properties of the Ti layer and create good conductivity. Despite these challenges the attraction of the DSC is that it lends itself well to roll to roll processing and is a technology that is far more developed than organic photovoltaics, which will be an important next generation of coating for such products.

5.5 Conclusions

This work has shown that a dye-ensitised solar cell (DSC) can be manufactured directly onto pre-painted aluminised steel in one embodiment using magnetron sputtered titanium. This DSC is capable of achieving 2.9% photovoltaic conversion efficiency compared to a solid Ti electrode produced under identical conditions of 3.2%. The principal reason for the lowering of efficiency of the thin PVD layer on pre-painted aluminised steel is a lower fill factor that is believed to be related to the micro-cracking introduced by differential CTEs which increases sheet resistance. Future work will be to investigate variations to the polymer type and coating pigmentation to obtain a closer match in thermal characteristics and to explore multi layer magnetron sputtered metals. Developments in low temperature sintering also offer the potential to expand the substrate choice to include galvanised zinc-aluminium alloy coated steels, which are more typical of those used for high durability construction products. A multi-target PVD facility would allow the deposition of more than one material at a time allowing a greater insight into what these coatings may offer.

5.6 References

1. B. O'Regan and M. Gratzel: "A Low-Cost, High-Efficiency Solar-Cell Based on Dye-Sensitized Colloidal TiO_2 Films", *Nature*, 1991, 353, p. 737-740.
2. M. K. Nazeeruddin, A. Kay, I. Rodicio, R. Humphry-Baker, E. Muller, P. Liska, N. Vlachopoulos, and M. Gratzel: "Conversion of Light to Electricity by Cis-X_2bis(2,2'-Bipyridyl-4,4'-Dicarboxylate)Ruthenium(II)Charge-Transfer Sensitizers (X = Cl^-, Br^-, I^-, CN^-, and SCN^-) on Nanocrystalline TiO_2 Electrodes", *Journal of the American Chemical Society*, 1993, 115, p. 6382-6390.
3. A. Kay and M. Gratzel: "Low cost photovoltaic modules based on dye sensitized nanocrystalline titanium dioxide and carbon powder", *Solar Energy Materials for Solar Cells*, 1996, 44, p. 99-117.

4. X. M. Fang, T. L. Ma, M. Akiyama, G. Q. Guan, S. Tsunematsu, and E. Abe: "Flexible counter electrodes based on metal sheet and polymer film for dye-sensitized solar cells", *Thin Solid Films*, 2005, 472, p. 242-245.

5. M. G. Kang, N. G. Park, K. S. Ryu, S. H. Chang, and K. J. Kim: "Flexible metallic substrates for TiO_2 film of dye-sensitized solar cells", *Chemistry Letters*, 2005, 34, p. 804-805.

6. S. Ito, N. L. C. Ha, G. Rothenberger, P. Liska, P. Comte, S. M. Zakeeruddin, P. Pechy, M. K. Nazeeruddin, and M. Gratzel: 'High-efficiency (7.2%) flexible dye-sensitized solar cells with Ti-metal substrate for nanocrystalline-TiO_2 photoanode', *Chemical Communications*, 2006, (38), p. 4004-4006.

7. M. G. Kang, N. G. Park, K. S. Ryu, S. H. Chang, and K. J. Kim: "A 4.2% efficient flexible dye-sensitized TiO_2 solar cells using stainless steel substrate", *Solar Energy Materials for Solar Cells*, 2006, 90, p. 574-581.

8. M. M. Gómez, E. Magnusson, E. Olsson, A. Hagfeldt, S. E. Lindquist, and C. G. Granqvist: "Nanocrystalline Ti-oxide-based solar cells made by sputter deposition and dye sensitization: Efficiency versus film thickness", *Solar Energy Materials for Solar Cells*, 2000, 62, p. 259-263.

9. M. M. Gómez, J. Rodriguez, S. E. Lindquist, and C. G. Granqvist: "Photoelectrochemical studies of dye-sensitized polycrystalline titanium oxide thin films prepared by sputtering", *Thin Solid Films*, 1999, 342, p. 148-152.

10. M. M. Gómez, J. Rodriguez, S. Tingry, A. Hagfeldt, S. E. Lindquist, and C. G. Granqvist: "Photoelectrochemical effect in dye sensitized, sputter deposited Ti oxide films: The role of thickness-dependent roughness and porosity", *Solar Energy Materials for Solar Cells*, 1999, 59, p. 277-287.

11. M. M. Gómez, N. Beermann, J. Lu, E. Olsson, A. Hagfeldt, G. A. Niklasson, and C. G. Granqvist: "Dye-sensitized sputtered titanium oxide films for photovoltaic applications: influence of the O_2/Ar gas flow ratio during the deposition", *Solar Energy Materials for Solar Cells*, 2003, 76, p. 37-56.

12. M. M. Gómez, J. Lu, E. Olsson, A. Hagfeldt, and C. G. Granqvist: "High efficiency dye-sensitized nanocrystalline solar cells based on sputter deposited Ti oxide films", *Solar Energy Materials for Solar Cells*, 2000, 64, p. 385-392.

13. M. Gómez, J. Lu, J. L. Solis, E. Olsson, A. Hagfeldt, and C. G. Granqvist: "Dye-sensitized nanocrystalline titanium-oxide-based solar cells prepared by sputtering: Influence of the substrate temperature during deposition", *Journal of Physical Chemistry B*, 2000, 104, p. 8712-8718.

14. M. Toivola, F. Ahlskog, and P. Lund: "Industrial sheet metals for nanocrystalline dye-sensitized solar cell structures", *Solar Energy Materials for Solar Cells*, 2006, 90, p. 2881-2893.

15. L. W. McKeen, Fluorinated Coatings and Finishes Handbook, in Plastics Design Handbook, William Andrew, 2006, p. 205-218.

16. M-K. Son, H. Seo, S-K. Kim, Na-Y. Hong, B.-M. Kim, S. Park, K. Prabakar, H-J. Kim, "Improved long-term durability of a parallel-type dye-sensitized solar cell module using a platinum metal grid fabricated by direct current magnetron sputtering with heat treatment", *Journal of Power Sources*, 2013, 222, p. 333-339.

Chapter 6

PVD Metallic Bi-layers for Fabrication of DSCs on Organic Polymer Coatings

6.1 Introduction

This chapter describes studies aimed at minimising the Internal Resistance of Dye-Sensitized Solar Cells Fabricated on Organic Coated Steel Products using Magnetron Sputtering. This work is a continuation from the studies in Chapter 5 where it had been deemed possible for DSC technology to be successfully fabricated onto an organic polymer coated steel product. This had been achieved by rendering the polymer coating electronically conducting through the application of a physical vapour deposited thin Ti film. However, a change in focus had been revealed once again by the sponsor, Tata Steel. The bakeware coating studied in Chapter 5 has it limitations from the point of view of thermal expansion. However, due to the fact that it contains an aluminium pigment, worries about its effect on the DSC redox electrolyte, revealed from work carried out in Chapter 4, sparked an interest in a more inert polymer coating system. Attention was now shifted to the use of an organic polymer coating called polyimide. This system was noted to have excellent thermal and chemical stability properties that would maybe lend itself favourably for use in DSC fabrication. Polyimide was readily available as thin films of varying thickness, or also in a liquid form with the view to be coated on to a given substrate. The substrate chosen by the sponsor was an electrical chromium coated steel (ECCS) product, coated in a layer of polyimide at a thickness off around 50 – 100 microns. In order for DSC technology to be applied to this polyimide-ECCS system, once again PVD Ti was used in order to provide electrical conductivity. However, early developmental work revealed some very interesting findings. Varying thicknesses of

Ti deposited on polyimide coated ECCS displayed very poor sheet resistance vales after a heat treatment that simulated the DSC semiconductor sintering process. SEM revealed cracking within the Ti layer as seen in Chapter 5 when Ti was deposited on bakeware. As a comparison a metal with a higher co-efficient of thermal expansion, Al, was deposited at the same thickness, 500nm, and the electrical conductivity of the film was tested. Far superior values of sheet resistance were witnessed. A bilayer was then proposed to conserve the beneficial properties of electrical conductivity and corrosion resistance for Al and Ti respectively.

This Chapter details the developmental work and investigates methods of reducing a DSCs internal ohmic resistance through the use of a magnetron sputtering to produce electrically conducting films to act as collector electrode contacts. Ti, Al and Al-Ti bi-layer films have been applied, as mentioned above, to a polymer coated ECCS substrate. The metallised substrates produced have been used in the assembly of conventional DSCs. Cells have also been fabricated on Ti and Al foil for comparison. The metal layers are proposed to provide low electrical resistance and also to prohibit any corrosive attack by the tri-iodide electrolyte on the steel substrate product. This work focuses on the suitability of these materials as conducting layers for DSCs on organically coated substrates. The assembly of such a DSC incorporating thin film technology offers material cost savings and exciting scale up potential for metal roofing and cladding products.

6.2 Experimental Design

6.2.1 Substrate material

Due to the relatively high manufacturing temperatures, around 450 - 500°C, associated with the fabrication of DSCs, a 0.3mm gauge electro-chromium coated steel substrate, coated with an organic insulating and high temperature resistant layer of polyimide was used. The material was produced on a trial coil coating line on a roll to roll process, and oven curing was performed to achieve a suitable polymer

structure. The substrate was guillotined to the required dimensions prior to sputtering.

6.2.2 Sputtering of Ti and Al

Sputtering was performed as detailed in section 2.7.1 and 2.7.2.

6.2.3 Sputtering of Al-Ti Bi-layer

In order to sputter a bi-layer of Al and Ti, the exact same procedure as above was applied; however both target materials were placed in separate power sources. 0.5μm of Al was deposited first, and then Ti of 0.5μm, 1μm and 2μm thick was applied to the surface of the sputtered Al, under the same vacuum. This procedure negated the need to vent the chamber to change the target material after the deposition of Al, where a built up of surface oxide would prevail. Details are also explained in section 2.7.3.

6.2.4 Preparation of the TiO_2 Photoelectrode

The Preparation of the photoelectrodes was carried out as detailed in 2.4.2. A commercially available paste containing TiO_2 nanoparticles, ethyl cellulose and terpineol (Dyesol DSL 18NRT) was used as it provides a more successful mesoporous titania structure through its ability to be sintered under higher temperatures.

6.2.5 Preparation of counter electrodes

Counter electrodes were prepared as detailed in section 2.4.3.

6.2.6 Device fabrication

Devices were fabricated as detailed in section 2.4.4. The geometry of the final cell design is shown in schematically Figure 6.1.

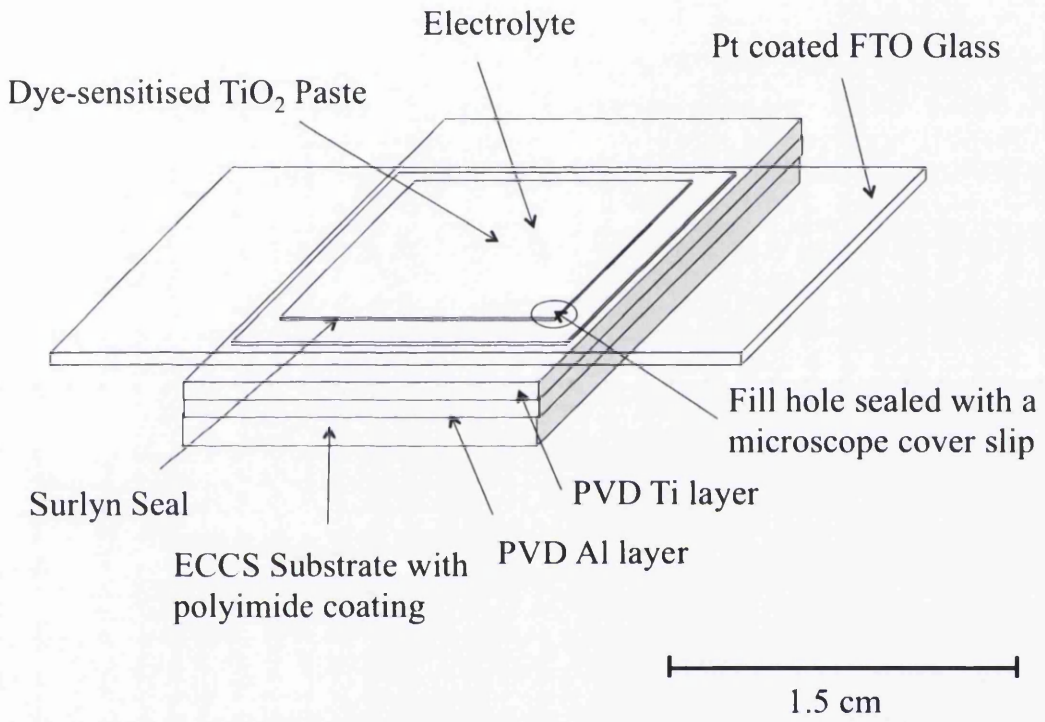

Figure 6.1: *Schematic illustration of the geometry of a DSC on an organically coated steel substrate*

6.2.7 Substrate corrosion testing

The corrosion mechanisms involved when iodine tri-iodide redox electrolyte is in contact with Al and Ti substrate surfaces (0.5 micron PVD on polymer coated ECCS and bulk material), were characterised using UV/Vis spectrophotometry in the same manner as detailed in Chapter 2 and the work in Chapter 4.

6.3 Results and Discussion

6.3.1 Ti and Al films

The sputter deposited Ti and Al films showed excellent adhesion to the underlying polymer coated ECCS substrate using industrial standard tape pull off tests. The Al film showed an average sheet resistance of 0.4 ohm/square, using a four point probe measurement method. However, the Ti film gave a considerably larger value of 12 ohm/square post deposition. Both materials were introduced to a simulated heat treatment or annealing process (similar to the environment expected during the TiO_2 calcination) at 450°C for various time intervals before the titania application, and sheet resistance measurements were made once again to evaluate the integrity of the films undergoing such treatment, shown in Table 6.1. An improvement in the electrical resistance was associated with the Al film. However a severe loss in conductivity was witnessed for the Ti film. Graphs of sheet resistance with respect to annealing times at 450°C for PVD Al can be seen in figure 6.2. No graphs were produced for Ti as sheet resistances for these films were very high and in the order of kΩ. To explain the decrease in resistance for Al, it can be correlated to work published by Tellier *et al* [9], where an improvement in resistance has been seen for aluminium films that have undergone annealing processes, the resistance recovery is said to be attributed to a surface reordering phenomenon. This is a promising result regarding the use of Al thin films. However, the resistance results obtained for PVD Ti films seem to strongly disfavour its use as a photoelectrode substrate. As witnessed in Chapter 4, metallised polymer surfaces that are exposed to high temperature environments are sometimes prone to crack formation within the metal film, which results in a significant increase in its electrical resistance. Work by Gao *et al* shows that the extent of this cracking phenomenon is said to strongly depend upon residual stress created within the film, with a major contributor being that of thermal stresses, resulting from a coefficient of thermal expansion mismatch between the film and substrate material during heating and cooling [10].

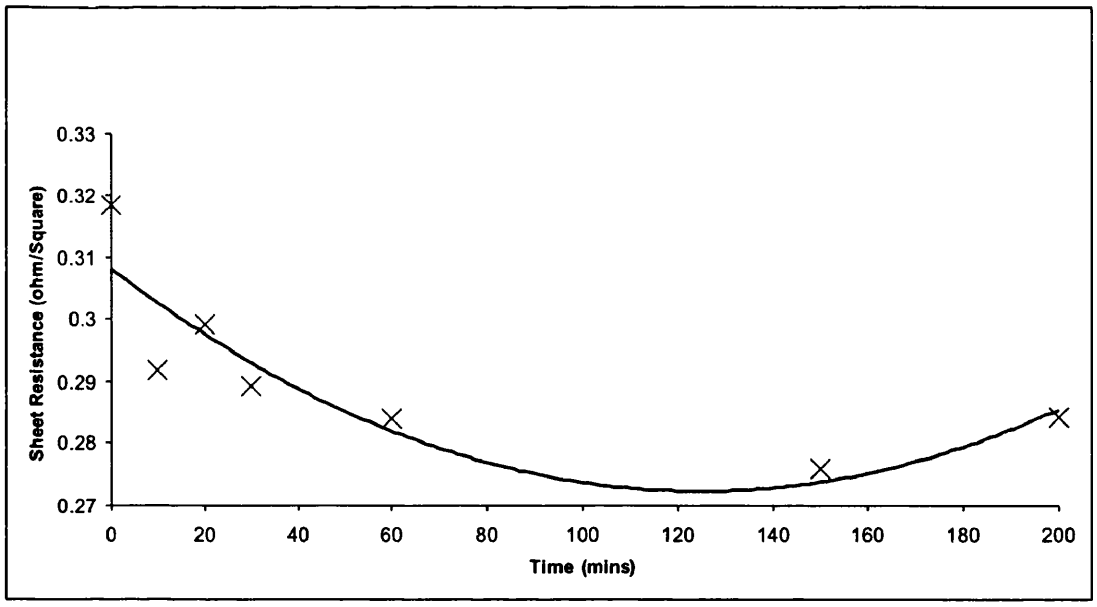

Figure 3: *Sheet resistance of 500nm thin film of Al against time in minutes during a simulated sinter process at 450°C*

Gao *et al* have developed a quantitative model for predicting thermal stresses in a similar three layer system; film-polymer-substrate metal. However this model is only valid for heat associated during a metallic deposition process and not further heat treatments of the three-layer system. This may aid in explaining the loss of electrical conductivity for our Ti film. Al has a significantly higher coefficient of thermal expansion (24 (10^{-6}m/m K)) than Ti (8.4 (10^{-6}m/m K)), and slightly higher but more similar to that of the high temperature resistant organic coating (around 16 (10^{-6}m/m K)). Therefore, Al may flow over the surface more freely, as opposed to resisting the expansion/contraction of the polymer used in this system during heating or cooling, resulting in cracking.

Figure 6.3 illustrates optical microscopy images of PVD Ti and Al samples post sintering (without a titania layer). There is no sign of crack formation for Al, the film is continuous, but the presence of micro cracking is evident for Ti producing huge discontinuity in the film.

a)

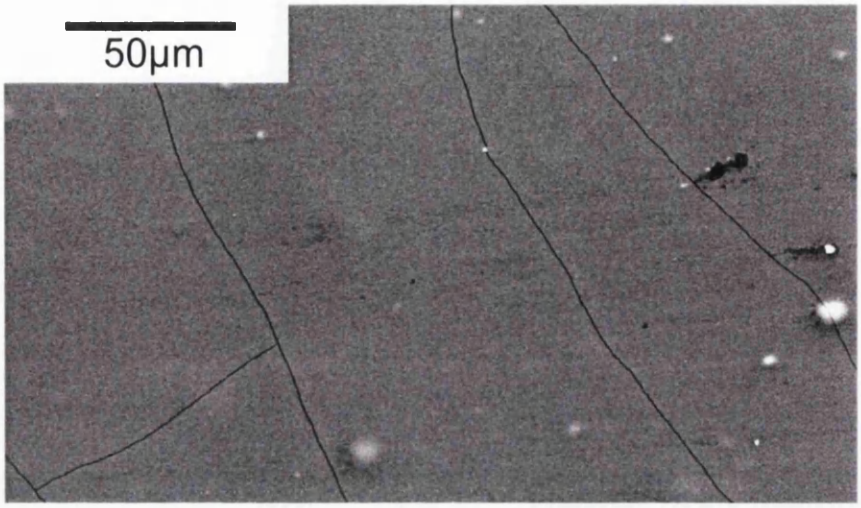

b)

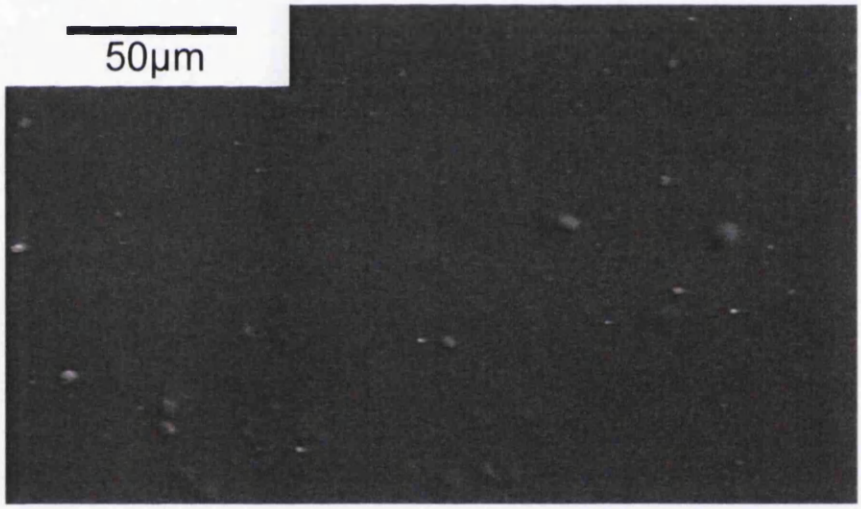

***Figure 6.3**. SEM surface images, after heat treatment at 450°C for 30 minutes, of a) 500nm PVD Titanium deposited on polyimide ECCS b) 500nm PVD Aluminium deposited on polyimide ECCS showing a more continuous surface property.*

Table 6.1: *Four point probe determined sheet resistance values for PVD layers of Al (0.5μm) and Ti (0.5μm) deposited on polyimide coated ECCS before the calcination step and after application of a heating step at 450°C for 30 minutes without prior titania deposition. Also values for Ti and Al foil controls are shown.*

Material	Sheet Resistance before annealing procedure (ohm square)	Sheet Resistance after 10 minutes annealing (ohm square)	Sheet Resistance after 20 minutes annealing (ohm square)	Sheet Resistance after 30 minutes annealing (ohm square)	Sheet Resistance after 60 minutes annealing (ohm square)
PVD Al	0.32	0.299	0.291	0.29	0.284
PVD Ti	12	2000	8000	-	-
Al foil	0.0033	0.0033	0.0033	0.0033	0.0033
Ti foil	0.0044	0.0044	0.0044	0.0044	0.0044

No IV curves could be produced from DSCs fabricated on either Ti or Al sputtered on the polymer coated ECCS, or for cells fabricated on Al foil. DSCs prepared under identical conditions on Ti foil gave an efficiency of 3.2%. It can be seen from the average cell performance data in Table 6.2 that the cells fabricated on PVD Al and Ti produced very poor efficiencies. This is also the case for cells manufactured on Al foil substrates for comparison purposes. The performance data extracted from cells built on the 1mm coupon of Ti foil shadows that of the others. As can be seen from the SEM images, the poor performances for cells built on PVD Ti film will have been caused by the loss of conductivity during the sintering procedure. However we should expect to see a more promising result from cells built on the PVD Al films, as excellent conductivity is maintained after sintering. This was not the case and was due to the effects of corrosion when Al is in contact with DSC electrolyte as detailed in Chapter 4.

In addition, the electrolyte used for cell production had not been optimised for reverse cell set up (i.e. the high tri-iodide concentration reduces the photons reaching the sensitising layer whereas in forward set up the first layer the photons hit is the sensitising layer on glass). But this couldn't be the sole reason for the zero efficiency, as we would expect higher values even with this scenario.

Table 6.2: *Efficiency data for 1cm² dye sensitised solar cells mounted on Ti foil, Al foil, PVD Al and Ti films mounted on polymer coated ECCS substrates at one sun illumination.*

Cell Type	Voc (V)	Isc (mA/cm^2)	FF	Efficiency (%)
PVD Al	0.66	0.0	16	0.0
PVD Ti	0.2	0.0	10	0.1
Al foil	0.0	0.0	0.0	0.0
Ti foil	0.73	6.0	72	3.2

After the studies mentioned above, we were essentially left with the notion that PVD Al films deposited on polyimide coated ECCS showed excellent electrical conductivity, whilst Ti films showed poor electrical conductivity. At the same time Al films showed to be poor from a corrosion point of view, whilst Ti films showed excellent longevity when in contact with DSC electrolyte. To try and solve this problem, I came up with the idea of combining the both films in a single system in order to reap the benefits of both materials. The next section details work carried out on a PVD Al-Ti bilayer.

6.3.2 Al-Ti Bilayer

The Al-Ti bilayer was proposed for conservation of the advantageous properties of both single film aluminium and titanium. By depositing a layer of Al we can maintain excellent electrical conduction, and then by applying a film of Ti on top of the Al we may be able to achieve a barrier layer that prevents any interaction between the Al and the redox electrolyte, but still allowing percolation of electrons from the underlying Al. The sputter deposited Al-Ti bilayer showed excellent adhesion to the underlying polymer coated ECCS substrate using industrial standard tape pull off tests once again. The average sheet resistances pre and post heat treatment can be seen in table 6.3.

Table 6.3: *Four point probe determined sheet resistance values for PVD Al-Ti bilayers with varying thicknesses of Ti (0.5, 1, 2 microns) deposited on polyimide coated ECCS before the calcination step and after application of a heating step at 450°C for various times without prior titania deposition.*

Material	Sheet Resistance before annealing procedure (ohm square)	Sheet Resistance after 10 minutes annealing (ohm square)	Sheet Resistance after 20 minutes annealing (ohm square)	Sheet Resistance after 30 minutes annealing (ohm square)	Sheet Resistance after 60 minutes annealing (ohm square)
Al-Ti 0.5	0.44	0.4	0.42	0.42	0.4
Al-Ti 1	0.4	1.2	1.5	2	2.2
Al-Ti 2	0.21	0.93	1.59	2.4	2.5

Figure 6.4 shows the IV curves produced from DSCs produced on the Al-Ti bilayers.

It can be seen from the average cell performance data in Table 6.4 that the cells fabricated on these layers give very positive results. Intriguingly, an increase in efficiency, Voc and FF can be seen with increasing Ti thickness.

a)

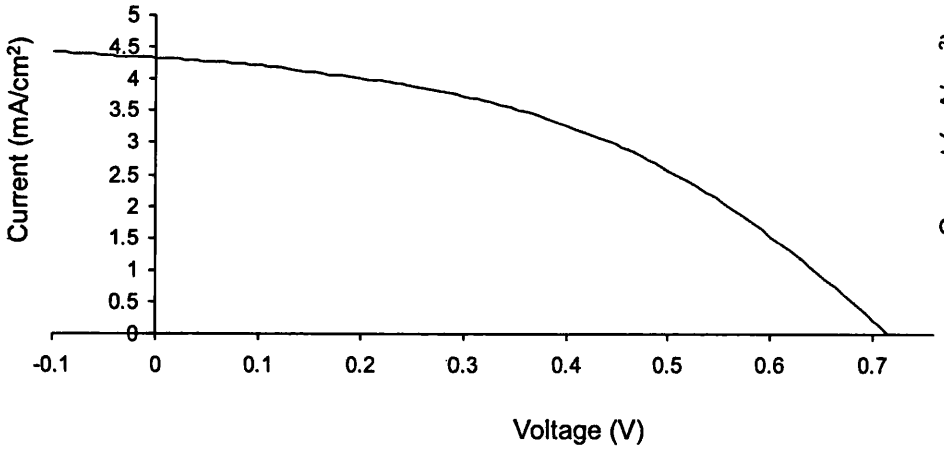

b)

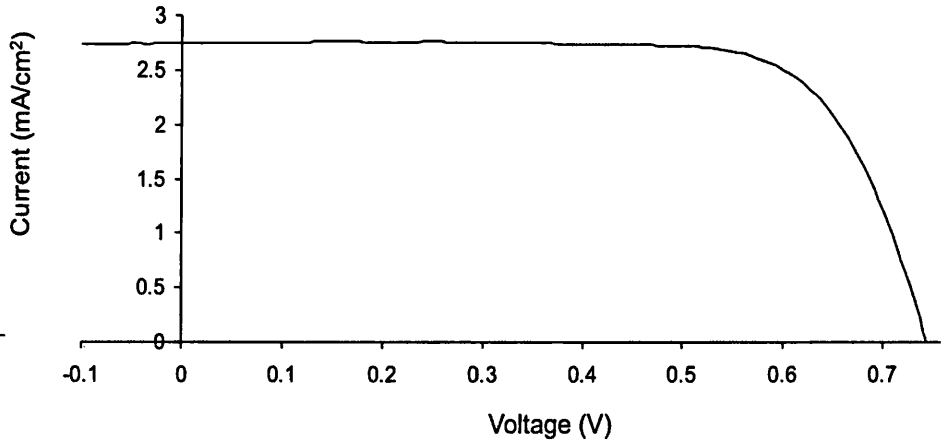

c)

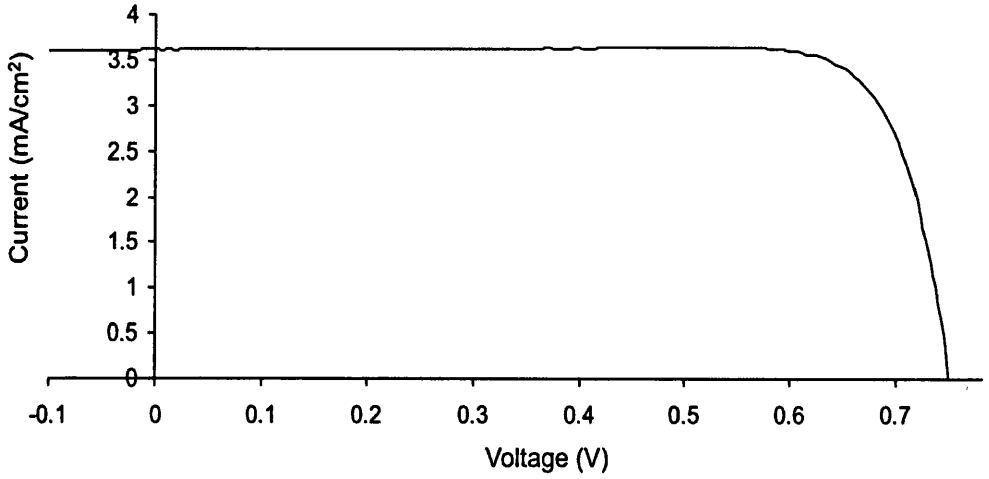

Figure 6.4: *IV characteristics under 1 sun illumination for cells produced on PVD Al-Ti bilayer with varying thicknesses of Ti. a) 0.5 μm, b) 1 μm, c) 2 μm.*

Table 6.4: *Efficiency data for 1cm² dye sensitised solar cells fabricated on Al-Ti bilayers with Ti thicknesses of 0.5, 1 and 2 microns, deposited on PI coated ECCS substrates and tested at one sun illumination.*

Cell Type	PVD Al Thickness (nm)	PVD Ti Thickness (nm)	Voc (V)	Isc (mA/cm²)	FF (%)	Efficiency (%)
Al-Ti 0.5	500	500	0.71	4.3	44	1.3
Al-Ti 1	500	1000	0.74	2.7	74	1.5
Al-Ti 2	500	2000	0.75	3.6	82	2.2

The 1 mm Ti coupon data presented in Chapter 5, shows that the bilayer cells still have some way to go to match a solid substrate. Nevertheless the Al-Ti bilayers have been shown to be capable of providing sufficient electron transport to sustain a dye sensitized solar cell at an efficiency of over 2%. This provides a novel method for creating steel based dye-sensitised solar cell in one embodiment in a roll-to-roll process. In other words following paint curing a metallisation unit could be incorporated to apply metallic layers that would then form the foundations for subsequent dye cell components. Furthermore given that deposition of TiO_2 *via* magnetron sputtering has already been demonstrated elsewhere [8-13] there is an opportunity to produce DSCs entirely within one PVD operation.

6.3.3 Cell longevity

The bilayer cells were retested after 24 hours, and after longer time periods if permitted in order to ascertain whether their performance had been affected by the presence of aluminium in the system, resulting in deactivation of the triiodide within electrolyte. Tables 6.5, 6.6, 6.7 and 6.8 show the retest performance of the cells.

The bilayer consisting of 2 microns of Ti was the only system to maintain is efficiency for over 48 hours. In fact only a slight decrease in efficiency had been witnessed for this system for several weeks. Fill factor remains at an encouragingly high value also. The thinner Ti layer barriers (0.5 and 1 micron) do not seem sufficient enough to totally segregate the Al conducting layer from contacting the redox electrolyte. In order to gain a better understanding of the morphology of these bilayers, SEM and GDOES analysis was performed. Figure 6.5 shows the SEM images and GDOES elemental makeup of the bilayer consisting of 1 micron of Ti.

It can be seen from the SEM image that there appears to be 'tear' like structures within the Ti top layer. Elemental analysis was performed by EDAX in the region of the tear and the findings are shown in Table 6.9.

Table 6.5. *Retest data for Al-Ti bilayer cells 24 hours after production*

Cell Type	Voc (V)	Isc (mA/cm^2)	FF (%)	Efficiency (%)
Al-Ti 0.5	0.69	2	46	0.7
Al-Ti 1	0.7	1.7	52	0.6
Al-Ti 2	0.73	3.7	80	2.2

Table 6.6. *Retest data for Al-Ti bilayer cells 48 hours after production*

Cell Type	Voc (V)	Isc (mA/cm^2)	FF (%)	Efficiency (%)
Al-Ti 0.5	-	-	-	-
Al-Ti 1	-	-	-	-
Al-Ti 2	0.73	3.5	80	2.2

Table 6.7. *Retest data for Al-Ti bilayer cells a week after production*

Cell Type	Voc (V)	Isc (mA/cm²)	FF (%)	Efficiency (%)
Al-Ti 0.5	-	-	-	-
Al-Ti 1	-	-	-	-
Al-Ti 2	0.72	3.6	81	2.1

Table 6.8. *Retest data for Al-Ti bilayer cells 2 weeks after production*

Cell Type	Voc (V)	Isc (mA/cm²)	FF (%)	Efficiency (%)
Al-Ti 0.5	-	-	-	-
Al-Ti 1	-	-	-	-
Al-Ti 2	0.72	3.0	79	2

Table 6.9: *Elemental composition of a PVD Al-Ti bilayer with 1 micron thickness of Ti deposited on polymer coated ECCS after heat treatment at 450°C for 30 minutes.*

	Within 'tears'	**Intact Region**
Element	**Element %**	**Element %**
Carbon	34.99	35.01
Oxygen	20.08	20.11
Aluminium	41.91	0.1
Titanium	0	42.2
Calcium	0.14	0.1
Iron	2.88	2.5

Intriguingly, within these 'tear' like regions, the results shown above confirm that no titanium is present and aluminium is. It seems has though Ti has delaminated in these areas. These features proved to be a common occurrence over the entire surface of the bilayer, meaning that in a cell format, aluminium presenting itself to the redox electrolyte initiating corrosion. The triiodide redox mediator is broken down over a period of 48 hours, and the cell becomes deactivated.

For comparison elemental analysis was also performed on an intact region of the surface film, i.e. at a 'non torn' region, and this indicated that titanium was predominant, and no aluminium was detected, thus confirming that tearing or porosity is a significant issue with this system. GDOES results seen in Figure 6.9, show that titanium diffuses into the aluminium layer during deposition and even more so after heat treatment, however titanium seems to remain at the surface of the aluminium. The GDOES analysis has no stand in explaining the exposure of aluminium as it has been used only as a depth profile, and gives no indication of porosity of surface features such as 'tears'.

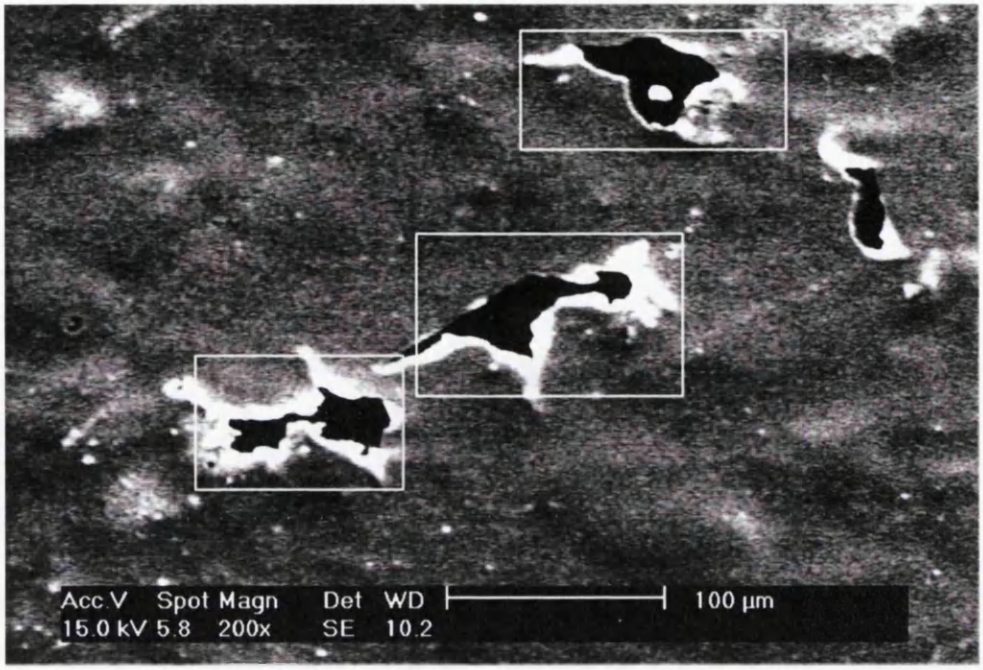

Figure 6.5. *SEM image of 'tear' like structures in the Ti top layer of an Al-Ti bilayer, after heat treatment at 450°C for 30 minutes. The areas within the boxes were the areas analysed.*

Increasing the thickness of Ti however must have a lowering effect on the amount of aluminium being introduced to the electrolyte due to the longevity of this film when DSC electrolyte is present in a cell format. A two microns layer of Ti seems to significantly increase the life of the cell. Two weeks after production the cell, we are still achieving an energy conversion efficiency of 2%. In an industrialisation of this system, greater thicknesses of sputtered films will correspond to a significant cost increase, through time and material cost, which is obviously not desirable.

a)

There is some Ti penetration. There is less O with Ti

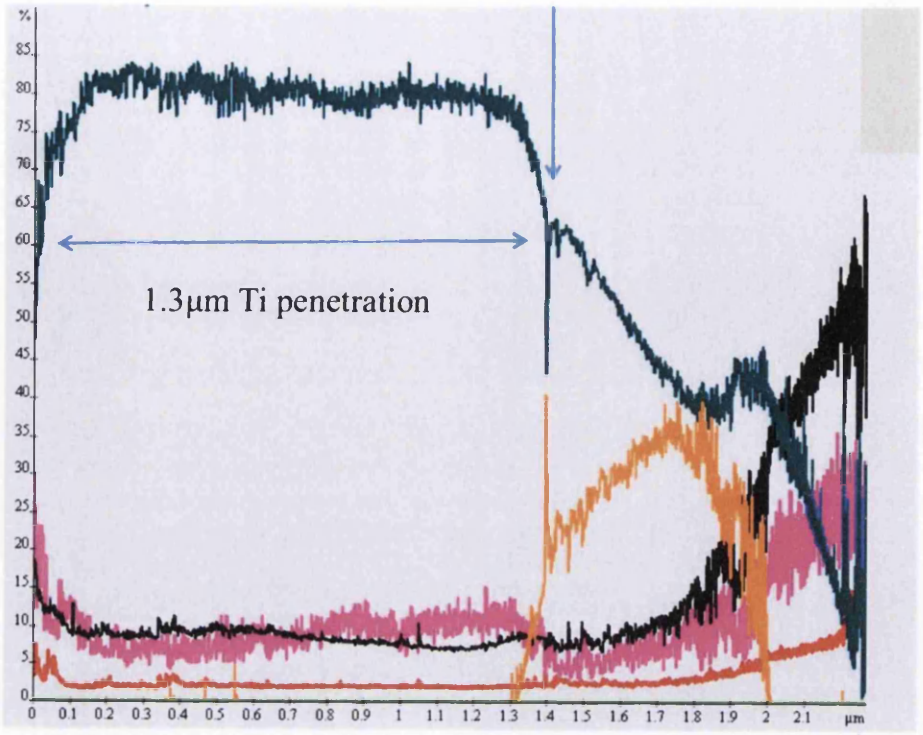

b)

There is Ti with O but no O with Al. Ti is only 0.5 microns thick. There is little Fe present

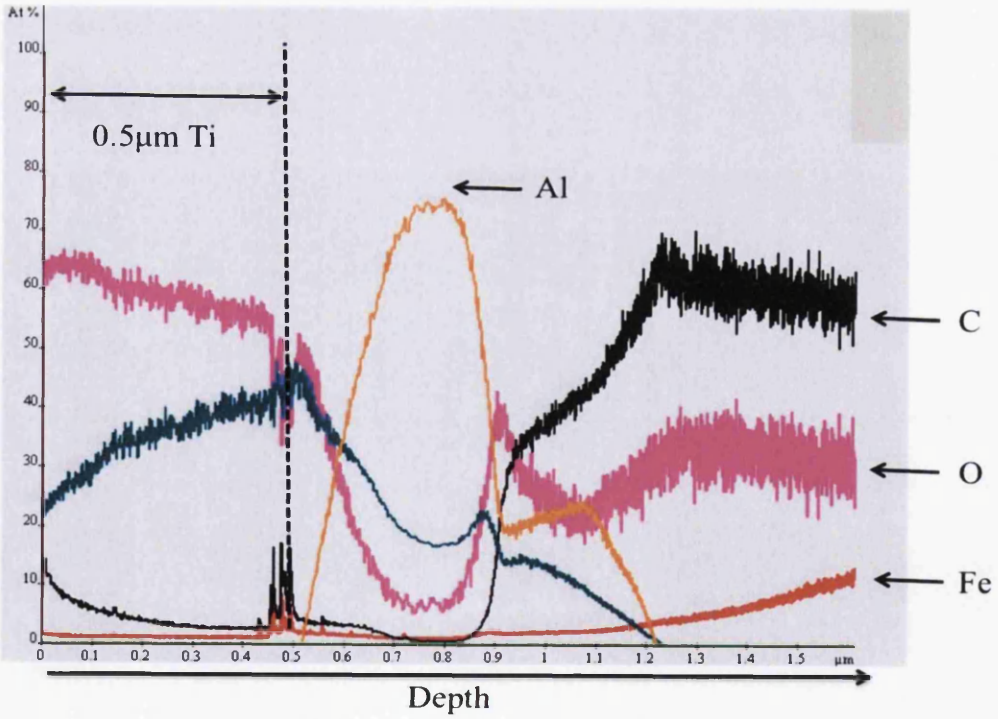

Figure 6.6. *GDOES surface composition results for Al-Ti bilayer consisting of 1 micron of Ti a) before and b) after heat treatment at 450°C for 30 minutes*

6.4 Conclusion

This work has shown that there is potential for a dye sensitized solar cell to be manufactured directly on to PI ECCS substrates in one embodiment using a magnetron sputtered Al-Ti bilayer. However some work is needed in improving the morphology of the film to totally block any of the redox mediator form presenting itself to the aluminium layer, banishing the effects of corrosion within the cell.

6.5 References

1. B. O'Regan, and M. Gratzel, "A low-cost, high-efficiency solar cell based on dye-sensitized colloidal TiO_2 films", *Nature*, 1991, 353, p. 737-740.
2. M. Toivola, F. Ahlskog, and P. Lund, "Industrial sheet metals for nanocrystalline dye-sensitized solar cell structures", *Solar Energy Materials and Solar Cells*, 2006, 90, p. 2881-2893.
3. K. Onoda, S. Hgamsinlapasathian, T. Fujieda, S. Yoshikawa, "The superiority of Ti plate as the substrate of dye-sensitized solar cells", *Solar Energy Materials and Solar Cells*, 2007, 91, p. 1176-1181.
4. M. M. Gómez, J. Rodriguez, S. -E. Lindquist, C. G. Granqvist, "Photoelectrochemical studies of dye-sensitized polycrystalline titanium oxide thin films prepared by sputtering", *Thin Solid Films,* 1999, 342(1-2), p. 148-152.
5. M. M. Gómez, J. Rodriguez, S. Tingry, A. Hagfeldt, S. -E. Linquist, G. C. Granqvist, "Photoelectrochemical effect in dye sensitized, sputter deposited Ti oxide films: The role of thickness-dependent roughness and porosity", *Solar Energy Materials and Solar Cells*, 1999, 59, p. 277-287.
6. M. M. Gómez, N. Beermann, J. Lu, E. Olsson, A. Hagfeldt, G. A. Niklasson, C. G. Grandqvist, "Dye-sensitized sputtered titanium oxide films for photovoltaic applications: influence of the O-2/Ar gas flow ratio during the deposition", *Solar Energy Materials and Solar Cells*, 2003, 76, p. 37-56.

7. M. M. Gómez, J. Lu, E. Olsson, A. Hagfeldt, G. C. Granqvist, "High efficiency dye-sensitized nanocrystalline solar cells based on sputter deposited Ti oxide films", *Solar Energy Materials and Solar Cells*, 2000, 64, p. 385-392.

8. M. Gómez, E. Magnusson, E. Olsson, A. Hagfeldt, S. -E. Lindquist, C. G. Granqvist, , "Dye-sensitized nanocrystalline titanium-oxide-based solar cells prepared by sputtering: Influence of the substrate temperature during deposition", *Journal of Physical Chemistry B*, 2000, 104, p. 8712-8718.

9. C. R. Tellier, A.J. Tosser, "Resistivity Recovery of Thin Sputtered Aluminum Films", *Electrocomponent Science and Technology*, 1976, 3, p. 85-89.

10. J. Gao, Y. Bao, D.T. Gawne, "Failure mechanisms of PVD films on organic coatings, *5th International Conference on Advances in Corrosion Protection by Coatings, Cambridge, U.K., 2009.*

Chapter 7

Conclusions and Future Work

7.1 Preventing Organic Coating Delamination using PVD

Thin PVD-deposited layers of Al on an iron substrate have been investigated as a means of stopping corrosion-driven organic coated delamination by a cathodic disbondment mechanism. A novel combinatorial method involving the deposition of a PVD Al thin wedge of graded thickness enabled the influence of Al layer thickness on the kinetics of organic coating disbondment to be studied on a single specimen in one 24 h experiment. Although cathodic disbondment has been seen to diminish, instead the corrosion proceeds anodically in the form of filiform corrosion.

7.2 Novel Substrates for DSC Technology

At the outset of this project a vast array of coated and uncoated metallic materials were deemed to be potential supporting substrates for the construction of DSCs. A number of experimental techniques were developed, which have revealed many interesting features regarding these substrates, highlighted potential issues concerning DSC fabrication techniques and re-enforced existing beliefs. We have also developed a novel technique of quantitatively characterising the interaction between redox mediator and different substrate material.

Experiments have identified those substrates that perform very poorly as a DSC substrate and have provided an approximate order to those that showed greater promise. This improved encapsulation of lower electrolyte volumes in combination

with novel monitoring techniques has revealed more about the substrate electrolyte interactions. This provided a clearer picture of those materials which did not deteriorate on prolonged exposure to the iodide / tri-iodide electrolyte, making them suitable substrates for the construction of DSCs *via* either a high or low temperature processing route. These were: titanium, stainless steel (316 grade in particular) and molybdenum (for high temperature processing).

Characterisation of other substrate/counter electrode combinations have revealed the following points of interest when considering the construction of metal based, flexible DSCs. From chapter 5, it may be said that thin metal conducting layers such as Titanium may present an option for the construction of DSCs *via* a lower temperature processing route to alleviate the deterioration of the PVD Titanium layer on polymer coated steel samples due to an inherent difference in thermal expansion.

Lastly there has been promising results for a sample of polyimide coated ECCS to become rendered electrically conducting through the application of an Al-Ti bilayer. The morphologies of the film have been studied and an optimum coating thickness advised.

This project has been able to demonstrate some important features that need to be considered when designing a metal mounted dye sensitised solar cell such as the interaction between the metal material and the DSC electrolyte. However, the up-scaling of PVD technology in conjunction with the industrialisation of DSC technology may have a way to go before becoming a realistic venture. The reason I believe this is purely due to the lack of large scale strip metal coating technologies available. From the literature, it seems apparent that deposition rates are much lower than those needed, if coating strip meals at speeds comparable to that of current coating processes, such as hot dip galvanising, are to be achieved.

There are many avenues of further work that need to be explored and these are briefly detailed here.

Clearly the substrate needs to be corrosion resistant. The substrates identified to-date are titanium, stainless steel and molybdenum. It is also clear that ECCS is promising particularly in combination with a polymer coating such as polyimide. The next phases of work should probe further into the vapour deposition methods to apply very thin layers of metals like titanium to allow the substrate to have the electrochemical properties of titanium without the associated cost.

A variety of techniques have been developed and can now be deployed to study corrosion and yet there are further advances possible. Time-lapse photography is a means of monitoring substrate corrosion rate / electrolyte decomposition on DSCs (without sensitised titania layer). RGB analysis would also allow for kinetic information to be obtained on a wide range of samples at once through use of a timelapsed digital camera. Further use of UV Vis spectroscopy could be used to a monitor a large array of PVD sputtered electrodes. Investigating the components of the electrolyte should also be an area to develop also, namely the amount of tert-butylpyridine used. It has been mentioned in the literature that mild steel can resist the corrosive nature of the DSC electrolyte, which is believed to be related to the components of the specific DSC electrolyte used.

7.3 Personal Outcomes

During my time on the engineering doctorate course, I believe that there were many beneficial learning outcomes and skills acquired, that I feel I will be able to transfer to any future endeavour. A major component of the course was to present information to colleagues, fellow scientists and industrial professionals. I found this very difficult at first, especially during the first year, due to a lack of confidence during public speaking. By the end of the course I had presented at a conference in Las Vegas and also at a seminar, which was attended by over one hundred academics and industrial professionals. Another learning outcome I feel I have achieved is the awareness of issues regarding developing sustainability and the use and development of alternative energy sources. I feel I now understand the need for change within the

community, and also feel that I have contributed to an area of research that is of huge interest currently. I enjoyed building knowledge of how dye-sensitised solar cells work, and also found pleasure in the problem solving nature of the work.

Appendix

A list of publications that arose from work carried out in this thesis is detailed below.

1. G.J. Reynolds, Z.S. Barrett, H.N. McMurray, G. Williams, "An investigation of the influence of physical vapour deposited aluminium layers on the kinetics of organic coating disbondment on iron", *Corrosion Science*, 2013, 70, p. 82-92. doi: 10.1016/j.corsci.2013.01.015

2. T. Watson, G. Reynolds, D. Wragg, G. Williams, and D. Worsley, "Corrosion Monitoring of Flexible Metallic Substrates for Dye-Sensitized Solar Cells," *International Journal of Photoenergy*, 2013, vol. 2013, Article ID 791438, 8 pages. doi:10.1155/2013/791438

3. G. J. Reynolds, T. M. Watson, G. Williams, and D. Worsley, "Corrosion Resistance of Metallic Substrates for the Fabrication Dye-Sensitized Solar Cells", *ECS Transactions*, 2011, 33, p. 129-138. doi: 10.1149/1.3553355

4. T. M. Watson, G. J. Reynolds, D. A. Worsley, "Painted steel mounted dye sensitised solar cells: titanium metallisation using magnetron sputtering", *Iron & Steelmaking*, 2011, 38, p. 168-172. doi:10.1179/1743281210Y.0000000003